SELECTIVE OXIDATION OF ALKANES AND ALKENES BY POLYOXOMETALATES USING GREEN OXIDANTS

A THESIS

SUBMITTED TO THE

UNIVERSITY OF PUNE

FOR THE DEGREE OF

DOCTOR OF PHILOSOPHY

IN CHEMISTRY

BY

Research Student

ROHIT INGLE

Research Guide

DR. P. MANIKANDAN

CATALYSIS DIVISION

NATIONAL CHEMICAL LABORATORY

PUNE 411 008

INDIA

February 2008

CERTIFICATE

This is to certify that the work discussed in the thesis entitled **"SELECTIVE OXIDATION OF ALKANES AND ALKENES BY POLYOXOMETALATES USING GREEN OXIDANTS"** by **ROHIT INGLE**, submitted for the degree of *Doctor of Philosophy in Chemistry* was carried out under my supervision at the Catalysis and Inorganic Chemistry Division of the National Chemical Laboratory, Pune, India. Such materials as have been obtained by other sources have been duly acknowledged in this thesis. To the best of my knowledge, the present work or any part thereof has not been submitted to any other University for the award of any other degree or diploma.

Date: **Dr. P. Manikandan**

Place: Pune   (Research Supervisor)

<u>DECLARATION</u>

I hereby declare that the work described in this thesis entitled **"SELECTIVE OXIDATION OF ALKANES AND ALKENES BY POLYOXOMETALATES USING GREEN OXIDANTS"** submitted for the degree of *Doctor of Philosophy in Chemistry* has been carried out by me at the Catalysis and Inorganic Chemistry Division of the National Chemical Laboratory, Pune, India under the supervision of Dr. P. Manikandan. Such materials as have been obtained by other sources have been duly acknowledged in this thesis. The work is original and has not been submitted in part or full by me for award of any other degree or diploma in any other University.

Date: **Rohit Ingle**

Place: Pune   (Research Student)

Dedicated

to my

Parents

Acknowledgements

I sincerely acknowledge my research guide Dr. P. Manikandan for his invaluable guidance, constructive suggestions and support given throughout the course of this investigation.

I wish to express my sincere gratitude and indebtedness to Dr. S. B. Halligudi, Dr. R. Nandini Devi and Dr. N. K. Kala Raj for all the help rendered by them in any form during this period.

I express my sincere gratitude to Dr. S. Sivasanker, Dr. Rajiv Kumar, Dr. D. Srinivas, Dr. A. P. Singh, Dr. M. K. Dongare, Dr. Veda Ramaswamy, Dr. C. V. V. Satyanarayana, Dr. C. S. Gopinath, Dr. Mirajkar, Dr. T. Raja, Dr. Pardhy, Dr. Deshpande, Dr. Awate, Dr. Belhekar, Dr. Shubhangi, Ms. Agashe, Ms Jacob, Mr. Niphadkar, Mr. Tejas, Mr. Jha and Ms Violet, Catalysis Division, National Chemical Laboratory, Pune for their valuable discussions, academic aid and ethical guidance throughout the course of work. I would also like to thank Mr. Purushottaman, Mr. Kashinathan, Mr. Madhu, Mr. Milind, Mr. Katti and other supporting staff of Catalysis Division.

I am genuinely thankful to my Lab mates Dr. Sankar, Sreeja, Sankaranarayanan, Tushar, Shashikant, Srikant, Asha, Aany, Reji, Anju, Vineetha and Srinidhi for their cheerful cooperation and affection.

I don't have words to express my feelings towards my friends Shanbhag, Shekhar, Dr. Hrishikesh, Dr. Amit, Mahesh, Ankur, Suman, Lakshi, Dr. Vasudev, Naresh, Dr. Prashant and Prasad for their whole hearted love and encouragement throughout my research activity.

I would also like to thank all the students in Catalysis Division especially Atul, Ramakant, Srikant, Ankush, Devendra, Sachin, Ganesh, Sivaram, Dr. Rajendra, Pallavi, Neelam, Maitri, Dr. Surekha, Dr. Smita and Dr. Dhanashree for their motivation and fruitful discussions. I have no words to articulate my feelings towards my other friends Kaustubh, Dr. Vivek, Archika, Poorva, Dr. Mahesh, Unmani and Shivani for their unconditional love and unfailing moral support.

Finally, I owe my acknowledgements to the University Grants Commission (UGC) for financial assistance in the form of Junior Research Fellowship and Dr. S.

Abbreviations

15 wt% HPA/MO$_2$	15 w/w percent of heteropoly acid dispersed on TiO$_2$ or ZrO$_2$
AAS	Atomic Absorption Spectroscopy
ACN	Acetonitrile
APTES	Aminopropyltriethoxysilane
BET	Brunauer-Emmett-Teller
BJH	Barret-Joyner-Halenda
DCE	1,2 dichloroethane
DRS-UV-Vis	Diffuse Reflectance Scattering Ultra-Violet Visible Spectroscopy
EO$_{20}$-PO$_{70}$-EO$_{20}$	Polyethylene glycol-Polypropylene glycol-Triblock copolymer
EDX or EDAX	Energy Dispersive X-Ray Absorption Spectroscopy
EPR	Electron Paramagnetic Resonance Spectroscopy
FT-IR	Fourier Transformed Infra-Red Spectroscopy
GC-MS	Gas Chromatography coupled with Mass Spectrometry
GLC or GC	Gas-Liquid Chromatography
HPA	Heteropoly acid
ICP	Inductively Coupled Plasma Spectroscopy
MCM-41	Mobil Composite Material (A mesoporous material)
MO$_2$	TiO$_2$ or ZrO$_2$
Mo$_6$Al-As	(NH$_4$)$_3$AlMo$_6$H$_6$O$_{24}$.7H$_2$O, as synthesized
Mo$_6$Al-Cal	(NH$_4$)$_3$AlMo$_6$H$_6$O$_{24}$.7H$_2$O, calcined at 350 °C
MoVAlO$_x$	Mo$_1$V$_{0.33}$Al$_{0.16}$O$_x$ composition of the catalyst
MoVAlO$_x$-1, MoVAlO$_x$-2, MoVAlO$_x$-3 and MoVAlO$_x$-4	Mo$_1$V$_{0.33}$Al$_{0.16}$O$_x$ synthesized at pH conditions of 1, 2, 3 and 4, respectively
[MTCA]	Methyltricaprylammonium group
[MTCA][SbW9O33] Q$_9$[SbW9O33]	Sodium counter cations of Na$_9$[SbW$_9$O$_{33}$] replaced by [MTCA] group (cations)
[MTCA]$^+$Cl$^-$	Methyltricaprylammonium chloride

NH$_2$-SBA	Amino Functionalized SBA-15
NH$_2$-SBA- V$_x$HPA, x = 1, 2 , 3	Amino Functionalized SBA-15, on which the vanadium heteropoly acid V$_x$HPA is anchored
NMR	Nuclear Magnetic Resonance Spectroscopy
PMA	Phosphomolybdic (molybdophosphoric) acid
PTA	Phosphotungstic (tungstophosphoric) acid
PTC	Phase Transfer Catalyst
Q$_9$[SbW9O33]	Sodium counter cations of Na$_9$[SbW$_9$O$_{33}$] replaced by [MTCA] group (cations)
Raman	Fourier Transformed Raman Spectroscopy
SAXS	Small Angle X-Ray Scattering Spectroscopy
SBA-15	Santa Barbara Amorphous (A mesoporous material)
[SbW$_9$O$_{33}$]	Anionic part of Na$_9$[SbW$_9$O$_{33}$] polyoxometalate
SEM	Scanning Electron Microscopy
TBHP	Tertiary Butyl Hydroperoxide (aqueous)
TBHP/DCE	Tertiary Butyl Hydroperoxide extracted in 1,2 dichloroethane
TEOS	Tetraethylorthosilicate
TG-DTA	Thermogravimetry-Differential Thermal Analysis
UV-vis or UV-visible	Ultraviolet-Visible Spectroscopy
V$_x$HPA	Vanadium substituted heteropoly acids
V$_1$HPA	Monovanadomolybdophosphoric acid
V$_2$HPA	Divanadomolybdophosphoric acid
V$_3$HPA	Trivanadomolybdophosphoric acid
XRD	Powder X-Ray Diffraction

Contents

Chapter 1:

Introduction

1.1 Overview

Polyoxometalates belong to a large class of nanosized metal-oxygen cluster anions [1, 2]. These form by a self-assembly process, typically in an acidic aqueous solution as illustrated by equation 1.1 and 1.2 and can be isolated as solids with an appropriate counter cation, for example H^+, alkali metal cation, NH_4^+etc.

$$8\ H^+ + 7\ WO_4^{2-} \rightarrow [W_7O_{24}]^{6-} + 4\ H_2O \qquad\qquad (1.1)$$

$$23\ H^+ + HPO_4^{2-} + 12\ MoO_4^{2-} \rightarrow [PMo_{12}O_{40}]^{3-} + 12\ H_2O \qquad\qquad (1.2)$$
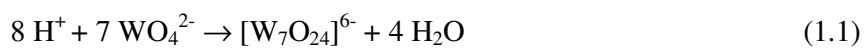
Generally, two types of polyoxometalates are distinguished, based on their chemical compositions - isopoly anions and heteropoly anions. These anions may be represented by the general formulae:

$[M_mO_y]^{p-}$ Isopoly anions

$[X_xM_mO_y]^{q-}$ ($x \leq m$) Heteropoly anions
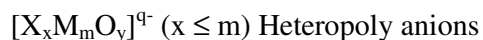
where M is the addenda atom and X is the heteroatom also called the central atom when located in the centre of the polyanion. The distinction between the two groups is frequently artificial, especially in the case of mixed-addenda polyoxometalates [2]. Heteropoly compounds are by far most important for catalysis as well as for other applications; hence this work is mainly focused on them. Heteropoly acids - strong acids composed of heteropoly anions and protons as the counter cations - constitute a special case of heteropoly compounds that is particularly important for catalytic applications.

The most common addenda atoms are molybdenum or tungsten, less frequently vanadium and niobium or mixtures of these elements in their highest oxidation states (d^0, d^1). Much broader range of elements act as heteroatoms; as such, almost all elements of the Periodic Table can be incorporated in heteropoly anions, most typical ones being P^{5+}, As^{5+}, Si^{4+}, Ge^{4+}, B^{3+} etc. Molybdenum (VI) and tungsten (VI) are the best polyoxometalate forming elements, as the result of a favorable combination of ionic radius and charge and of accessibility of empty *d*-orbitals for metal-oxygen π bonding [2].

1.2 Structures of Polyoxometalates

Dozens of structural types and stoichiometries of polyoxometalates are known to date. The minimum degree of condensation of addenda atoms is arbitrarily set to be in the range of 2 to 6 [2, 3]. The maximum can go to as high as a few hundred. For example, the giant heteropoly tungstate $[La_{16}As_{12}W_{148}O_{524}]^{76-}$ includes 28 heteroatoms (La, As) and 148 addenda atoms (W) [4].

Two general principles apply to polyoxometalate structure: [2-5]

1. Addenda atoms occupy a metal-oxygen polyhedron MO_x that is most commonly an octahedron. In this polyhedron, the metal atom is displaced from the inversion centre towards the peripheral vertices because of metal-oxygen π bonding.

2. Structures with MO_6 octahedra that contain more than two free vertices are generally not found among the typical polyoxometalates. This is known as the Lipscomb restriction, which may be explained as a result of the strong *trans* influence of the terminal M=O bonds that facilitates dissociation of MO_3 from the polyanion [6].

According to Pope and Muller, it is convenient to discuss the variety of polyoxometalate structure starting from a few highly symmetrical 'parent' polyanions; then many other polyoxometalate structures maybe considered as their 'derivatives' [2, 5]. There are three such parent structures, with a tetrahedron, an octahedron and an icosahedron as their central polyhedron XO_n (n = 4, 6 or 12) that determines the symmetry of the whole polyanion. These structures, that have already been mentioned, are: the Keggin structure (T_d symmetry); the structure of a hypothetical anion $[XM_{12}O_{38}]$ (O_h), that has not yet been observed itself but its derivatives, for example the Anderson-Evans anion $[XM_6O_{24}]$, are well known and the Dexter-Silverton structure (I_h). These structures will be briefly discussed below.

1.2.1 The Keggin structure

This is the first characterized and the best known structure that is adopted by many polyoxometalates [7]. Among a wide variety of heteropoly compounds, the Keggin are the most stable and more easily available. These, together with some of their derivatives, are the most important for catalysis.

The Keggin heteropoly anions are typically represented by the formula $[XM_{12}O_{40}]^{x-8}$, where X is the heteroatom, x is its oxidation state and M is the addenda atom (usually Mo^{6+} or W^{6+}). The M^{6+} ion can be substituted by many other metal ions e.g, V^{5+}, Co^{2+}, Zn^{2+}etc. The Keggin anion has a diameter of *ca.* 1.2 nm and is composed of a central tetrahedron XO_4 surrounded by 12 edge- and corner-sharing metal-oxygen octahedra MO_6 (Figure 1). The octahedra are arranged in four M_3O_{13} groups. Each group is formed by three octahedra sharing edges and having a common oxygen atom which is also shared with the central tetrahedron XO_4. The total assemblage contains 40 close-packed oxygen atoms. The oxygen atoms are of four types: twelve terminal M=O, twelve edge-bridging angular M-O-M shared by the octahedra within a M_3O_{13} group, twelve corner-bridging quasi-linear M-O-M connecting two different M_3O_{13} groups and four internal X-O-M. These oxygen atoms can be discriminated by ^{17}O NMR [2]. The corresponding bonds exhibit characteristic infrared bands in the range of 600-1100 cm^{-1} [2].
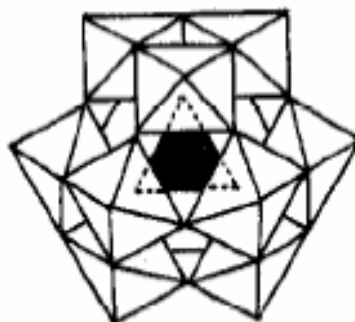
Figure 1: The Keggin structure of the $[X^xM_{12}O_{40}]^{x-8}$ anion (α-isomer) [2]

Each of the M_3O_{13} groups can be rotated by 60° about its 3-fold axis which leads to geometrical isomers. The structure shown in Figure 1 is the most common α isomer of the Keggin structure. Rotation of one of its M_3O_{13} group produces the β isomer. In some cases, these isomers can be separated, e.g, by fractional crystallization. Rotation of two, three or all four M_3O_{13} produces the γ, δ and ε isomers, respectively [2].

Lacunary derivatives of the Keggin anion result from the removal of one or more M atoms. Examples of the lacunary derivatives (one monovacant and two trivacant) of the α-Keggin anions are shown in Figure 2. The two trivacant species correspond to loss of a corner-shared group of MO_6 octahedra (A-type $[XM_9]$) or an

edge-shared group (B-type $[XM_9]$) [2]. Such species can assemble into larger polyoxometalate structures, either directly or without incorporation of metal ion linkers.
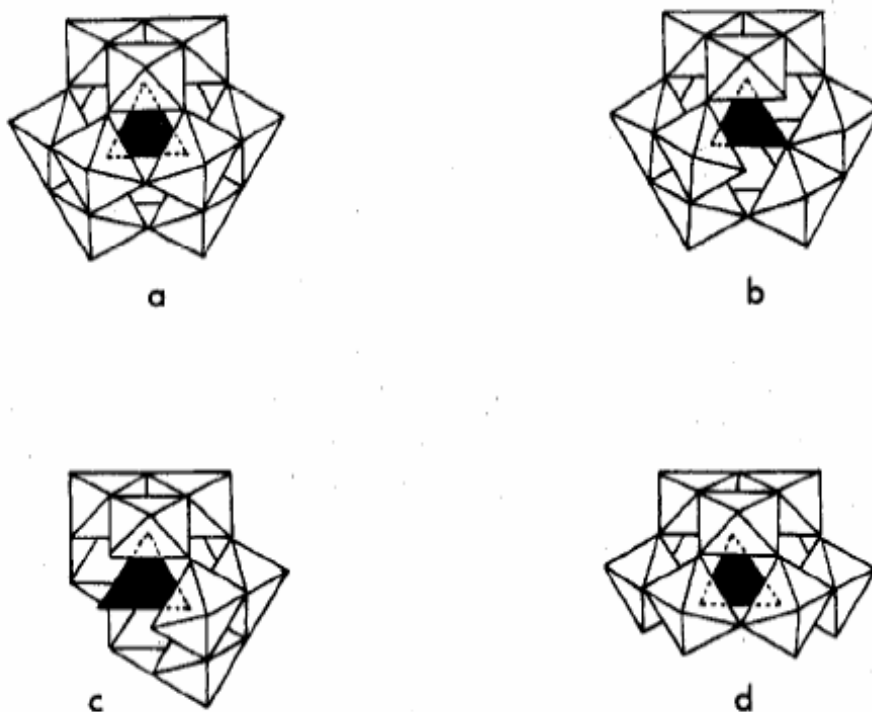
Figure 2: The structures of the α-Keggin anion $[XM_{12}O_{40}]^{x-8}$ (a) and its lacunary derivatives: (b) monovacant, (c) trivacant B-$[XW_9]$ and (d) trivacant A-$[XW_9]$ [2]

1.2.2 The Well-Dawson structure

One of these derivatives is the Well-Dawson dimeric (2:18) heteropoly anion $[X_2M_{18}O_{62}]^{2x-16}$ ($M = Mo^{6+}$ or W^{6+}, $X = P^{5+}$ or As^{5+}, x = charge on the 'X' atom). Its structure (α-isomer) is shown in Figure 3. The anion consists of two trivacant lacunary Keggin species A-$\{XM_9\}$ linked directly across the lacunae. The Well-Dawson structure contains two M_3O_{13} groups. A 60° rotation of one of these groups about its 3-fold axis gives the β-isomer. The molybdenum anion is chiral because of a displacement of the molybdenum atoms within their MoO_6 octahedra. The tungsten complex shows no such chirality probably because of the greater rigidity of the tungsten framework [2, 8].
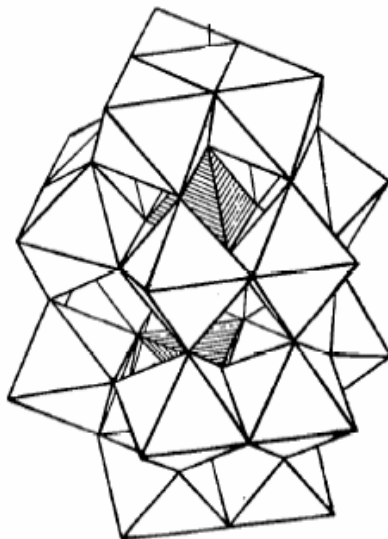
Figure 3: The Well-Dawson structure of the $[X_2M_{18}O_{62}]^{2x-16}$ anion (α-isomer) [8]

1.2.3 The Anderson-Evans structure

This example represents a different structural type with an octahedron as a central polyhedron. The Anderson-Evans structure is adopted by 6-heteropoly anions (e.g. $[Te^{6+}Mo_6O_{24}]^{6-}$) [2, 9]. It consists of six coplanar MO_6 octahedra arranged in a closed ring sharing edges. The heteroatom occupies the octahedral pocket in the centre of the ring (Figure 4).
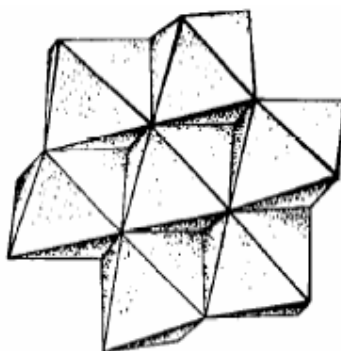
Figure 4: The Anderson-Evans structure of the $[X_6M_6O_{24}]^{2x-16}$ anion [9]

1.2.4 The Dexter-Silverton structure

A less common type of 12-heteropoly anions $[XM_{12}O_{42}]^{x-12}$, where M is molybdenum (VI) and X is cerium (IV), uranium (IV)or thorium (IV), adopt this structure (Figure 5). In this anion, the central atom is surrounded by twelve oxygen

atoms that form an icosahedron as a central polyhedron. The MO_6 octahedra are arranged in face-sharing pairs [2, 10].
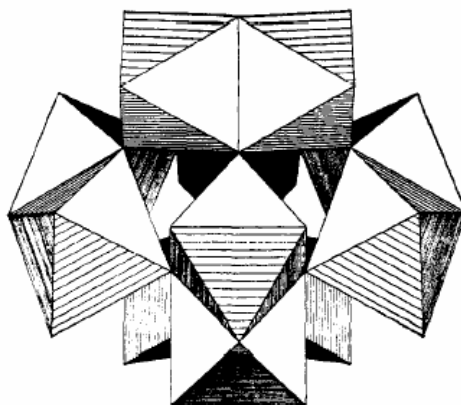
Figure 5: The Dexter-Silverton structure of the $[XM_{12}O_{42}]^{x-12}$ anion [10]

1.2.5 Transition metal substituted Sandwich type Polyoxometalates

In 1973 Tourne *et al* reported a 'sandwich-type' polyoxometalate for the first time, which dawned new area in the polyoxometalate world [11]. The reported polyoxometalate was formulated as $[P_2Co_4(H_2O)_2W_{18}O_{68}]^{10-}$ and it was observed that the four cobalt atoms were actually sandwiched between two lacunary trivacant Keggin units composed of $(PW_9O_{34})^{9-}$, as can be seen in Figure 6, hence the name sandwich type polyoxometalates.
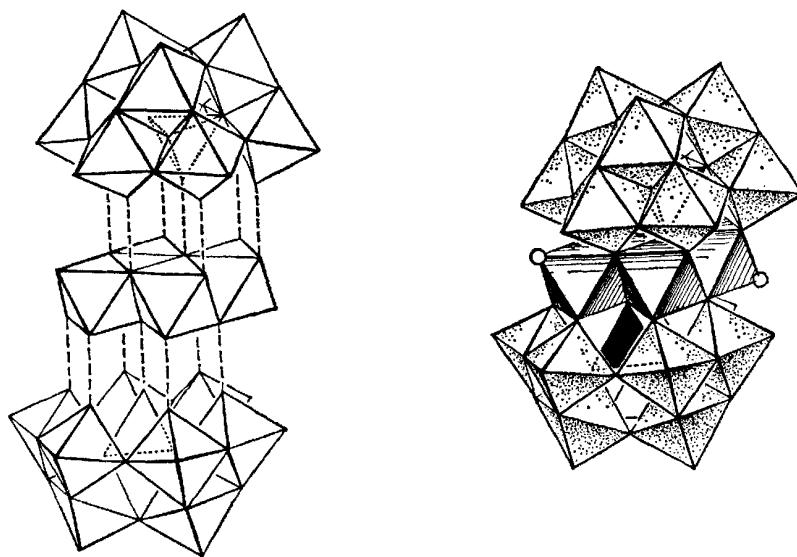
Figure 6: The $[P_2Co_4(H_2O)_2W_{18}O_{68}]^{10-}$ anion, where the four Co atoms occupy the central octahedra and the circles denote water molecules [11]

Soon after this polyoxometalate was reported; a variety of other sandwich type polyoxometalates with similar structure, but with different central atoms and transition metal ions followed the suite. Some prominent amongst them were, $[M_4(H_2O)_2(XW_9O_{34})_2]^{n-}$ (n = 12, X = Ge^{IV}, Si^{IV}, M = Mn^{2+}, Cu^{2+}, Zn^{2+}, Cd^{2+}; n = 10, X = P^V, As^V, M = Mn^{2+}, Co^{2+}, Ni^{2+}, Cu^{2+}, Zn^{2+}, Cd^{2+}; n = 6, X = P^V, As^V, M = Fe^{3+}; n = 14, X = Ga^{III}, M = Cu^{2+}, Zn^{2+}) [12-32]. The central atom in all these sandwich type polyoxometalates assumes a tetrahedral geometry.

Similar to these sandwich type polyoxometalates, some other structurally different sandwich type polyoxometalates were also reported, as shall be seen further. The fundamental difference in these polyoxometalates and the above sandwich type polyoxometalates was that, here the geometry of the central atom was pyramidal. Additionally, in these polyoxometalates either three or four transition metal ions could be sandwiched between the two lacunary trivacant Keggin units, depending on the central atoms and the transition metal atoms. The structures of these two kinds of polyoxometalates are shown in Figure 7. Some examples of three transition metal ions sandwiched between two lacunary trivacant Keggin units are, $[M_3(H_2O)_3(XW_9O_{33})_2]^{n-}$ (n = 12, X = As^{III}, Sb^{III}, M = Mn^{2+}, Co^{2+}, Ni^{2+}, Cu^{2+}, Zn^{2+}; n = 10, X = Se^{IV}, Te^{IV}, M = Cu^{2+}) and $[(VO)_3(XW_9O_{33})_2]^{n-}$; n = 12, X = As^{III}, Sb^{III}, Bi^{III}; n = 11, X = As^{III} [33-40]. Further, few examples of four transition metal ions sandwiched between two lacunary trivacant Keggin units are $([M_2(H_2O)_6(WO_2)_2(SbW_9O_{33})_2]^{(14-2n)-}$ (M^{n+} = Fe^{3+}, Co^{2+}, Mn^{2+}, Ni^{2+}), $([M_2(H_2O)_6(WO_2)_2(BiW_9O_{33})_2]^{(14-2n)-}$ (M^{n+} = Fe^{3+}, Co^{2+}, Ni^{2+}, Cu^{2+}, Zn^{2+}), $[(VO(H_2O)_2)_2(WO_2)_2(BiW_9O_{33})_2]^{10-}$, $[Sn_{1.5}(WO_2(OH))_{0.5}(WO_2)_2(XW_9O_{33})_2]^{10.5-}$ (X = Sb^{III}, Bi^{III}), $[M_3(H_2O)_8(WO_2)(TeW_9O_{33})_2]^{8-}$ (M = Ni^{2+}, Co^{2+}), $[(Zn(H_2O)_3)_2(WO_2)_{1.5}(Zn(H_2O)_2)_{0.5}(TeW_9O_{33})_2]^{8-}$, $[(VO(H_2O)_2)_{1.5}(WO(H_2O)_2)_{0.5}(WO_2)_{0.5}(VO(H_2O))_{1.5}(TeW_9O_{33})_2]^{7-}$ and $[M_4(H_2O)_{10}(XW_9O_{33})_2]^{n-}$ (n = 6, X = As^{III} and Sb^{III}, M = Fe^{3+} and Cr^{3+}; n = 4, X = Se^{IV}, Te^{IV}, M = Fe^{3+} and Cr^{3+}; n = 8, X = Se^{IV}, Te^{IV}, M = Mn^{2+}, Co^{2+}, Ni^{2+}, Zn^{2+}, Cd^{2+} and Hg^{2+}) [40-45].
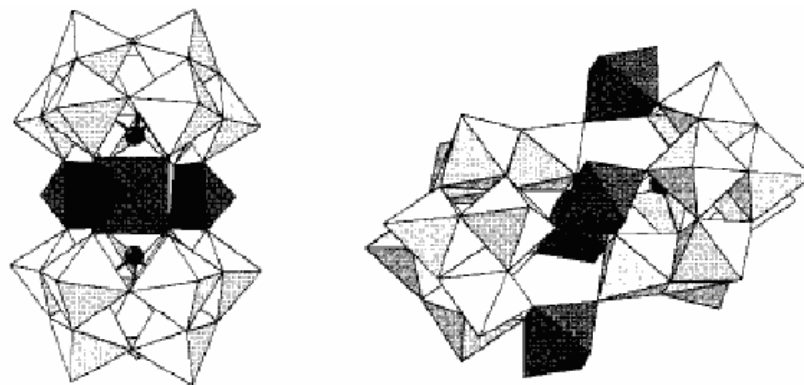
Figure 7: Structure of sandwich type polyoxometalates with three (left) and four (right) transition metal atoms sandwiched by two lacunary trivacant Keggin units, with pyramidal central atoms (seen as black circles, in the lacunary trivacant Keggin unit). The black polyhedrons represent the transition metal polyhedrons, which are square pyramidal in the case of 'left', while octahedral in the case of 'right' [34]

1.2.6 Zinc and Cobalt based Sandwich type Polyoxometalates

In 1991 Tourne *et al* reported zinc and cobalt central atoms based sandwich type polyoxotungstates, using common chemicals and simpler reaction conditions, with the general formula $[WM_3(H_2O)_2(MW_9O_{34})_2]^{12-}$, where M = Zn^{2+}, Co^{2+} [46]. The structure of these two sandwich type polyoxoanions was similar to the structure, seen in Figure 6. However, here in the central belt of transition metal atoms, one of the inner side transition metal atoms is replaced by a tungsten atom. The other three atoms, as well as the two central atoms above and below are zinc or cobalt atoms. Thus total three kinds of zinc/cobalt atoms are present in these polyoxoanions, first is the central atoms, second is the inner side atom of the central belt and thirdly the outer side atoms of the central belt, surrounded by a labile water molecule on one side each (please see Figure 6).

Although the structure appears to be very complicated, the synthesis is relatively very simple. The experimental procedure follows as, dropwise addition of zinc or cobalt nitrate solution to a hot solution of sodium tungstate (temperature maintained at 90-95 °C). Prior to the addition of the nitrate solution, appropriate amount of concentrated nitric acid is added to the sodium tungstate solution under stirring, to adjust the pH. Once the addition of nitrate solution is over, the mixture is transferred to a dish and left covered for crystallization of the desired polyoxometalate

21

to take place. It can be noted that he syntheses of all the other sandwich type polyoxometalates normally follow a two step procedure, the first is synthesis of the lacunary trivacant Keggin unit and the next step is synthesis of the desired polyoxoanion, by treating this lacunary trivacant Keggin unit with the appropriate transition metal salt solution.

Interestingly, in the case of these zinc and cobalt containing sandwich type polyoxotungstates, the outer side zinc or cobalt atoms in the central belt, that are attached to labile water molecules can be relatively easily and selectively knocked out, without affecting the original structure polyoxoanion. Thus a variety of transition metal ions can be introduced in the polyoxoanion frame work depending on the choice or requirement. The substituting transition metal atoms reported in the case of zinc polyoxoanion are Co^{2+}, Mn^{2+}, Mn^{3+}, Ni^{2+}, Cu^{2+}, Fe^{2+}, Fe^{3+}, VO^{2+}, Pd^{2+} and Pt^{2+}, while in the case of cobalt polyoxoanion are Zn^{2+}, Mn^{2+}, Cu^{2+} and Ni^{2+}. In the case of former, even Ru^{3+} and Rh^{3+} have been reported to substitute the zinc atoms by other groups in later reports [47, 48]. In the case of zinc polyoxoanion, even the third zinc atom in the central belt can be substituted by increase of the reaction times and/or the concentration of the transition metal salt solutions. Thus, trisubstituted derivatives of the zinc polyoxoanions with Co^{2+}, Mn^{2+}, Mn^{3+}, Ni^{2+}, Cu^{2+} and Fe^{3+} were also reported by the original authors.

1.3 Historical Background

The history of polyoxometalates dates back to 1826 when Berzelius discovered the first heteropoly salt, ammonium 12-molybdophosphate [49]. Later on in 1848, Svanberg and Struve introduced this compound in analytical chemistry as the basis for the determination of phosphorus that has been widely used since [50]. By 1908, approximately 750 heteropoly compounds had been reported. However, the structure of polyoxometalates had remained a mystery for more than a century since their discovery. Werner, Miolati, Rosenheim and Pauling proposed structures based on sharing metal-oxygen polyhedra [51-54]. It was Keggin who in 1933 solved the structure of the most important 12:1 type of heteropoly anion by a powder diffraction study of $H_3[PW_{12}O_{40}]$ [7]. This structure, now named after its discoverer, contained 12 WO_6 octahedra linked by edge and corner sharing, with the heteroatom occupying a tetrahedral hole in the centre. In 1948, Evans determined the structure of another widespread type - the Anderson's 6:1 heteropoly anion - by single-crystal X-ray

analysis of $[Te^{6+}Mo_6O_{24}]^{6-}$ salts; this structure is now referred as the Anderson-Evan's structure [9]. In 1953, Dawson reported the next new structure (now frequently referred as the Well-Dawson's) of an 18:2 (or 9:1) heteropoly anion $[P_2W_{18}O_{62}]^{6-}$ [8]. This structure was shown to be closely related to the Keggin structure. Next, in 1968, Dexter and Silverton reported the X-ray structure of $[Ce^{4+}Mo_{12}O_{42}]^{8-}$ and showed the large Ce heteroatom to be in a CeO_{12} central icosahedron [10]. By early 1970s, the chemistry of polyoxometalates had been greatly expanded. This period is associated with extensive work of many groups all over the world and in the 1980-90s; the number of groups involved in the field further increased with expanding applications of polyoxometalates in various areas.

By 1995, the X-ray structure of approximately 180 polyoxometalates had been reported [3]. Among them, salts of giant heteropoly anions such as $[La_{16}As_{12}W_{148}O_{524}]^{76-}$ (ion mass *ca.* 40000, diameter 40 Å) and others were prepared and characterized by Muller *et al* [4]. The application of modern characterization techniques had led to much better understanding of the structural principles of polyoxometalates and their properties. However, there is still plenty of scope for further work in this field, as many fundamental questions regarding the structural principles, mechanisms of synthesis and reactivity of polyoxometalates remain unanswered.

1.4 Nomenclature in Heteropolyoxometalates

A systematic nomenclature of polyoxometalates has been developed [2, 55]. It uses a labeling system for the metal atoms and, in some cases, for the oxygen atoms to avoid ambiguity. The resulting names, however, are too long and complicated; these are practically never used for routine purposes.

In catalytic applications, only a relatively small number of well-known types of polyoxometalates have been involved so far, largely limited to the Keggin compounds and their derivatives. Usually, simplified conventional nomenclature, sometimes even trivial names, are sufficient for reporting and retrieving information in the field. Here we adopt the current nomenclature that treats polyoxometalates (also referred to as heteropoly anions, heteropoly compounds, polyoxoanions or polyanions) as quasi coordination complexes [2]. The heteroatom, if present is considered as the central atom of the complex and the addenda as the ligands. In the formulae of heteropoly anions, the heteroatoms are placed before the heteroatoms; the

heteropoly anion is placed in square brackets and thus separated from the counter cations as illustrated by the following examples:

$[SiW_{12}O_{40}]^{4-}$	12-tungstosilicate or dodecatungstosilicate
$H_3[PMo_{12}O_{40}]$	12-molybdophosphoric acid
$Na_5[PMo_{10}V_2O_{40}]$	Sodium decamolybdodivanabdophosphate

For simplicity, the counter cations and the charge of polyanion and even the oxygen atoms may be omitted; for example, $Na_6[P_2Mo_{18}O_{62}]$ may be abbreviated to $\{P_2Mo_{18}O_{62}\}$ or P_2Mo_{18}.

1.5 Crystal Structure of Keggin type Polyoxometalates

1.5.1 Primary structure

The heteropoly acids in the solid state are ionic crystals (sometimes amorphous) which consist of large polyanions that are linked together. This polyanionic Keggin structure specially the α-type has T_d symmetry and consists of a centrally located XO_4 tetrahedron (X = central atom or central atom) surrounded by twelve edge and corner sharing MO_6 octahedra (M = addenda atom). The octahedra are arranged in four M_3O_{13} groups. Each group is formed by three octahedra sharing edges and having a common oxygen atom which is also shared with the central tetrahedron XO_4. The oxygen atoms in the Keggin structure are classified into four classes of symmetry equivalent oxygen atoms: $X-O_a-M$, $M-O_b-M$ ('inter' bridges between corner sharing octahedra), $M-O_c-M$ ('intra' bridges between edge sharing, i.e., within a M_3O_{13} set) and $M-O_d$ (the terminal oxygen atoms) where M is the addenda atom and X is the central atom. The anion contains twelve quasi-linear M-O-M linkages between the octahedra forming part of different M_3O_{13} triads twelve angular M-O-M bonds between the octahedra within a single triad, four X-O-M bonds where the triads are joined to the central atom and twelve terminal M=O bonds.

1.5.2 Secondary structure

The three dimensional arrangement consisting of the large polyanions, cations, water of crystallization and other molecules constitute the secondary structure of heteropoly compounds. Acid forms of heteropoly compounds in solid state, contain

counter cations or the protons which play an important role in the structure of the crystal, by linking the neighboring heteropoly anions. For e.g., protons of crystalline $H_3PW_{12}O_{40}.6H_2O$ are presented in hydrated species, $H_5O_2^+$, each of which links four neighboring heteropoly anions by hydrogen bonding to the terminal $W\text{-}O_d$ oxygen atoms and the polyanions are packed in a bcc structure. This is shown in the following Figure.

$$W = O \text{----} H$$
$$\searrow$$
$$O\text{--------}H\text{-------}O$$
$$W = O \text{----} H \nearrow \qquad\qquad \searrow H \text{----} O = W$$
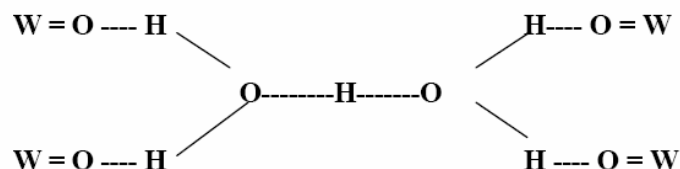
Secondary structures may also contain organic molecules for e.g., $H_4SiW_{12}O_{40}.9DMSO$ which contains nine molecules of DMSO in a unit cell where there are weak hydrogen bonds between methyl groups and oxygen atom of the heteropoly anions. Another interesting example is $PW_{12}O_{40}. [(C_5H_5N)_2H]_3$ is obtained by the reaction of anhydrous $H_3PW_{12}O_{40}$ with pyridine.

1.5.3 Tertiary structure

Structure of the solid heteropoly acid as assembled constitutes the tertiary component of the complex. The size of the particles, pore structure and distribution of protons in particles are the elements of the tertiary structure. The primary, secondary and tertiary structures are represented in Figure 8 [56].

$\oslash$: $H^+(H_2O)_n$, Cs^+, pyH^+, etc.
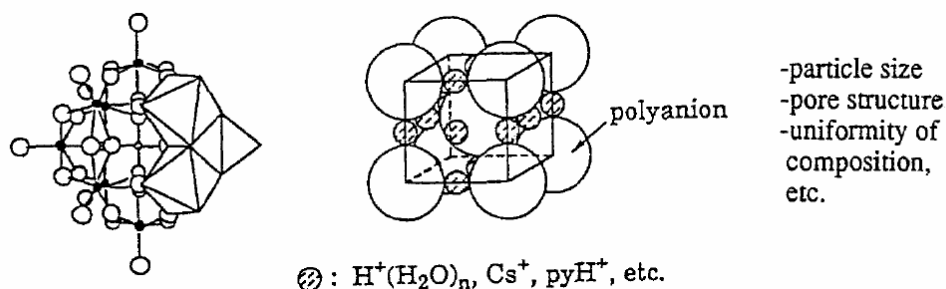
Figure 8: Primary, secondary and tertiary structure of $H_3[PW_{12}O_{40}]$ [56]

1.6 General Properties of Heteropoly Compounds

1.6.1 Solubility of heteropoly compounds

Free acids and most salts of heteropoly anions are extraordinarily soluble in water and are often very soluble in a wide range of organic solvents.

In water: Most free acids are generally extremely soluble (up to 85 % by weight of solution). In general, the heteropoly salts of small cations, including those of many heavy metals, are also very soluble. Heteropoly acids with large size counter cations are less soluble. Thus Cs^+, Ag^+, Tl^+, Hg^{2+}, Pb^{2+} and the larger alkaline earth metal salts are often insoluble. The NH_4^+, K^+ and Rb^+ salts of some of the important series of heteropoly anions are insoluble. Salts of heteropolymolybdate and heteropoly tungstate anions with cationic coordination complexes, alkaloids or organic amines are usually insoluble. Solubility of the heteropoly compounds in water must be attributed to very low lattice energies and solvation of cations. Solubility is governed by packing considerations in the crystals. The counter cations are fitted in between the large negative anions. When large cations like Rb^+, Cs^+ are present they allow stable packing in the large interstices, causing sufficient lowering of lattice energy to produce insolubility.

In organic solvents: Many of the free acids and a few of the salts are very soluble in organic solvents, especially if the latter contain oxygen. Ethers, alcohols and ketones (in that order) are generally the best solvents. Free acids are insoluble in non-oxygen solvents such as benzene, chloroform and carbon disulphide. The dehydrated salts sometimes dissolve readily in organic solvents; the hydrated salts are insoluble.

Many studies show that the typical Keggin heteropoly acids retain the structure of polyanion in aqueous solution, at least at a relatively high concentration [2]. This has been demonstrated by XRD, IR and Raman spectroscopy as well as by ^{17}O NMR [57]. However, in dilute ($<10^{-2}$ mol^{-1}) solutions, degradation of polyanion may occur.

Generally, the stability of 12-heteropoly anions towards hydrolysis in aqueous solution decreases in the order of addenda atoms [1, 58].

$$W (VI) > Mo (VI) > V (V)$$
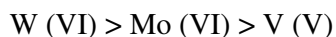
12-Heteropolymolybdates with different central atoms differ markedly in their stability to degradation in water solution in the following decreasing order [1, 58].

$$Si > Zr, Ti > Ge > P > As$$
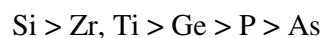
The crystalline free acids and salts of heteropolymolybdate and heteropoly tungstate anions are almost always highly hydrated. A given acid or salt will often form several solid hydrates. Most of the heteropolymolybdate series form isomorphous 30-hydrates.They melt in their own water of hydration between 40 and 100°C. In dry air they begin to lose water and they give up all thirty water molecules in vacuum over sulfuric acid.

1.6.2 Redox properties of heteropoly compounds

Some heteropoly compounds especially heteropolymolybdates are strong oxidizing agents and can be very readily changed to fairly stable, reduced heteropolymolybdates. These reduced species are called 'heteropoly blues'. Redox chemistry of polyoxometalates is extremely diverse [1, 2]. It has been subject of many studies and found many applications in chemical analysis as well as in selective oxidation reactions [58].

According to Pope, polyoxometalates, regarding their redox abilities, can be divided into two groups- 'mono-oxo' (type I) and 'cis-dioxo' (type II) [1, 5]. This classification is based on the number of terminal oxygen atoms attached to each addenda atom. Examples of type I polyanions are the Keggins, the Well-Dawsons and their derivatives that have one terminal M=O per each addenda atom. Type II polyanions can be represented by the Dexter-Silverton anion which has two terminal oxygen atoms in cis positions on each addenda atoms. In type I octahedra MO_6, the LUMO is a nonbonding metal-centered orbital, whereas for type II MO_6 octahedra, the LUMO is antibonding with respect to the terminal M=O bonds. Consequently, type I polyoxometalates are reduced easily and frequently reversibly to form mixed-valence species (heteropoly blues), which retain the structure of the parent oxidized anions. In contrast, type II polyoxometalates are reduced with more difficulty and irreversibly to complexes with yet unknown structures [1, 5]. For this reason, only

type I heteropoly compounds, by and large the Keggins, are of interest for oxidation catalysis.

The total number of accepted electrons on reduction of type I polyoxometalates can be quite high. As the anion structure retains upon this process, the additional negative charge is compensated for by protonation of the anion from solvent. Thus the reduction is frequently pH dependent, which is represented by the following equation

$$[XM_{12}^{6+}O_{40}]^{x-8} + p\ e^- + q\ H^+ \leftrightarrow H_q[XM_{12-p}^{6+}M_p^{5+}O_{40}]^{x+q-p-8}$$
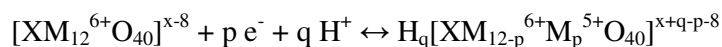
where $q \leq p$ [1, 2]. On reduction in acidic solution pH = 1, the Keggin tungsten anions, e.g., $[SiW_{12}O_{40}]^{4-}$, can add two electrons without protonation, i.e. the anion charge becoming -6. In a more neutral solution, the pH independent reduction can proceed up to the anion charge of -9. The reduced Well-Dawsons anions $\{X_2W_{18}O_{62}\}$ can bear up to -12 without protonation [2].

1.6.3 Acidic properties of heteropoly compounds

Heteropolytungstates and molybdates are strong acids. The acidity is generally determined by dissociation constants and the Hammet acidity function [59]. The free acids generally have several replaceable hydrogen ions. Protons are dissociated completely from the structure in aqueous solution. Since in heteropoly acids the negative charge of similar value is spread over much larger anions than those from mineral acid and the electrostatic interactions between proton and the anion is much less for heteropoly acids than for mineral acids. An additional important factor is possibly the dynamic delocalization ability of the charge or electron. The change in the electronic charge caused by de-protonation may be spread over the entire polyanion unit.

The strength and the number of acid centers as well as related properties of heteropoly acids can be controlled by the structure and composition of heteropoly anions, the extent of hydration, the type of support, the thermal treatment etc. Solid heteropoly acids such as $H_3PW_{12}O_{40}.xH_2O$ and $H_3PMo_{12}O_{40}.xH_2O$ are pure Brønsted acids and are stronger than conventional solid acids such as $SiO_2-Al_2O_3$ or H-X and H-Y zeolites [56, 60, 61]. Thermal desorption of basic molecules also reveals the

acidic properties. Pyridine adsorbed on $SiO_2\text{-}Al_2O_3$ is completely desorbed at 573 K. On the other hand, sorbed pyridine in $H_3PW_{12}O_{40}$ mostly remains at 573 K, indicating that $H_3PW_{12}O_{40}$ is a very strong acid. The acid strength can also be demonstrated by temperature programmed desorption (TPD) with NH_3. The general trend for acid strength among the common heteropoly acids is as follows [62].

$$H_3PW_{12}O_{40} > H_4SiW_{12}O_{40} \geq H_3PMo_{12}O_{40} > H_4SiMo_{12}O_{40}$$
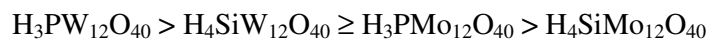
1.6.4 Thermal properties of heteropoly compounds

Thermal stability of the free acids of the heteropolymolybdates and heteropolytungstates is quite high and is of great importance for their use in heterogeneous catalysis [56, 63]. The stability is dependent on the nature of the central atom and addenda atom. Complexes containing phosphorous as the central atom are generally more stable than the compounds containing silicon as the central atom. Heteropoly compounds containing tungsten as the addenda atom are more stable than those with molybdenum atoms. The decomposition at high temperatures causes loss of acidity. The phosphomolybdic acid gets decomposed to the corresponding MoO_3 and P_2O_5 [63]. The Keggin structure is reconstructed when the complex is exposed to an atmosphere containing water vapour whereas in the case of less labile polyoxotungstates this kind of reconstruction is less likely.

Heteropoly acids are used as solid acid catalysts for vapour phase reactions at high temperatures. The substitution of transition metals in the anionic framework generally reduces the thermal stability in these complexes. The substitution of molybdenum in phosphomolybdic acid by addenda atoms such as vanadium reduces the thermal stability of the resulting phosphomolybdovanadates. The thermal stability reduces with the vanadium atoms in the polyanion framework. At higher temperature there is eviction of vanadium from the primary structural framework and the subsequent degradation into simple oxides i.e., MoO_3 and V_2O_5. The formation of such species is detected by X-ray diffraction analysis which clearly distinguishes between the heteropoly and the metal oxide phases. The structure of such complexes can be reconstructed on exposure to atmosphere of water vapour.

1.7 Catalytic Applications of Polyoxometalates

1.7.1 Polyoxometalates as catalysts in Industrial processes

Catalysis by heteropoly acids (HPA) and related compounds is a field of growing importance, attracting attention worldwide in which many novel and exciting developments are taking place, both in the areas of research and technology. Among numerous applications of heteropoly compounds, catalysis is by far the most important. Presently, over 80% of the patent applications concerning with polyoxometalates is related to catalysis [64]. First attempts to use polyoxometalates as catalysts can be traced back to the beginning of the twentieth century.

Heteropoly compounds have several advantages as catalysts, the most important being their multifunctionality and structural mobility. On one hand they have a very strong Brønsted acidity; on the other hand, they are efficient oxidants, exhibiting fast reversible multi-electron redox transformations under mild conditions. Their acid-base and redox properties can be varied over a wide range by changing the chemical composition. Solid heteropoly compounds possess a discrete ionic structure, comprising fairly mobile structural units - heteropoly anion and counter cations - unlike the network structure of zeolites or metal oxides. The structure is frequently preserved upon substitution or oxidation/reduction and manifests itself to exhibit extremely high proton mobility. On the top of that many heteropoly compounds have a very high solubility in polar solvents and fairly high thermal stability in the solid state.

Because of their unique properties heteropoly compounds are promising acid, redox and bifunctional (acid and redox) catalysts. The catalytic reactions can be performed in homogeneous as well as heterogeneous (gas-solid, liquid-solid or biphasic liquid-liquid) systems. Heteropoly compounds are frequently used as model systems for fundamental research providing unique opportunities for mechanistic studies on the molecular level. At the same time, they become increasingly important for applied catalysis.

In the late 1970-80s several new industrial chemical processes utilizing polyoxometalate catalysts were developed and commercialized in Japan [65, 66]. The first commercial process was the liquid phase hydration of propene to 2-propanol launched in 1972. It was followed by the vapour-phase oxidation of methacrolein to methacrylic aid in 1982, the liquid-phase hydration of isobutene for its separation from the butane-butene fraction in 1984, the biphasic polymerization of

tetrahydrofuran to polymeric diol in 1985, the hydration of n-butenes to 2-butanol in 1989 and other processes. More recently, in 1997, the direct oxidation of ethylene to acetic acid was industrialized by Showa Denko and, in 2001; the production of ethyl acetate using a heteropoly acid catalyst was launched by BP AMOCO.

1.7.2 Catalytic applications of the Keggin type Polyoxometalates in Oxidation reactions

As soon as one (or more) molybdenum atom(s) of phosphomolybdic acid are replaced by vanadium atom(s), a redox center gets generated in the Keggin unit, thereby making it an excellent redox catalyst. Over the years several reports have been published displaying the excellent catalytic activity of molybdovanadophosphoric acids with both aqueous hydrogen peroxide as well as molecular oxygen as the oxidants [67-76]. Thus it can be seen that these vanadium incorporated Keggin units are active for the oxidation of several types of substrates viz. alkene epoxidation, aromatic hydroxylation, cyclohexane oxidation to KA oil, adamantane hydroxylation, ketonization of active methylene groups, oxidation of cyclic ketones etc.

Not only in academia, but also vanadium substituted phosphomolybdic acid is the first and perhaps the only heteropoly anion based redox catalyst till date that has been used for any of the oxidation processes by chemical industries. It is used as a catalyst in the making of methacrylic acid from methacrolein with molecular oxygen as the oxidant. At a methacrolein conversion of 70-90%, the selectivity of methacrylic acid is between 80-85%, in the temperature range of 270-350 °C [77].

Similar to vanadium substituted phosphomolybdic acid, even the transition metal substituted polyoxotungstates (TMSP) are reported to be efficient catalysts with a variety of oxidants *viz.* molecular oxygen, hydrogen peroxide, ozone, TBHP, PhIO, $NaIO_4$, NaOCl etc. In these TMSP compounds, one or more of the tungsten atoms of the Keggin unit are replaced by transition metal ions from the first series like Mn^{2+}, Fe^{3+}, Co^{2+}, Ni^{2+}, Cu^{2+} etc, thus generating a redox center thereby, which catalyzes the oxidation reactions similar to the salen or porphyrin complexes of these transition metals [78-83].

1.7.3 Catalytic applications of the Sandwich type Polyoxometalates in Oxidation reactions

The structure and the synthesis of the zinc polyoxoanion along with its di- and tri-substituted derivatives were reported in 1991 by Tourne *et al* [46]. Within three years since then, Ronny Neumann and coworkers reported the catalytic applications of all these polyoxoanions for the epoxidation of alkenes and ketonization of alcohols [84, 85], especially with $[WZnMn_2(H_2O)_2(ZnW_9O_{34})_2]^{12-}$ as the catalyst. Very high turnover numbers with excellent selectivities for the desired product were reported in the presence of a phase transfer catalyst in a liquid-liquid biphasic solvent system, with aqueous hydrogen peroxide as the oxidant. Additionally, it was also claimed that these sandwich type polyoxometalates are not only oxidatively and thermally but also solvolytically more stable than the simple Keggin type polyoxoanions.

The detailed procedure followed the dissolution of the corresponding polyoxoanion in water in the first step. Subsequently, a phase transfer catalyst like Aliquat 336 (i.e. methyltrioctylammonium chloride) was dissolved in 1,2 dichloroethane. The two solutions were mixed in a separating funnel, where upon the polyoxoanion was transferred to dichloroethane layer under the virtue of Aliquat 336. The dichloroethane layer was collected and dried and to it was added known amount of alkene/alcohol and calculated amount of the oxidant. The reaction was carried out in the temperature range of 2-70 °C for a desired time interval or till the completion of the reaction. A variety of other reports by the same group in the years to follow showed the versatility of the system and the increasing scope of polyoxometalates as catalysts in oxidation reactions with hydrogen peroxide and molecular oxygen, as well as other oxidants [47, 48, 86-98].

Amongst other Sandwich type polyoxometalates, Hill's group has reported $[Co_4P_2W_{18}O_{68}]^{10-}$ as well as $[Fe_3P_2W_{18}O_{68}]^{9-}$ as redox catalysts with molecular oxygen as the oxidant for the epoxidation of alkenes and autoxidation of aldehydes respectively [99, 100].

1.7.4 Catalytic applications of the Anderson type Polyoxometalates in Oxidation reactions

There is only one report in the literature till date, where an Anderson type polyoxometalate $[IMo_6O_{24}]^{5-}$ has been used a catalyst for the oxidation of vicinal diols with molecular oxygen as the oxidant [101]. Thus, the major application of this type of polyoxometalates seems to be; as catalyst precursors for making different varieties of mixed metal oxides, as shall be seen in Chapter 5 of this thesis.

1.8 Heterogenization of Polyoxometalates

The diversity of research fields connected to the chemistry of polyoxometalates is significant and includes their application in many areas, including structural chemistry, analytical chemistry, surface chemistry, medicine, electrochemistry and photochemistry [102]. However, one of the most extensively studied applications of polyoxometalates has been in the area of catalysis, where their use as both Brønsted acid catalysts and oxidation catalysts has been going on since the late 1970's. A basic premise behind the use of polyoxometalates in oxidation chemistry is the fact that polyoxometalates are oxidatively stable. This leads to the conclusion that for practical purposes polyoxometalates would have distinct advantages over widely investigated organometallic compounds that are vulnerable to decomposition due to oxidation of the ligand bound to the metal center.

Along with the development of concepts, synthetic techniques and mechanistic understanding of the use of polyoxometalates as efficient oxidation catalysts, future practical application of polyoxometalate oxidation catalysis will also require methods for catalyst 'engineering' to aid in catalyst recovery and recycle. The basic approach is to immobilize a catalyst with proven catalytic properties onto a solid support leading to a catalytic system that may be filtered and reused. Such approaches include concepts such as simple use of catalysts as insoluble bulk material, impregnation of a catalyst onto a solid and usually inert matrix and attachment through covalent or ionic bonds of a catalyst to a support. These approaches or strategies are described in details in further paragraphs.

The strategy followed by Yamaguchi and Mizuno was usage of a solvent that won't dissolve the polyoxometalate under reaction conditions. Thus they used $[(n-C_4H_9)_4N]_4H[SiW_{11}Ru^{III}(H_2O)O_{39}].2H_2O$ as the catalyst and used isobutyl acetate, trifluorotoluene, 1,2dichloroethane and tert-butyl acetate as solvents for the oxidation

of a variety of organic substrates with molecular oxygen, *viz.* adamantane, cyclohexane and cyclooctane to name a few [103]. Earlier in 2001, Zuwei *et al* reported an interesting method of taking advantage of both homogeneous and heterogeneous nature of catalysts. Thus, the catalyst $[C_5H_5NC_{16}H_{33}]_3[PO_4(WO_3)_4]$ was used for the epoxidation of propylene with *aq.* H_2O_2 as the oxidant and 2-ethylanthraquinone as the co-reductant, with aqueous/oil biphasic solvent system. The catalyst was observed to be heterogeneous in oil phase before the addition of H_2O_2 and was homogeneous in the same after the addition of H_2O_2 due to its transformation into a new species, *viz.* $[C_5H_5NC_{16}H_{33}]_3[PO_4[W(O)_2(O_2)]_4]$. Once all the H_2O_2 was consumed, the new species reverted back to the original one and again became heterogeneous in the oil layer. It could be noted that the reactant, product and co-reactant were always present in the oil layer, so the catalyst could be easily separated after the reaction and reused again [104]. In another example, Okun *et al* reported $[(Fe^{III}(OH_2)_2)_3(A-\alpha-PW_9O_{34})_2]^{9-}$ supported on cationic silica nanoparticles as a new material for selective aerobic oxidation reactions. This material was used for oxygenation of sulfides and autoxidation of aldehydes. The principle behind the binding of the polyoxoanions to the cationic silica nanoparticles was electrostatic force between the positively charged cationic silica nanoparticles on one side and negatively charged polyoxoanions on the other side [99].

In the preceding years, Ronny Neumann reported the modification of support of MCM-41 by amine functionalization and anchoring of $H_5PV_2Mo_{10}O_{40}$ and using this catalytic system for the aerobic oxidation of hydrocarbons, with isobutyraldehyde as sacrificial oxidant. Maintaining appropriate conditions, it was observed that there was not any leaching of catalyst and the catalyst could be easily separated and reused without much loss of activity [105]. In another report, the same author replaced the protonic/ sodium or potassium counter cations with tripodal polyammonium cations that made it insoluble in solvents, otherwise which dissolve these $[WZn_3(ZnW_9O_{34})_2]^{12-}$ based polyoxometalates. The polyoxometalates thus formed were reported for hydrogen peroxide mediated oxidation reactions of allylic alcohols [106]. In the following report, Neumann reported the use of silica tethered poly-ethylene-poly-propylene oxide as support for the polyoxoanions, in order to use the catalytic system in a heterogeneous fashion. Thus silicates containing combinations of hydrophilic poly ethylene oxide PEO, hydrophobic poly propylene oxide PPO and

cationic quaternary ammonium 'Q' groups were prepared. These silicates coupled with $[WZnMn_2(ZnW_9O_{34})_2]^{12-}$ based polyoxometalates led to active catalytic assemblies. Thus, heterogeneous catalysts with hydrogen peroxide as the oxidant, for the oxidative dehydrogenation of dihydroanthracene with improved activity and selectivity, as compared to the unsupported polyoxoanions, were obtained [107, 108].

1.9 Scope and Organization of the Thesis

1.9.1 Scope and Objective of the present work

As mentioned above, polyoxometalates constitutes an important class of materials and their catalytic applications, both as acid catalysts on one side and as redox catalysts on the other side are truly very versatile. Of these two major classes of reactions we will be chiefly concentrating on redox reactions. This is because; selective oxidation reactions are one of the most encountered ones in academia and industry. All the oxidation products of all such reactions find lot of applications in various areas. Millions of tons of these products are produced annually and find applications in all areas of chemical industries ranging from pharmaceutical to large scale commodities.

Currently most of the oxidation processes involve the common use of stoichiometric oxidants resulting in tedious work up procedures at the end of reaction processes. Alternatively, they also lead to the formation of large amount of chromium, manganese and other toxic salts as by-products. Thus developing a process that will use environment friendly oxidants like molecular oxygen or hydrogen peroxide is highly desirable. However, it is known that both these eco friendly oxidants generally do not show any direct activity towards the organic substrates. Thus the important challenge involved here is make use of catalysts that will make these oxidants react with the organic substrates at ambient conditions.

Currently there are various transition metal ions based catalyst systems that are known to activate molecular oxygen or hydrogen peroxide. However, most of them are of metal-organic ligand origin like metal-salen complexes or metal-porphyrin complexes. The problem with these systems is that the organic part of the catalyst is vulnerable to oxidation itself, thus the further activity is lost. In order to overcome this problem, various strategies have been adopted *viz.* polyfluorination of the porphyrin ligand etc. An alternative to the process is use of robust molecules like polyoxometalates, substituted by transition metals or otherwise. The advantages of

polyoxometalates are that they are easy to synthesize as compared to zeolites or molecular sieves and they are compatible with dioxygen and hydrogen peroxide.

Although the polyoxometalates are gaining popularity as catalysts for oxidation reactions, in most of the cases they are used as catalysts in a homogeneous fashion. Since the separation of catalyst from the product mixture involves costly and time staking procedures, it is always preferred to make the use of any catalyst in heterogeneous manner. Similarly, not much work has been done on mechanism elucidation and investigation of the active intermediates responsible for the oxidation process. Albeit there are some reports on the mechanistic aspects, there is some ambiguity in the literature when it comes to the exact nature of the active intermediates and overall reaction mechanism. Thus a detailed study in which all the shortcomings seen above could be overcome is certainly desired.

1.9.2 Organization of the Thesis

The thesis is divided into six chapters which includes a general introduction (Chapter 1).

Chapter 2

Chapter 2 describes the synthesis and characterization of manganese and zinc containing sandwich type polyoxotungstates with antimony, bismuth and tellurium as the heteroatoms and the applications of the same towards the epoxidation of a variety of olefins is described further. The in-depth studies were carried out to investigate the exact role of manganese ions and tungsten octahedrons with hydrogen peroxide as the oxidant. Attempts have also been made to study the active intermediate and possible mechanism of the reactions by UV-visible and FT-IR and also towards the recycling of the catalyst. Further, the catalyst system is extrapolated for the ketonization a variety of secondary alcohols as well as allylic alcohols.

Chapter 3

Chapter 3 describes the synthesis and characterization of neat as well as anchored vanadium substituted phosphomolybdic acids. The anchoring of heteropoly acids was carried on amine functionalization of SBA-15. The details of synthesizing SBA-15 and its amine functionalization, followed by characterization of the same by ICP, UV-visible, N_2 sorption, SEM, XRD, FT-IR and ^{31}P-NMR is mentioned. After

anchoring, sufficient discussion is provided to show the presence of the heteropoly acids inside the pores of SBA-15. A detailed comparison has been done between the activities shown by neat as well as the anchored vanadium substituted phosphomolybdic acids with both, hydrogen peroxide and TBHP as the oxidants. For the anchored heteropoly acids, leaching test and recycling studies are also described as a part of the study.

Chapter 4

Chapter 4 describes the activity of simple and vanadium substituted phosphomolybdic acids supported on titania or zirconia towards the epoxidation of a variety of olefins. Details for the preparation of titania and zirconia and the wet impregnation of heteropoly acids on the same are briefly discussed. The supported heteropoly acids are characterized by powder XRD, solid state UV-visible and FTIR studies. Further, the use of organic solvent extracted TBHP as the oxidant and hydrophobic volatile liquids as the solvents in the epoxidation studies is justified. Synergistic effect observed between titania and vanadium substituted phosphomolybdic acids is also discussed.

Chapter 5

Chapter 5 describes the selective oxidation of ethane to ethylene and acetic acid over molybdenum-vanadium mixed metal oxides as catalyst. Initially the background and the scope of this work are discussed. This is followed by introduction to fixed bed vapor phase reactors. The experimental details, including hydrothermal synthesis of mixed metal oxides at various pH's, pretreatment of catalysts, precautions followed, step by step reaction procedure and characterization of the catalysts and the reaction system by ICP, EDAX, XRD, UV-visible, Raman, EPR and SEM is thoroughly discussed. The best catalyst for the selective oxidation of ethane to ethylene and acetic acid is also subjected to some further studies. These studies are to observe the effect of change in temperature, pressure and flow rate of reactants on the same reaction. The possible reaction mechanism is also described further.

Chapter 6

Chapter 6 summarizes the overall conclusion from the work presented in this thesis.

References

1. P. Souchay, Ions Mineraux Condenses; Paris, 1969

2. M. T. Pope, Heteropoly and Isopoly Oxometalates ; Springer: Berlin, 1983

3. G. M. Maksimov, Russ. Chem. Rev. 64 (1995) 445

4. A. Muller, W. Plass, E. Krickemeyer, S. Dillinger, H. Bogge, A. Armatage, A. Proust, C. Beugholt, U. Bergmann, Angew. Chem. Int. Ed. Engl. 33 (1994) 849

5. M. T. Pope, A. M. Muller, Angew. Chem. Int. Ed. Engl. 30 (1991) 34

6. W. N. Lipscomb, Inorg. Chem. 4 (1965) 132

7. J. F. Keggin, Proc. Roy. Soc. London A 144 (1934) 75

8. B. Dawson, Acta Crystallogr. 6 (1953) 113

9. H. T. Evans, Jr. J. Am. Chem. Soc. 70 (1948) 1291

10. D. D. Dexter, J. V. Silverton, J. Am. Chem. Soc. 90 (1968) 3589

11. T. J. R. Weakley, H. T. E. Jun, J. S. Showell, G. F. Tourne and C. M. Tourne, J. Chem. Soc. Chem. Comm. 1973, 139

12. R. G. Finke, M. W. Droege, J. R. Hutchinson, O. Gansow, J. Am. Chem. Soc. 103 (1981) 1587

13. R. G. Finke, M. W. Droege, Inorg. Chem. 22 (1983) 1006

14. H. T. Evans, C. M. Tourne, G. F. Tourne, T. J. R. Weakley, J. Chem. Soc., Dalton Trans. 1986, 2699

15. R. G. Finke, M. W. Droege, P. J.Domaille, Inorg. Chem. 26 (1987) 3886

16. S. H. Wasfi, A. L. Rheingold, G. F. Kokoszka, A. F. Goldstein, Inorg. Chem. 26 (1987) 2934

17. T. J. R. Weakley, R. G. Finke, Inorg. Chem. 29 (1990) 1235

18. C. J. Gomez Garcia, E. Coronado, J. J. Borras-Almenar, Inorg. Chem. 31 (1992) 1667

19. N. Casan-Pastor, J. Bas-Serra, E. Coronado, G. Pourroy, L. C. W. Baker, J. Am. Chem. Soc. 114 (1992) 10380

20. C. J. Gomez-Garcia, E. Coronado, P. Gomez- Romero, N. Casan-Pastor, Inorg. Chem. 32 (1993) 3378

21. C. J. Gomez- Garcia, J. J. Borras Almenar, E. Coronado, L. Ouahab, Inorg. Chem. 33 (1994) 4016

22. X.-Y. Zhang, G. B. Jameson, C. J. O'Connor, M. T. Pope, Polyhedron 15 (1996) 917

23. X. Zhang, Q. Chen, D. C. Duncan, C. Campana, C. L. Hill, Inorg. Chem. 36 (1997) 4208

24. X. Zhang, Q. Chen, D. C. Duncan, R. J. Lachicotte, C. L. Hill, Inorg. Chem. 36 (1997) 4381

25. J. L. Clemente-Juan, E. Coronado, J. R. Gala'n-Mascaros, C. J. Gomez-Garcia, Inorg. Chem. 38 (1999) 55

26. L.-H. Bi, E.-B. Wang, J. Peng, R.-D. Huang, L. Xu, C.-W. Hu, Inorg. Chem. 39 (2000) 671

27. L.-H. Bi, R.-D. Huang, J. Peng, E.-B. Wang, Y.-H. Wang, C.-W. Hu, J. Chem. Soc. Dalton Trans. 2001, 121

28. U. Kortz, S. Isber, M. H. Dickman, D. Ravot, Inorg. Chem. 39 (2000) 2915

29. E. M. Limanski, M. Piepenbrink, E. Droste, K. Burgemeister, B. Krebs, J. Clust. Sci. 13 (2002) 369

30. C. Rosu, D. C. Crans, T. J. R. Weakley, Polyhedron 21 (2002) 959

31. U. Kortz, S. Nellutla, A. C. Stowe, N. S. Dalal, U. Rauwald, W. Danquah, D. Ravot, Inorg. Chem. 43 (2004) 2308

32. D. Drewes, E. M. Limanski, B. Krebs, Eur. J. Inorg. Chem. 2005, 1542

33. F. Robert, M. Leyrie, G. Herve, Acta Crystal. B-38 (1982) 358

34. M. Bosing, A. Noh, I. Loose, B. Krebs, J. Am. Chem. Soc. 120 (1998) 7252

35. U. Kortz, N. K. Al-Kassem, M. G. Savelieff, N. A. Al Kadi, M. Sadakane, Inorg. Chem. 40 (2001) 4742

36. B. Botar, T. Yamase, E. Ishikawa, Inorg. Chem. Comm. 4 (2001) 551

37. T. Yamase, B. Botar, E. Ishikawa, K. Fukaya, Chem. Lett. 2001, 56

38. P. Mialane, J. Marrot, E. Riviere, J. Nebout, G. Herve, Inorg. Chem. 40 (2001) 44

39. U. Kortz, S. Nellutla, A. C. Stowe, N. S. Dalal, J. van Tol, B. S. Bassil, Inorg. Chem. 43 (2004) 144

40. D. Drewes, E. M. Limanski, M. Piepenbrink, B. Krebs, Z. Anorg. Allg. Chem. 630 (2004) 58

41. M. Bosing, I. Loose, H. Pohlmann, B. Krebs, Chem. Eur. J. 3 (1997) 1232

42. Loose, E. Droste, M. Bosing, H. Pohlmann, M. H. Dickman, C. Rosuu, M. T. Pope, B. Krebs, Inorg. Chem. 38 (1999) 2688

43. B. Krebs, E. Droste, M. Piepenbrink, G. Vollmer, C. R. Acad. Sci. Paris, Ser. II c 3 (2000) 205

44. U. Kortz, M. G. Savelieff, B. S. Bassil, B. Keita, L. Nadjo, Inorg. Chem. 41 (2002) 783

45. E. M. Limanski, D. Drewes, E. Droste, R. Bohner, B. Krebs, J. Mol. Struct. 656 (2003) 17

46. C. F. Tourne, G. F. Tourne, F. Zonnevijlle, J. Chem. Soc. Dalton Trans. 1991, 143

47. R. Neumann, A. M. Khenkin, J. Mol. Catal. A. 114 (1996) 169

48. R. Neumann, M. Dahan, J. Am. Chem. Soc. 120 (1998) 11969

49. J. J. Berzelius, Poggendorffs Ann. Phys. Chem. 1826, 6, 369, 380

50. L. Svanberg, H. Struve, J. Pract. Chem. 61 (1854) 449

51. A. Werner, Ber. Dtsch. Chem. Ges. 40 (1907) 40

52. A. Miolati, R. Pizzighelli, J. Prakt. Chem. 77 (1908) 417

53. A. Rosenheim, Handbuch der Anorganischen Chemie; Abbeg, R., Auerbach, F., Eds; Hirzel Verlag: Leipzich, 1921; Vol. 4. Part 1, ii, pp. 997-1064

54. L. Pauling, J. Am. Chem. Soc. 51 (1929) 2868

55. Y. Jeannin, M. Fournier, Pure Appl. Chem. 59 (1987) 1529

56. T. Okuhara, N. Mizuno, M. Misono, Adv. Catal. 41 (1996) 113

57. I. V. Kozhevnikov, K. I. Matveev, Russ. Chem. Rev. 51 (1982) 1075

58. G. A. Tsigdinos, Top. Curr. Chem. 76 (1978) 1

59. I. V. Kozhevnikov, Russ. Chem. Rev. 56 (1987) 811

60. M. Misono, Catal. Rev. Sci. Eng. 29 (1987) 269

61. M. Misono, Catal. Rev. Sci. Eng. 30 (1988) 339

62. Y. Izumi, R. Hasebe, K. Urabe, J. Catal. 84 (1983) 402

63. J. B. Moffat, Metal-Oxygen Clusters. The Surface and Catalytic Properties of Heteropoly Oxometalates; Kluwer: New York, 2001

64. D. E. Katsoulis, Chem. Rev. 98 (1998) 359

65. M. Misono, N. Nojiri, Appl. Catal. 64 (1990) 1

66. Y. Izumi, K. Urabe, M. Onaka, Zeolite, Clay and Heteropoly Acid in Organic Reactions ; Kodansha/VCH: Tokyo, 1992

67. S. Yamada, A. Sakaguchi, Y. Ishii, J. Mol. Catal. A. 262 (2007) 48

68. M. Khenkin, R. Neumann, Angew. Chem. 2000, 112

69. S. Shinachi, M. Matsushita, K. Yamaguchi, N. Mizuno, J. Cat 233 (2005) 81

70. K. Nomiya, K. Yagishita, Y. Nemoto, Tada-aki Kamataki, J. Mol. Catal. A 126 (1997) 43

71. N. A. Alekar, V. Indira, S. B. Halligudi, D. Srinivas, S. Gopinathan, C. Gopinathan, J. Mol. Catal. A. 164 (2000) 181

72. K. Nomiya, S. Matsuoka, T. Hasegawa, Y. Nemoto, J. Mol. Catal. A. 156 (2000) 143

73. T. Ilkenhans, B. Herzog, T. Braun, R. Schlogl, J. Catal. 153 (1995) 275

74. M. Akimoto, K. Shima, H. Ikeda, E. Echigoya, J. Catal. 86 (1984) 173

75. M. Misono, N. Mizuno, K. Inumaru, G. Koyano, Lu Xin-Hong, Stud. Surf. Sci. Catal. 110 (1997) 35

76. K. Nomiya, Y. Nemoto, T. Hasegawa, S. Matsuoka, J. Mol. Catal. A: Chem. 152 (2000) 55

77. Catalysis by Polyoxometalates, Ivan Kozhevnikov, Wiley

78. Y. Liu, K. Murata, M. Inaba, Catal. Comm. 6 (2005) 679

79. M. M. Q. Simoes, C. M. M. Conceicao, J. A. F. Gamelas, P. M. D. N. Domingues, A. M. V. Cavaleiro, J. A. S. Cavaleiro, A. J. V. Ferrer-Correia, R. A. W. Johnstone, J. Mol. Catal. A. 144 (1999) 461

80. J. A. F. Gamelas, A. R. Gaspar, D. V. Evtuguin and C. P. Neto, App. Catal. A. 295 (2005) 134

81. D. Mansuy, J-F. Bartoli, P. Battioni, D. K. Lyon, R. G. Finke, J. Am. Chem. Soc. 113 (1991) 7222

82. Y. Nishiyama, Y. Nakagawa, N. Mizuno, Angew. Chem. Int. Ed. 40 (2001) 3639

83. N. Mizuno, C. Nozaki, I. Kiyoto, M. Misono, J. Am. Chem. Soc. 120 (1998) 9267

84. R. Neumann, M. Gara, J. Am. Chem. Soc. 116 (1994) 5509

85. R. Neumann, M. Gara, J. Am. Chem. Soc. 117 (1995) 5066

86. R. Neumann, D. Juwiler, Tetrahedron, 52 (1996) 8781

87. R. Neumann, A. M. Khenkin, Inorg. Chem. 34 (1995) 5753

88. R. Neumann, A. M. Khenkin, M. Dahan, Angew. Chem. Int. Ed. Engl. 34 (1995) 1587

89. R. Neumann, A. M. Khenkin, Chem. Comm. 1998, 1967

90. D. Sloboda-Rozner, P. L. Asters, R. Neumann, J. Am. Chem. Soc. 125 (2003) 5280

91. W. Adam, P. L. Asters, R. Neumann, C. R. Saha-Moller, D. Seebach, A. K. Beck, R. Zhang, J. Org. Chem. 68 (2003) 8222

92. W. Adam, P. L. Alsters, R. Neumann, C. R. Saha-Moller, D. Sloboda-Rozner, R. Zhang, J. Org. Chem. 68 (2003) 1721

93. P. T. Witte, P. L. Asters, W. Jary, R. Mullner, P. Pochlauer, D. Sloboda-Rozner, R. Neumann Org. Pro. Res. Dev. 8 (2004) 524

94. D. Sloboda-Rozner, P. Witte, P. L. Alsters, R. Neumann, Adv. Synth. Catal. 346 (2004) 339

95. P. T. Witte, S. R. Chowdhry, J. E. ten Elshof, D. Sloboda-Rozner, R. Neumann, P. L. Alsters, Chem. Comm. 2005, 1206

96. A. Haimov, G. Cohen, R. Neumann, J. Am. Chem. Soc. 126 (2004) 11762

97. R. Neumann, A. M. Khenkin, D. Juwiler, H. Miller, M. Gara, J. Mol. Catal. A. 117 (1997) 169

98. R. Ben-Daniel, L. Weiner, R. Neumann, J. Am. Chem. Soc. 124 (2002) 8788

99. N. M. Okun, T. M. Anderson, C. L. Hill, J. Am. Chem. Soc. 125 (2003) 3194

100. X. Zhang, K. Sasaki, C. L. Hill, J. Am. Chem. Soc. 118 (1996) 4809

101. A. M. Khenkin, R. Neumann, Adv. Synth. Catal. 344 (2002) 1017

102. C. L. Hill, Chem. Rev. 98 (1998) 1

103. K. Yamaguchi, N. Mizuno, New J. Chem. 26 (2002) 972

104. X. Zuwei, Z. Ning, S. Yu, L. Kunlan, Science. 292 (2001) 1139

105. A. M. Khenkin, R. Neumann, A. B. Sorokin, A. Tuel, Catal. Lett. 63 (1999) 189

106. M. V. Vasylyev, R. Neumann, J. Am. Chem. Soc. 126 (2004) 884

107. R. Neumann, M. Cohen, Angew. Chem. Int. Ed. Engl. 36 (1997) 1738

108. M. Cohen, R. Neumann, J. Mol. Catal. A. 146 (1999) 291

Chapter 2:

Selective Oxidation of alkenes and alcohols over [SbW$_9$O$_{33}$] based catalyst system with aq. H$_2$O$_2$

2.1 Introduction

Epoxidation of olefins is one of the most studied reactions in organic synthesis, as the epoxides are useful intermediates in the manufacturing of a variety of chemicals. Similarly, selective oxidation of alcohols to their carbonyls is also of paramount importance in organic synthesis. Generally all these oxidation reactions involve stoichiometric quantities of inorganic/organic oxidants [1], toxic or hazardous oxidizing agents [2-5]. Developing new catalysts that will utilize environmental friendly oxidants for these oxidation reactions, as an alternative to the stoichiometric oxidation processes still continues to be a subject of interest [6-9]. Many catalysts of metal-organic ligand origin (like metal-salen or metal-porphyrin complexes) are reported for epoxidation of alkenes and oxidation of alcohols, but the limitations with these catalysts are that the organic part of these catalysts itself is vulnerable to oxidation, thereby reducing its activity significantly. To overcome this problem various approaches have been employed like dispersion of transition metal ions on inert supports like zeolites, metal oxides, mesoporous materials and so on [10-14]. Alternatively polyoxotungstates based inorganic compounds have been reported in the recent years as efficient catalysts for selective oxidation reactions [15-19].

Amongst the various polyoxometalates based systems, the transition metal substituted polyoxometalates (TMSP) like vanadium substituted phosphomolybdic acid, or the transition metal containing sandwich type polyoxotungstates like $Na_{12}[WZnMn_2(ZnW_9O_{34})_2]$ were found to be robust catalysts for the selective epoxidation of alkenes as well as oxidation of alcohols. Both molecular oxygen and aqueous hydrogen peroxide were used as oxidants. The important advantage of polyoxotungstates is that, they are easy to synthesize as compared to zeolites or other molecular sieves, and are also compatible with aqueous hydrogen peroxide. While aerobic oxidation is certainly important, there are also certain advantages with H_2O_2 as the oxidants [20]. Hydrogen peroxide is preferred as an oxidant since it is cheap, environmental friendly and contains a high percentage of active oxygen. Further, with d^0 electronic configuration of tungsten (VI) and molybdenum (VI) species polyoxotungstates do not cause excessive catalytic dismutation of hydrogen peroxide, thus the later is fully available for the oxidation purpose [17].

Amongst the different types of polyoxometalates, manganese containing sandwich type polyoxometalates with bismuth, antimony or tellurium as the

heteroatoms reported by Bosing *et al* were found to highly efficient catalysts for the regioselective epoxidation of limonene [18]. In liquid-liquid biphasic systems these catalysts in conjunction with a methyl tricapryl ammonium chloride (PTC) displayed very high turn over numbers with *aq.* H_2O_2 as the oxidant, and were solvolytically and oxidatively stable. In the present chapter we have made an attempt to extend their work for the epoxidation of some other alkenes. We have also attempted the kinetic studies of the system as well as to explore the exact role of manganese, and the active intermediates that are responsible for the high activity.

During the re-investigation of the above catalytic systems, we were surprised to find that the tungsten octahedral clusters are in fact the active centers for the epoxidation of alkenes or oxidation of alcohols, irrespective of whichever transition metal or heteroatom that is present. We observed that the magnitude of limonene epoxidation with a manganese ions containing polyoxometalate *i.e.* $Na_{11}(NH_4)[Mn_3(H_2O)_3(SbW_9O_{33})_2]$ as well as with a manganese ions free polyoxometalate *i.e.* $K_{12}[Zn_3(H_2O)_3(SbW_9O_{33})_2].48H_2O$ was the same, and so was the activity of the capping agent $Na_9[SbW_9O_{33}].19.5H_2O$ itself. This shows that it is the tungstate species that are responsible for the catalytic activity, and not the manganese species as was believed in the original article.

Additionally, in the present studies 1,2-dichloroethane solvent was totally avoided and minimal amount of toluene was used whenever the substrate was a solid. Further, apart from alkenes, an attempt was made to extrapolate the activity of $Na_9[SbW_9O_{33}].19.5H_2O$ towards the oxidation of a variety of secondary and allylic alcohols, which also worked successfully, as shall be seen in the further sections.

2.2 Experimental

2.2.1 Materials

Sodium tungstate dihydrate, Sb_2O_3, $MnCl_2.4H_2O$ and $ZnCl_2$ were purchased from Loba Chemie Ltd, India. *Aq.* H_2O_2 (30 %) was purchased from Merck and exact strength at the time of usage was determined by iodometric titration. Substrates (both alkenes and alcohols) used were of highest purity purchased from Aldrich. Aliquat 336 (methyl tricapryl ammonium chloride) and chlorobenzene were obtained from S. D. fine chemicals India Ltd.

2.2.2 Catalyst synthesis

2.2.2.1 Synthesis of Na$_9$[SbW$_9$O$_{33}$].19.5H$_2$O

This compound was prepared by reaction of Na$_2$WO$_4$.2H$_2$O (40 g, 121 mmol) in boiling water (80 ml) and drop wise addition of Sb$_2$O$_3$ (1.96 g, 6.72 mmol) dissolved in concentrated HCl (12 M, 10 ml). The mixture was refluxed for 1 h and was allowed to cool slowly. Colorless crystals of Na$_9$[SbW$_9$O$_{33}$].19.5H$_2$O were formed after evaporation of one-third of the solution volume. Yield: 28.0 g (72 %). In a similar manner Na$_9$[BiW$_9$O$_{33}$] and Na$_8$[TeW$_9$O$_{33}$] were synthesized to perform some controlled reactions as shall be seen further.

2.2.2.2 Synthesis of Na$_{11}$(NH$_4$){[Mn(H$_2$O)]$_3$(SbW$_9$O$_{33}$)$_2$}.45H$_2$O

Na$_9$[SbW$_9$O$_{33}$].19.5H$_2$O (4 g, 1.4 mmol) was dissolved in water (8 ml) under gentle heating. To this pale yellow mixture was given slowly a solution of MnCl$_2$.4H$_2$O (0.414 g, 2.08 mmol) in water (10 mL), leading to a deep orange solution with pH 6-7. The mixture was refluxed for 1 h, and then NH$_4$NO$_3$ (0.673 g, 8.4 mmol) was added. After the mixture was cooled to ambient temperature, dark orange crystals of Na$_{11}$(NH$_4$){[Mn(H$_2$O)]$_3$(SbW$_9$O$_{33}$)$_2$}.45H$_2$O were obtained after several days. Yield: 2.6 g (63%). In a similar manner, Na$_{12}${[Cu(H$_2$O)]$_3$(SbW$_9$O$_{33}$)$_2$} and Na$_{12}${[Co(H$_2$O)]$_3$(SbW$_9$O$_{33}$)$_2$} were synthesized to perform some controlled reactions as shall be seen further.

2.2.2.3 Synthesis of K$_{12}${[Zn(H$_2$O)]$_3$(SbW$_9$O$_{33}$)$_2$}.46H$_2$O

A sample of ZnCl$_2$ (0.92 g, 6.7 mmol) was dissolved in 50 ml of H$_2$O and to it was added Na$_9$[SbW$_9$O$_{33}$].19.5H$_2$O (10.0 g, 4.1 mmol) dissolved in water (20 ml) was added drop wise. The solution was refluxed for 1 h and filtered after cooling (pH 6.6). The potassium salt of the heteropoly anion was isolated in high yield by precipitation of the above solution with solid KCl (15 g). This resulted in a white product, which was isolated and air-dried. Yield: 9.5 g (83%).

2.2.3 Characterization of the catalysts

The catalysts were subjected to elemental analysis and FT-IR for the confirmation of products formed. Elemental analysis of sodium, potassium, manganese, zinc, antimony, tellurium and bismuth was carried out by inductively

46

coupled plasma spectroscopy (ICP). The ICP was performed on Perkin Elmer Plasma Emission 1000 Spectrometer. Tungsten was estimated by gravimetric analysis using 8-hydroxyquinoline as the precipitating agent. The number of water molecules was determined by TG-DTA and were in agreement with the reported ones. The Thermal analysis was performed on a Seiko model instrument (TG DTA 32) and the thermograms recorded at a heating rate of 10 K min^{-1} from 303 to 873 K under N_2 atmosphere. FT-IR spectra were recorded on a Shimadzu FTIR 8201 PC instrument. The FT-IR spectra were recorded as KBr pellets.

2.2.4 Catalytic reactions

2.2.4.1 Preparation of catalyst stock solutions

[MTCA]$_9$[SbW$_9$O$_{33}$], [MTCA]$_9$[BiW$_9$O$_{33}$], [MTCA]$_8$[TeW$_9$O$_{33}$], [MTCA]$_{12}$[Mn$_3$(SbW$_9$O$_{33}$)$_2$], [MTCA]$_{12}$[Cu$_3$(SbW$_9$O$_{33}$)$_2$], [MTCA]$_{12}$[Co$_3$(SbW$_9$O$_{33}$)$_2$] and [MTCA]$_{12}$[Zn$_3$(SbW$_9$O$_{33}$)$_2$] were prepared by exchanging the sodium or potassium ions from the appropriate aqueous heteropoly salts with MTCA$^+$, and extracting the same into $C_2H_4Cl_2$ layer. Thus 0.064 mol of the alkali salt of polyoxometalate, dissolved in 10 ml of water was exchanged with 0.512 or 0.576 or 0.768 (depending on the charge on heteropoly anion) of [MTCA]$^+$Cl$^-$ dissolved in 10 ml of dichloroethane. ICP analysis of a well dried Na$_9$[SbW$_9$O$_{33}$] exchanged 1,2 dichloroethane layer showed the sodium concentration beyond detection limit, ruling out the possibility of partially exchanged Na$_x$[MTCA]$_{9-x}$[SbW$_9$O$_{33}$] species.

2.2.4.2 Procedure for the epoxidation of alkenes

The alkenes considered here for the epoxidation studies were limonene, norbornene, cyclooctene, cyclohexene, *cis*-stilbene, *trans*-stilbene, styrene and 1-octene. In a typical catalytic reaction, a 50 ml two-necked round bottom flask equipped with a condenser, was charged with the catalyst stock solution (corresponding to 0.01 mmol of [MTCA]$_9$[XW$_9$O$_{33}$] where X: Sb, Bi, Te or 0.005 mmol of [MTCA]$_{12}$[M$_3$(SbW$_9$O$_{33}$)$_2$] where M: Mn, Co, Cu, Zn), alkene (5 mmol), 30% *aq.* H$_2$O$_2$ (2.5 to 10.0 mmol) 1,2 dichloroethane (5 ml) and 30% *aq.* H$_2$O$_2$ (2.5 to 10.0 mmol), and further heated to the required reaction temperature with constant stirring. Alternatively, for epoxidation reaction in the absence of solvent, the round bottom flask was charged with 0.01 mol of Na$_9$[SbW$_9$O$_{33}$] (dissolved in minimum amount of water) and 0.09 mol of [MTCA]$^+$Cl$^-$, alkene (5.0 mmol) and 30% *aq.* H$_2$O$_2$

(2.5 to 10.0 mmol). For norbornene and *trans*-stilbene, 1 ml toluene was used for its dissolution. The catalyst will initially be in the aqueous phase but in the presence of PTC, it is pulled into the alkene layer. It may be noted that similar to ICP analysis of 1,2 dichloroethane layers as seen above, even the ICP analysis of alkene layers showed the sodium concentration beyond detection limit.

2.2.4.3 Procedure for the oxidation of alcohols

In a typical catalytic reaction, a 25 ml two-necked round bottom flask equipped with a condenser was charged with 0.01 mole of $Na_9[SbW_9O_{33}]$ and 0.09 mole of $MTCA^+Cl$, 10 mmol of the alcohols and 30 % *aq.* H_2O_2 (15 mmol) at constant stirring and then heated to the required reaction temperature. Reaction products were characterized and quantified using GLC (Hewlett-Packard 5890 gas chromatograph with a flame ionization detector and 50 m X 0.32 mm 5 % phenyl methyl silicone capillary column and with N_2 carrier gas) where chlorobenzene was used as the internal reference. Products were also identified by GC-MS (Shimadzu Gas Chromatograph, GC-17A fitted with QP-500MS Mass Spectrometer) as well as with NMR spectroscopy.

2.3 Results and Discussions

2.3.1 Characterization of the catalysts

The elemental analysis results are plotted in table 1, 2 and 3 for $Na_9[SbW_9O_{33}].19.5H_2O$, $Na_{11}(NH_4)\{[Mn(H_2O)]_3(SbW_9O_{33})_2\}.45H_2O$ and $K_{12}\{[Zn(H_2O)]_3(SbW_9O_{33})_2\}.46H_2O$ respectively.

Thus it can be observed in the tables that the obtained elemental compositions agree well with the expected elemental compositions. Similarly the FT-IR bands agree with the literature values. The FT-IR spectra as KBr pellets are shown in Figure 1, 2 and 3 for $Na_9[SbW_9O_{33}].19.5H_2O$, $Na_{11}(NH_4)\{[Mn(H_2O)]_3(SbW_9O_{33})_2\}.45H_2O$ and $K_{12}\{[Zn(H_2O)]_3(SbW_9O_{33})_2\}.46H_2O$ respectively. The values are attributed as; (1) 934 cm^{-1}: $W=O_t$, (2) 865 cm^{-1}: $W-O_c-W$, (3) 772 cm^{-1}: $W-O_e-W$, where *t*: terminal oxygen atoms, *c*: corner sharing oxygen atoms and *e*: edge sharing oxygen atoms [18].

Hence, at this point it was confirmed that the desired compounds $Na_9[SbW_9O_{33}].19.5H_2O$, $Na_{11}(NH_4)\{[Mn(H_2O)]_3(SbW_9O_{33})_2\}.45H_2O$ and

$K_{12}\{[Zn(H_2O)]_3(SbW_9O_{33})_2\}.46H_2O$ have been formed and the same were studied as potential catalysts for the oxidation of a number of alkenes and alcohols.

**Table 1:** Elemental compositions as obtained for $Na_9[SbW_9O_{33}].19.5H_2O$ compound

SL. No.	Element	Observed composition (%)	Expected composition (%)
1.	Na	7.14	7.23
2.	Sb	4.27	4.25
3.	W	57.67	57.80

Table 2: Elemental compositions as obtained for $Na_{11}(NH_4)\{[Mn(H_2O)]_3(SbW_9O_{33})_2\}. 45H_2O$ compound
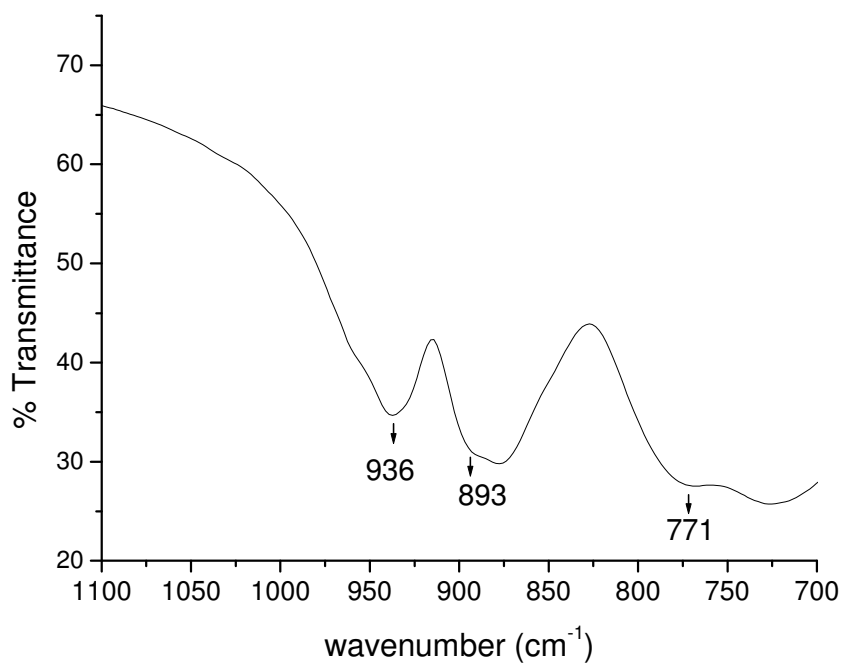
SL. No.	Element	Observed composition (%)	Expected composition (%)
1.	Na	4.17	4.28
2.	Mn	2.69	2.78
3.	Sb	4.24	4.12
4.	W	55.79	55.99

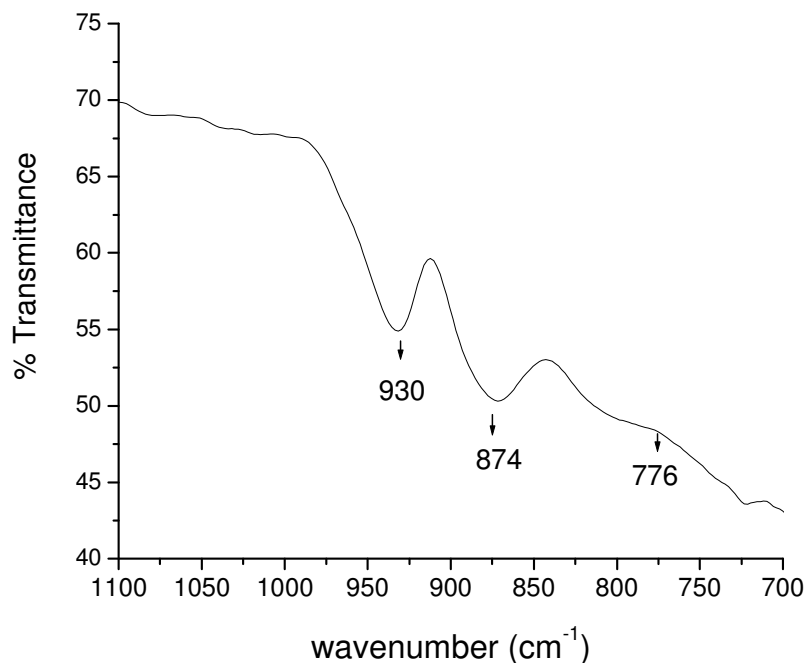**Table 3:** Elemental compositions as obtained for $K_{12}\{[Zn(H_2O)]_3(SbW_9O_{33})_2\}.46H_2O$ compound

SL. No.	Element	Observed composition (%)	Expected composition (%)
1.	K	7.54	7.61
2.	Zn	3.21	3.19
3.	Sb	3.88	3.96
4.	W	53.71	53.84
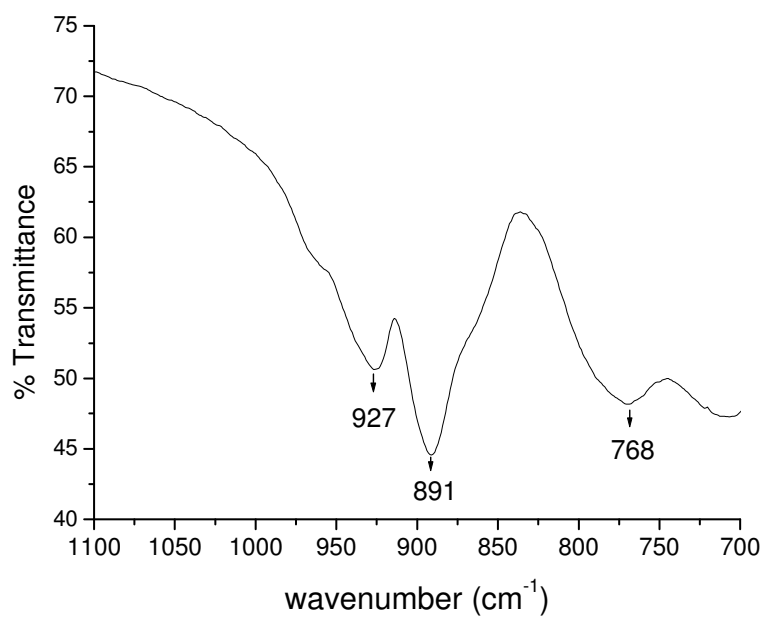
Figure 1: FT-IR spectrum of $Na_9[SbW_9O_{33}].19.5H_2O$ recorded as KBr pellet.

Figure 2: FT-IR spectrum of $Na_{11}(NH_4)\{[Mn(H_2O)]_3(SbW_9O_{33})_2\}.45H_2O$ recorded as KBr pellet.

Figure 3: FT-IR spectrum of $K_{12}\{[Zn(H_2O)]_3(SbW_9O_{33})_2\}.46H_2O$ recorded as KBr pellet.

2.3.2. Catalytic studies

2.3.2.1 Catalytic activity of $Na_{11}(NH_4)\{[Mn(H_2O)]_3(SbW_9O_{33})_2\}$

The manganese ion substituted sandwich type polyoxotungstate $Na_{11}(NH_4)[Mn_3(H_2O)_3(SbW_9O_{33})_2]$, was subjected for making of its stock solution as seen in experimental section. The above stock solution was investigated for the epoxidation of limonene with aqueous hydrogen peroxide as the oxidant as seen in the experimental section. The reaction was carried out at 60°C and substrate: oxidant mole ratio was 1:2. The limonene conversion was 90% in 3 h of time interval. The only reaction product obtained was *cis* and *trans* isomers of limonene 1,2 epoxide in almost 1:1 ratio. The epoxidation in the case of limonene was specific to the tri-substituted alkenyl group (forming limonene 1,2-epoxide as the product), as against the di-substituted alkenyl group (which gives limonene 8,9-epoxide as the product). The results are given in table 4.

Since manganese ions are the only species in the catalyst which can act as a redox centre, we thought of preparing analogous sandwich type polyoxometalates with other transition metal atoms like copper, cobalt and zinc. The copper and cobalt analogues were synthesized to see the individual activity of these metal ions and also to have a comparison of the same with the manganese ions. Similarly, since zinc is typically not a redox centre unlike manganese, copper or cobalt, it was chosen as a substitution towards some controlled reactions. Thus, the stock solutions of all these sandwich type polyoxotungstates were made and tested for limonene epoxidation, similar to the manganese ions substituted polyoxotungstate. The limonene epoxidation with all these polyoxotungstates were carried out and the results are given in the table 4.

From the Table 4, it can be observed that the copper and cobalt based polyoxotungstates showed the same activity as their manganese analogue towards limonene epoxidation, both in terms of conversion and selectivity. Interestingly, even the zinc analogue gave similar conversion and selectivity values. This observation was really surprising as zinc has no redox center like manganese, copper or cobalt. Further studies clearly showed that the tungsten octahedral clusters are in fact the active centers for the epoxidation of alkenes, irrespective of whichever transition metal is present in the polyoxometalate framework. We observed that the magnitude of limonene epoxidation with both, a manganese ions containing polyoxometalate i.e. $Na_{11}(NH_4)[Mn_3(H_2O)_3(SbW_9O_{33})_2]$ as well as a manganese ions free polyoxometalate i.e. $K_{12}[Zn_3(H_2O)_3(SbW_9O_{33})_2].48H_2O$ was the same, and so was the activity of the capping agent $Na_9[SbW_9O_{33}].19.5H_2O$ itself. Based on the above observations, it was inferred that manganese ions may really not be the active centre, unlike what was concluded before. Thus we assumed that the tungstate species are really the active centers towards the epoxidation reactions and not the manganese species as was believed in the original article.

And to substantiate this point further, the $[MTCA]_9[SbW_9O_{33}]$ stock solution, which does not contain any other transition metal ion substitutions, was also tested as a catalyst for the same epoxidation. However, in order to maintain the number of tungsten atoms with respect to manganese or zinc based sandwich type polyoxotungstates, here twice the number of mols of precursor was taken as catalyst. Interestingly, the results were identical to that of manganese based catalysts i.e. $([MTCA]_{12}[Mn_3(SbW_9O_{33})_2])$. Similar experiments were also carried out with

$[MTCA]_9[BiW_9O_{33}]$ and $[MTCA]_8[TeW_9O_{33}]$ in dichloroethane and the results obtained were similar to that of $[MTCA]_9[SbW_9O_{33}]$ in dichloroethane.

From the above results it was concluded that the tungsten octahedrons by themselves are active sites for the epoxidation with aq. H_2O_2 and there is no additional need of any transition metal atoms like manganese, cobalt or copper for the reaction. Similarly, even the antimony, bismuth or tellurium species do not play any major role except that, they help in the formation of the tungstate clusters. Further, these results prove yet another fact that the 'sandwich' structure is also not essential to demonstrate the catalytic activity for these polyoxotungstates. The typical structure of $[SbW_9O_{33}]^{9-}$ anion is shown in figure 4 [18].

Table 4: Controlled experiments for oxidation of limonene using *aq.* H_2O_2

SL. No.	Catalyst	Substrate: Catalyst	% Conversion	Time (h)
1	$[MTCA]_{12}[(Mn_3(SbW_9O_{33})_2]$ in $C_2H_4Cl_2$	1000:1	90	3
2	$[MTCA]_{12}[(Co_3(SbW_9O_{33})_2]$ in $C_2H_4Cl_2$	1000:1	92	3
3	$[MTCA]_{12}[(Cu_3(SbW_9O_{33})_2]$ in $C_2H_4Cl_2$	1000:1	89	3
4	$[MTCA]_{12}[(Zn_3(SbW_9O_{33})_2]$ in $C_2H_4Cl_2$	1000:1	91	3
5	$[MTCA]_9[SbW_9O_{33}]$ in $C_2H_4Cl_2$	500:1	92	3
6	$[MTCA]_9[BiW_9O_{33}]$ in $C_2H_4Cl_2$	500:1	90	3
7	$[MTCA]_8[TeW_9O_{33}]$ in $C_2H_4Cl_2$	500:1	91	3
8	$Na_9[SbW_9O_{33}]+ 9[MTCA]^+Cl^-$ in water	500:1	91	4
9	$Na_9[SbW_9O_{33}].19.5H_2O$	100:1	<1	6
10	$[MTCA]^+Cl^-$ in $C_2H_4Cl_2$	100:1	<1	6

Experimental condition: Temp: 60 °C, substrate: 30% *aq.* H_2O_2 (mol) was taken as 1:2. In all these cases, amounts of catalyst taken were based on the XW_9O_{33} unit content for a given amount of substrate (where X: Sb, Bi or Te).
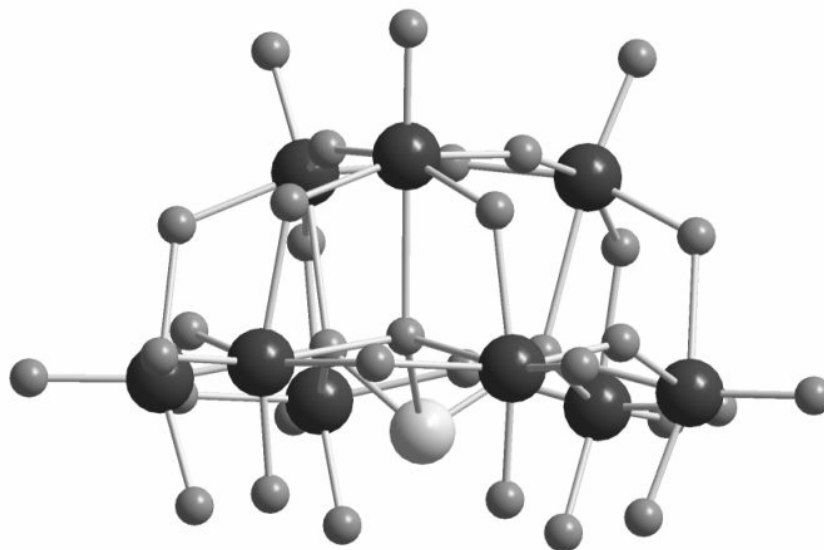
Figure 4: Ball and stick model of $[SbW_9O_{33}]^{9-}$ lacunary Keggin type polyoxometalate (Dark large circles: tungsten atoms, Light large circle: antimony atoms, Small circles: oxygen atoms) [18]

2.3.2.2 Effect of solvents on limonene epoxidation

      The epoxidation reaction was tested in various solvents like dichloroethane, dichloromethane, chloroform, methanol, acetonitrile and acetone. The reaction worked successfully in water immiscible solvents like dichloroethane, dichloromethane or chloroform, but failed in hydrophilic solvents like acetone, methanol or acetonitrile. Thus it was realized that liquid-liquid biphasic medium is very essential for the catalytic system to demonstrate the activity. Since limonene and aqueous H_2O_2 form a biphasic mixture, the activity of $Na_9[SbW_9O_{33}]$ in conjunction with $[MTCA]^+Cl^-$ was investigated in the absence of any additional solvent, as can be seen in the experimental section. This reaction was also observed to have worked successfully as can be seen in table 4. It may be noted that similar to limonene, all the liquid alkenes used by us were typically immiscible with water under reaction conditions and hence the present system is always necessarily a liquid-liquid biphasic system. In case of solid alkenes like norbornene or *trans*-stilbene, small amount of water immiscible solvent like toluene (a non-halogenated solvent) was used for its dissolution. The purpose of selecting toluene was to avoid the use of halogenated

solvents that are proven to be toxic contaminants that have an adverse effect on the environment.

However, it was observed that the reaction had slightly slowed down on *in-situ* addition of $Na_9[SbW_9O_{33}]$ and $[MTCA]^+Cl^-$ to limonene as compared to addition of equimolar amount of catalyst stock solution that is prepared separately. This retardation is because of the by-product NaCl that is formed on mixing $Na_9[SbW_9O_{33}]$ and $[MTCA]^+Cl^-$, as reported earlier by other groups [21]. Similar retardation was observed when 0.64 mol of NaCl was added to the reaction mixture, in which stock solution of $[MTCA][SbW_9O_{33}]$ was used as catalyst. Although the reactions decelerate, no decrease in the final conversion value was observed in the controlled experiments (Table 4).

2.3.2.3 Effect of temperature on limonene epoxidation

The rate of reactions increased with rise in the reaction temperature for all the alkenes. Figure 5 shows the typical trend for the epoxidation of limonene. Thus after 3 h of reaction interval only 41% conversion of limonene was observed at 35°C, however at 50 and 60°C it was 67 and 84% respectively for the same time interval (Figure 6). Accordingly, the energy of activation determined graphically was found to be 10.22 kcal K^{-1} mol^{-1} (Inset, Figure 6). The activation energy although low for catalytic reactions in general is quite typical for biphasic oxidation reactions [22]. Similarly, the values of the enthalpy of activation determined for limonene was 9.647 kcal K^{-1} mol^{-1}. As mentioned earlier in the case of limonene, stereoisomers of limonene-1,2-oxide was the only product obtained. No traces of limonene-8,9-oxide or limonene di-epoxide were observed in the product mixture even at lower or higher temperatures indicating the catalytic system is highly efficient for regioselective epoxidation reactions of such dienes. Limonene-1,2-epoxide existed in both *cis* and *trans* isomeric forms in almost an equimolar ratio as can be seen in Figure 7.
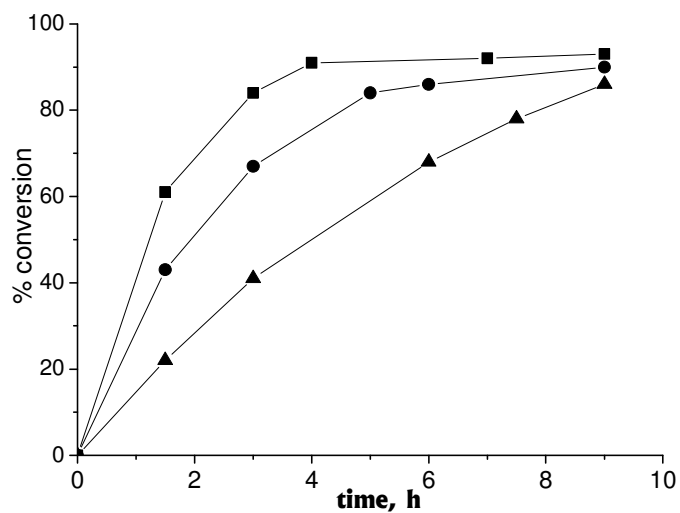
Figure 5: Kinetic plots of epoxidation of limonene over $Na_9[SbW_9O_{33}]$ + 9 $[MTCA]^+Cl^-$ at different temperatures in the range 35 - 60 °C. Reaction conditions: $Na_9[SbW_9O_{33}]$: 0.01 mmol, $[MTCA]^+Cl^-$: 0.09 mmol, limonene: 5 mmol, 30% *aq.* H_2O_2: 10 mmol (▲: 35°C, ●: 50°C, ■: 60°C)
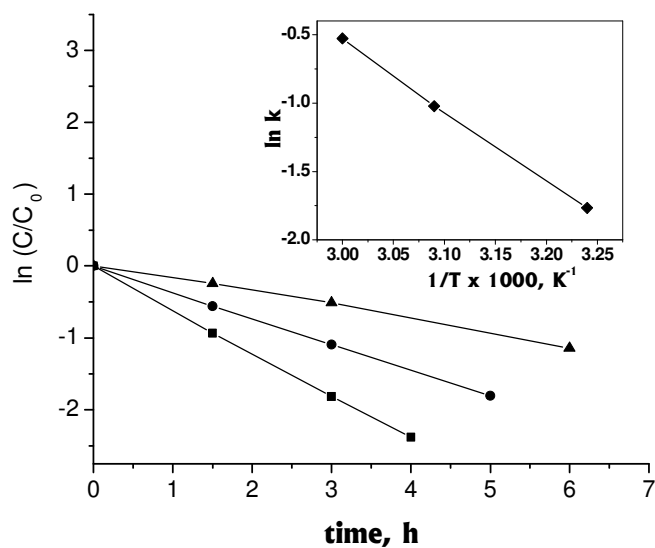
Figure 6: Kinetic profiles of limonene epoxidation reaction as a function of temperature and their linear fittings. *Reaction conditions:* Catalyst: 0.01 mmol, $[MTCA]^+Cl^-$: 0.09 mmol, limonene: 5 mmol, 30% *aq.* H_2O_2: 10 mmol (▲: 35°C, ●: 50°C, ■: 60°C). Inset: A plot of measured rate constants as a function of temperatures in an Arrhenius plot)
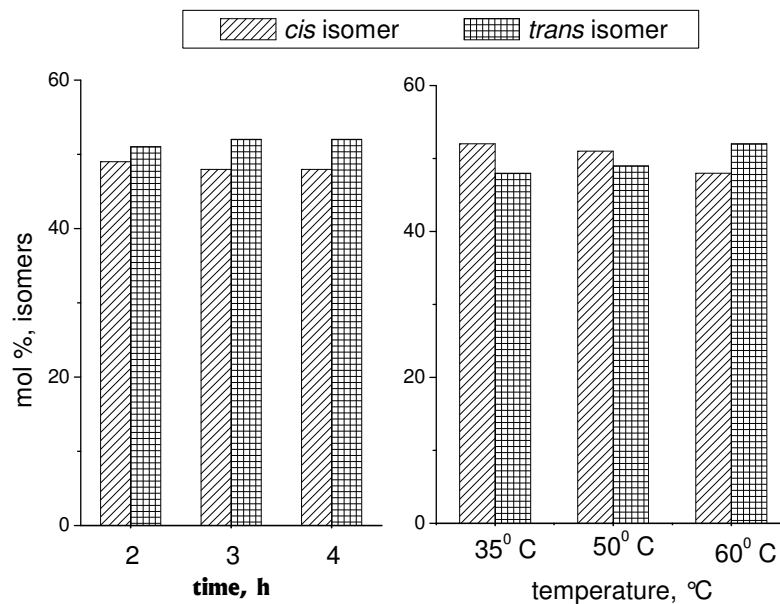
Figure 7: Selectivity of *cis* and *trans* isomers of Limonene 1, 2-epoxide:

   a. Left: with time at maximum conversion, *Reaction conditions*: $Na_9[SbW_9O_{33}]$: 0.01 mmol, $[MTCA]^+Cl^-$: 0.09 mmol, limonene: 5 mmol, 30% *aq.* H_2O_2: 10 mmol, Temp: 60^0 C

   b. Right: with reaction temperature at the maximum conversion, *Reaction conditions*: $Na_9[SbW_9O_{33}]$: 0.01 mmol, $[MTCA]^+Cl^-$: 0.09 mmol, limonene: 5 mmol , 30% *aq.* H_2O_2: 10 mmol

2.3.2.4 Epoxidation of other alkenes

A variety of other alkenes *viz.* norbornene, cyclohexene, cyclooctene, *cis*-stilbene, *trans*-stilbene, styrene and 1-octene were also tested for the epoxidation studies. In the case of norbornene and cyclohexene, a lower substrate : oxidant ratio gave excellent selectivity for the epoxide as can be seen in Table 5. On increasing the substrate : oxidant ratio, cyclohexene chiefly underwent allylic oxidation while norbornene mainly gave norbornanone. Similarly, increase in the temperature also favors allylic oxidation of the former, also reported by others [22]. Another cyclic alkene *viz.* cyclooctene gave only the epoxide with near quantitative yields, even at ambient temperature conditions. Cyclooctene has no tendency of undergoing allylic oxidation or cleaving of the epoxide like cyclohexene [23].

Terminal alkenes are normally very less reactive, but with the present catalytic system 1-octene gave a moderate conversion of 38 % and showed >99 % selectivity for the epoxide. With an activated terminal alkene like styrene, instead of epoxide formation the olefinic bond was cleaved and benzaldehyde was obtained as the major product. Another activated alkene *viz. cis*-stilbene gave a mixture of both *cis*-stilbene oxide (88 % selectivity) and *trans*-stilbene oxide (balance) as products at the maximum conversion of the substrate (*ca.* 57 %). *Trans*-stilbene on the other hand, gave only benzaldehyde as the product with very poor conversion.

Table 5: Oxidation of various alkenes over $Na_9[SbW_9O_{33}]+9[MTCA]^+Cl^-$ with *aq.* H_2O_2 as oxidant at different temperatures and different substrate: oxidant ratios

Substrate	Substrate: *aq.* H_2O_2	Temp, (°C)	Time, (h)	Conversion (%)	Selectivity, (%)
Limonene	1:2	60	4	91	*cis*-limonene 1,2-epoxide (49) *trans*-limonene 1,2-epoxide (51)
Norbornene [a]	1:1	60	5	85	Norbornene epoxide (80) Norbornanone (20)
Norbornene [a]	1:2	60	5	87	Norbornene epoxide (11) Norbornanone (89)
Cyclohexene	1:1	35	6	42	Cyclohexene epoxide (25) Cyclohexene-2-ol (41) Cyclohexene-2-one (34)
Cyclohexene	1:0.5	35	6	24	Cyclohexene epoxide (92) Cyclohexene diol (8)
Cyclooctene	1:1	60	6	97	Cyclooctene epoxide (>99)
Cyclooctene	1:2	35	9	95	Cyclooctene epoxide (>99)
cis-stilbene	1:2	60	6	57	*cis*-stilbene epoxide (88) *trans*-stilbene epoxide (12)
Trans-stilbene [a]	1:2	60	9	17	Benzaldehyde (>99)
Styrene	1:2	60	6	73	Benzaldehyde (>99)
1-octene	1:2	60	9	38	1-octene epoxide (>99)

Reaction conditions: $Na_9[SbW_9O_{33}]$: 0.01 mmol, $[MTCA]^+Cl^-$: 0.09 mmol, Substrate: Catalyst Ratio : 500:1, [a] 1 ml toluene was used as solvent.
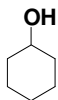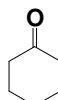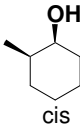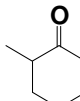
2.3.2.5 Oxidation of secondary and allylic alcohols
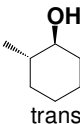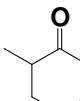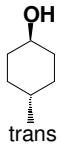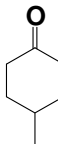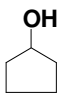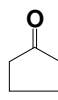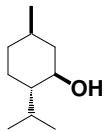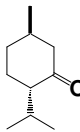
Having realized the activity of $Na_9[SbW_9O_{33}]$ in conjunction with a phase transfer catalyst, $MTCA^+Cl^-$ towards alkene epoxidation, the same was extrapolated towards the oxidation of a variety of secondary and allylic alcohols. The procedure for the same can be seen in experimental section. Although the catalyst showed some activity towards oxidation of secondary alcohols, it failed to show any activity towards the oxidation of primary alcohols; unless they were activated by an allylic or benzylic adjacency, as in the case of benzyl alcohol. In the case of secondary alcohols, the corresponding ketones was the only product, while in the case of allylic alcohol, the ketones, the epoxide and the epoxy-ketones were obtained, the major product being the ketone. Importantly, unlike alkenes, in the case of secondary as well as allylic alcohols the reaction had not slowed down on *in-situ* addition of $Na_9[SbW_9O_{33}]$ and $MTCA^+Cl^-$. Thus, the rate of reaction for *in-situ* addition of $Na_9[SbW_9O_{33}]$ and $MTCA^+Cl^-$ was same as that of addition of equimolar $Q_9[SbW_9O_{33}]$ stock solution, to the alcohol and hydrogen peroxide mixture.

In the case of secondary alcohols, oxidations of cyclic alcohols like cyclopentanol, cyclohexanol as well as *cis* and *trans*-isomers of methylated cyclohexanols were carried out, apart from linear alcohol like 2-hexanol. In all the cases near quantitative yields were obtained within two hours of reaction time. Structurally complex alcohols like borneol and menthol were also oxidized to corresponding ketones under the same condition and their yields were 87 and 93 % respectively. Benzylic and allylic alcohols also underwent a smooth oxidation to the corresponding aldehyde or ketones selectively, with this catalytic system. Oxidation of benzyl alcohol at 60 °C gave only 70 % convers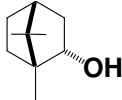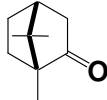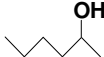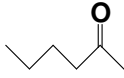ion with more than 99 % selectivity to benzaldehyde after 5 h. However, at 80 °C the yield was above 94 % in 2 h. In the case of benzyl alcohol no noticeable benzoic acid was observed even at substrate: *aq.* H_2O_2 mol ratio of 1:1.5.

Linear allylic alcohols with terminal olefinic bond like 1-hexene-3-ol and 1-octene-3-ol were completely transformed into corresponding ketones with selectivity of more than 99 % at 80 °C in 3 and 2 h respectively with the current catalyst system. Similarly, in the case of cyclohexene-2-ol, cyclohexene-2-one was the only product with more than 99 % yield in 1 h at 80 °C. For 1-phenyl ethanol, the product yield was higher than 96 % in 1 h at 80 °C.
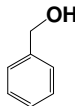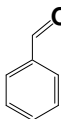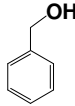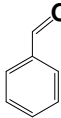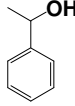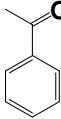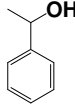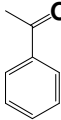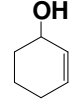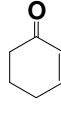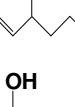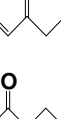
Turnover frequency (defined as moles of product found per mole of $Na_9[SbW_9O_{33}]$ per hour) approached $>15000\ h^{-1}$ for the oxidation of 1-phenyl ethanol when $Na_9[SbW_9O_{33}]$: substrate: *aq.* H_2O_2 mole ratio was 1:1,00,000:1,50,000 at 80 °C. The above results show that $Na_9[SbW_9O_{33}]$ + $MTCA^+Cl^-$ catalyst system was very efficient and selective for oxidation of wide range of alcohols, in the absence of any solvents. The results for the oxidation studies of secondary alcohols can be seen in Table 6 and for the oxidation studies of allylic and benzylic alcohols can be seen in Table 7.

Table 6: Selective oxidation of secondary alcohols over $Na_9(SbW_9O_{33})$ + $MTCA^+Cl^-$ using *aq.* H_2O_2.

SL. No.	Substrate	Time, h	Product	Yield, %	TON
1	OH (cyclohexanol)	2	O (cyclohexanone)	93	930
2	OH cis (2-methylcyclohexanol)	2	O (2-methylcyclohexanone)	> 99	990
3	OH trans (2-methylcyclohexanol)	2	O (2-methylcyclohexanone)	95	950
4	OH trans (4-methylcyclohexanol)	2	O (4-methylcyclohexanone)	98	980
5	OH (cyclopentanol)	2	O (cyclopentanone)	> 99	990
6	OH (menthol)	3	O (menthone)	89	890
7	OH (borneol/isoborneol)	3	O (camphor)	97	970
8	OH (2-hexanol)	2	O (2-hexanone)	> 99	990

Reaction conditions: $Na_9(SbW_9O_{33})$: 0.01 mmol, $MTCA^+Cl^-$: 0.09 mmol, alcohols: 10 mmol, 30 % *aq.* H_2O_2: 15 mmol, temperature: 80 °C. Yields were determined by GC analysis based on alcohol conversion and selectivity to the product.

Table 7: Selective oxidation of benzylic and allylic alcohols over $Na_9(SbW_9O_{33})$ + $MTCA^+Cl^-$ using *aq.* H_2O_2

SL. No.	Substrate	Temp, °C	Time, h	Product	Yield, %	TON
1	OH (benzyl alcohol)	60	5	O (benzaldehyde)	70	700
2	OH (benzyl alcohol)	80	2	O (benzaldehyde)	94	940
3	OH (1-phenylethanol)	60	2	O (acetophenone)	83	830
4	OH (1-phenylethanol)	80	1	O (acetophenone)	96	960
5	OH (2-cyclohexenol)	80	1	O (2-cyclohexenone)	68	990
6	OH (hex-1-en-3-ol)	80	1.5	O (hex-1-en-3-one)	72	990
7	OH (oct-1-en-3-ol)	80	1	O (oct-1-en-3-one)	78	990

Reaction conditions: $Na_9(SbW_9O_{33})$: 0.01 mmol, $MTCA^+Cl^-$: 0.09 mmol, secondary alcohols: 10 mmol, 30 % *aq.* H_2O_2 : 15 mmol. Yields were determined by GC analysis based on alcohol conversion and selectivity to the product.

2.3.2.6 Effect of temperature on cyclohexanol oxidation

Oxidation of cyclohexanol with *aq.* H_2O_2 over $Na_9[SbW_9O_{33}]$ + $MTCA^+Cl^-$ catalyst system was carried out with cyclohexanol: *aq.* H_2O_2 mol ratio of 1:1.5 in the temperature range 40-80 °C. Kinetics of the reaction were followed till maximum yield was obtained and the results are plotted in Figure 8. The cyclohexanol conversion and the reaction rate increase with increase in temperature without

affecting the selectivity of the required product, cyclohexanone. Accordingly, at 40 °C maximum conversion of ~ 74 % was obtained after 24 h whereas at 50 and 60 °C the cyclohexanol conversions were about 82 % after 8 and 5 h. However, at 80 °C maximum conversion of > 93 % was obtained within 2 h (Table 6).
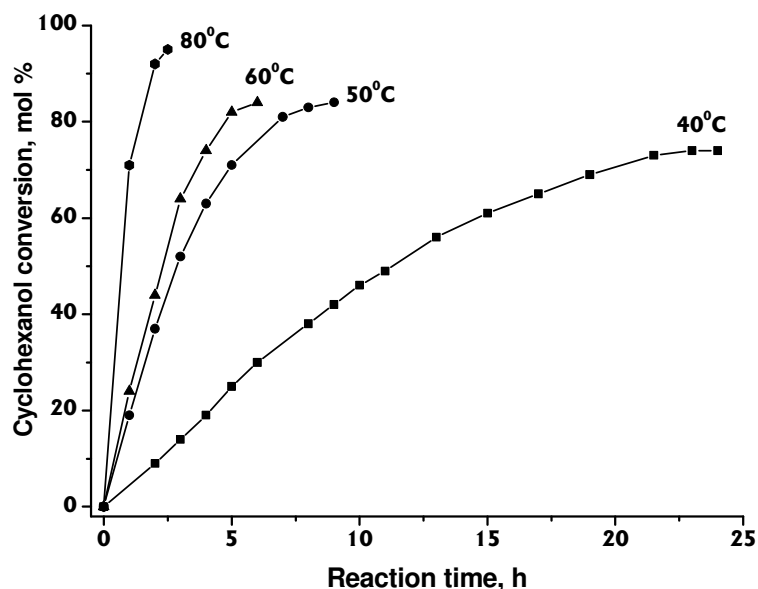
Figure 8: Kinetic plots of oxidation of cyclohexanol over $Na_9[SbW_9O_{33}]$ + 9 $MTCA^+Cl^-$ at different temperatures in the range 40 - 80 °C. Reaction conditions: $Na_9[SbW_9O_{33}]$: 0.01 mmol, $MTCA^+Cl^-$: 0.09 mmol, alcohol: 10 mmol, 30 % *aq.* H_2O_2: 15 mmol

Kinetic measurements for cyclohexanol oxidation reaction were carried at as a function of temperature and the results are plotted in Figure 9 and the data showed the reaction to be first order with respect to cyclohexanol. The rate constants at different reaction temperatures between 40 and 60°C were obtained by subjecting the data to linear regression as shown in the figure. Arrhenius equation was used with the above rate constant data to estimate the activation parameters for the cyclohexanol oxidation reaction (inset in Figure 9). The Energy of activation was obtained as 15.57 kcal/mol while the Enthalpy of activation was 10.2 kcal/mol. The obtained activation energy is typical for biphasic oxidation as observed in the literature, and as also seen above in the case of alkenes [22].

64
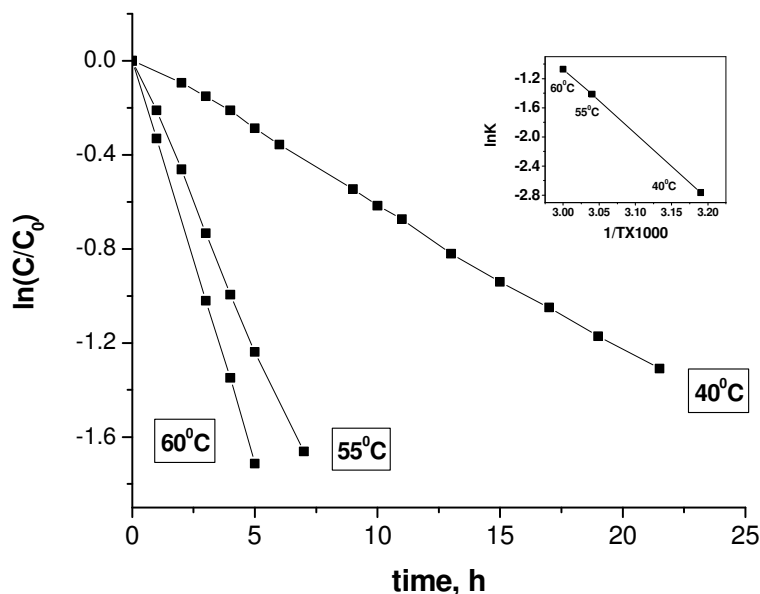
Figure 9: Kinetic profiles of cyclohexanol oxidation reaction as a function of temperature and their linear fitting. Reaction condition: catalyst: 0.01 mmol, MTCA$^+$Cl$^-$: 0.09 mmol, alcohol: 10 mmol, 30% *aq.* H$_2$O$_2$: 15 mmol. Inset: a plot of the measured rate constants as a function of temperatures in an Arrhenius plot.

2.3.2.7 Effect of substrate: oxidant ratio on cyclohexanol oxidation

In an attempt to optimize the amount of *aq.* H$_2$O$_2$ needed for cyclohexanol oxidation reaction, *experiments* were carried out with different cyclohexanol: *aq.* H$_2$O$_2$ mol ratios at 60 °C and results are plotted in Figure 10. With cyclohexanol: H$_2$O$_2$ mole ratio of 1:0.5 and 1:1 the conversions were 30 and 39 % respectively and no further increase in the conversion observed thereafter. With cyclohexanol: H$_2$O$_2$ mol ratio of 1:1.5 the conversion was as high as 84 % after 6 h and for 1:2 mol ratio, the cyclohexanol conversion was almost the same as that of 1:1.5 ratio, indicating that the substrate: *aq.* H$_2$O$_2$ mol ratio of 1:1.5 was optimum to obtain a satisfactory yield with the current catalytic system. Thus, the substrate: *aq.* H$_2$O$_2$ mol ratio of 1:1.5 was employed in all further reactions.
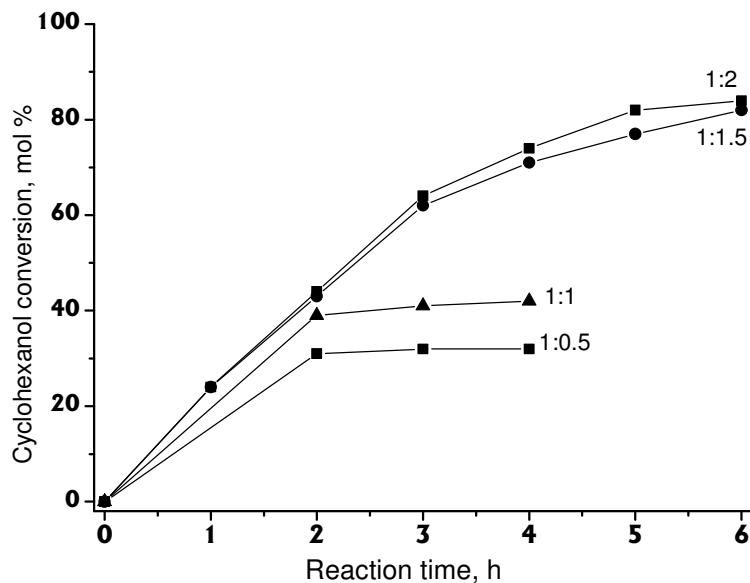
Figure 10: Oxidation of cyclohexanol over $Na_9[SbW_9O_{33}]$ + 9 $MTCA^+Cl^-$ with different substrate : *aq.* H_2O_2 ratio. *Reaction conditions*: $Na_9[SbW_9O_{33}]$: 0.01 mmol, $MTCA^+Cl^-$: 0.09 mmol, alcohol: 10 mmol, temperature: 60 °C

In an attempt to see whether multiple fractional addition of *aq.* H_2O_2 to substrates with certain time intervals is of any advantage over a single addition of the whole amount of *aq.* H_2O_2, experiments with addition of 1.5 mole equivalent of *aq.* H_2O_2 in one lot as well as in multiple fractional additions were carried out at 60 °C over the present catalyst system for cyclohexanol oxidation reaction and the results are shown in Figure 11. As seen in the figure, the total conversion of cyclohexanol, thus the yield of the cyclohexanone, was nearly the same whether the addition of 1.5 mol equivalent of *aq.* H_2O_2 was added in one lot or multiple fractions. In fact multiple fractional additions require more time than that required for one lot addition to achieve the same conversion as seen in the figure. Thus, addition of total amount of the oxidant was done in one lot for all other reactions.
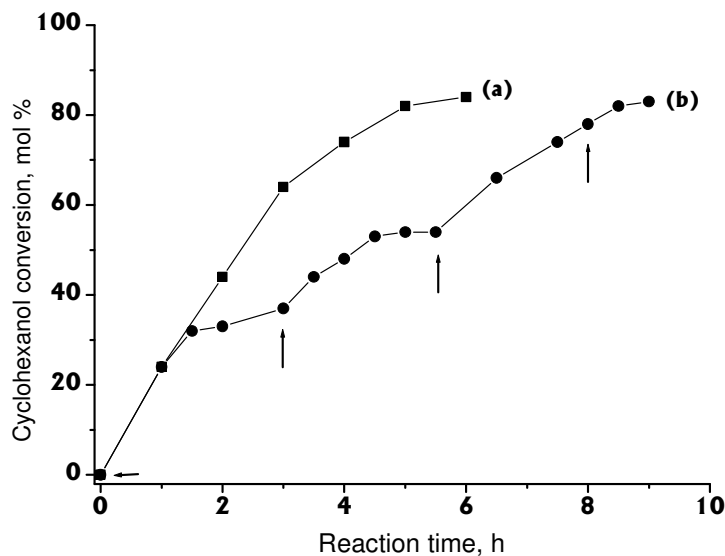
Figure 11: Oxidation of cyclohexanol over $Na_9[SbW_9O_{33}]$ + 9 MTCA$^+$Cl$^-$ with (a) one-lot addition and (b) fractional additional (3 X 0.5 mol) of 1.5 mol *aq.* H_2O_2 equivalent of with reference to cyclohexanol. Reaction conditions: catalyst: 0.01 mmol, MTCA$^+$Cl$^-$: 0.09 mmol, alcohol: 10 mmol, temperature: 60 °C. ↑ indicates the time when 0.5 mol fraction of *aq.* H_2O_2 added.

2.3.3 Active center of the catalyst and reaction mechanism

UV-visible studies were conducted for the separated and well-dried dichloroethane solutions of manganese containing polyoxotungstate (Figure 12, left) and the antimony based precursor (Figure 12, right) before and after interaction with aq H_2O_2. The spectra of both the polyoxotungstates before interaction with H_2O_2 were identical, which changed after with the addition of H_2O_2 in both the cases. However, the spectra of both the polyoxotungstates on treating with H_2O_2 were also identical to each other. The bands seen in the UV region correspond to [MTCA] group [18]. Upon interaction with H_2O_2, shifts in bands are observed due to changes in the environment of these anions. This indicates that the changes that are taking place in manganese containing polyoxotungstate are also occurring in the antimony based capping agent.
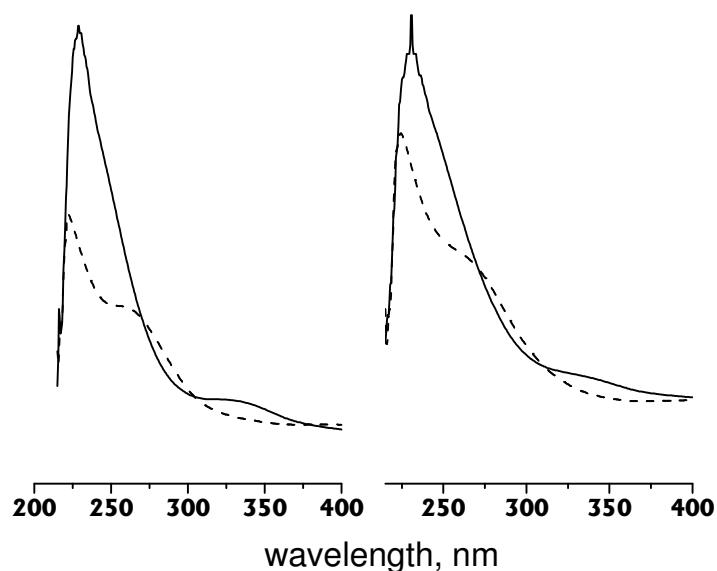
Figure 12: UV-visible spectra of [MTCA]$_9$[SbW$_9$O$_{33}$] (left) and [MTCA]$_{12}$ [Mn$_3$(SbW$_9$O$_{33}$)$_2$] (right) in 1, 2 dichloroethane (Dashed lines: before interaction with 30% *aq.* H$_2$O$_2$, Solid lines: after interaction with 30% *aq.* H$_2$O$_2$)

However, UV-visible spectra were not adequate in explaining the mechanism of reaction, thus IR spectroscopy was used as a probe to investigate the nature of active peroxo species, as well as to study the stability of the catalyst under the experimental conditions [22]. Due to the limitation of IR measurement with aqueous solution, IR measurements were made with the dichloroethane solution of [MTCA]$_9$[SbW$_9$O$_{33}$] on KBr discs before and after treating with *aq.* H$_2$O$_2$ and the spectra can be seen in Figure 13 (left). The peaks are assigned as follows: 944 (vs) (W=O$_t$); 880 (vs) (W-O$_c$-W); 769 (s) (W-O$_e$-W) (t: terminal, c: corner sharing, e: edge sharing). An additional peak appearing at 834 cm^{-1} after the above solution was treated with *aq.* H$_2$O$_2$, is attributed to the formation of tungsten-peroxo species in accordance with the literature [22]. On treatment with 10% *aq.* KI, the peroxide decomposes and the peak at 834cm^{-1} disappears. The resultant spectrum was identical to that of the fresh sample as can be seen in the figure. Similar spectral measurements were also done with dichloroethane solution of [MTCA]$_{12}$[Mn$_3$(SbW$_9$O$_{33}$)$_2$] and the spectra were identical to [MTCA]$_9$[SbW$_9$O$_{33}$] spectra (Figure 13, right). These studies indicate that tungsten-peroxo species was the possible intermediate species involved

in the selective oxidation of alkenes, and the results also prove that the catalyst is stable under the present experimental conditions. Further, our efforts to isolate the peroxo intermediate presumably forming during the hydrogen peroxide treatment with $[MTCA]_9[SbW_9O_{33}]$ in dichloroethane solvent became futile. However, number of peroxo species formed was estimated to be six per unit of $[SbW_9O_{33}]$ by titration between dichloroethane solutions of the peroxo intermediate complexes with methanolic Ce (IV) [24].
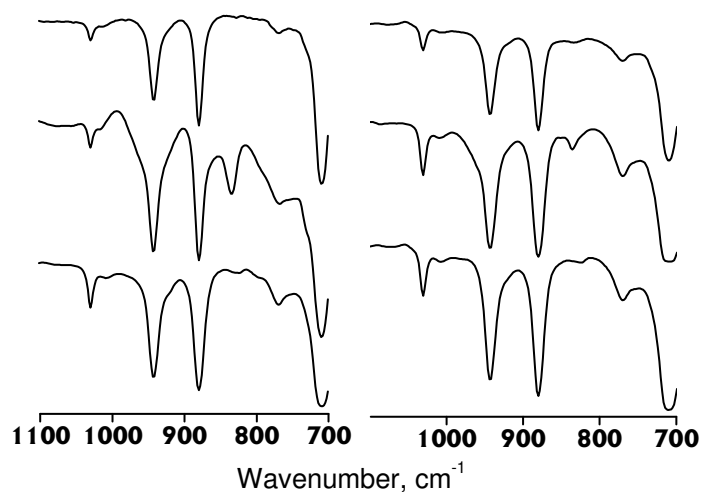
Figure 13: IR spectra of $[MTCA]_9[SbW_9O_{33}]$ (left) and $[MTCA]_{12}[Mn_3(SbW_9O_{33})_2]$ (right) in 1, 2 dichloroethane (Top: before reaction, Center: after addition of 30% *aq.* H_2O_2, Bottom: after decomposition of excess of peroxide with 10% KI solution)

Finally, on the basis of IR observations a model of the reaction mechanistic pathway for the epoxidation of alkenes (Scheme 1) or oxidation of alcohols (Scheme 2) is proposed. One or more tungstate octahedron of the $Na_9[SbW_9O_{33}]$ cluster bind to peroxo species with possible seven coordination and the original structure is retained on the completion of oxidation reaction.
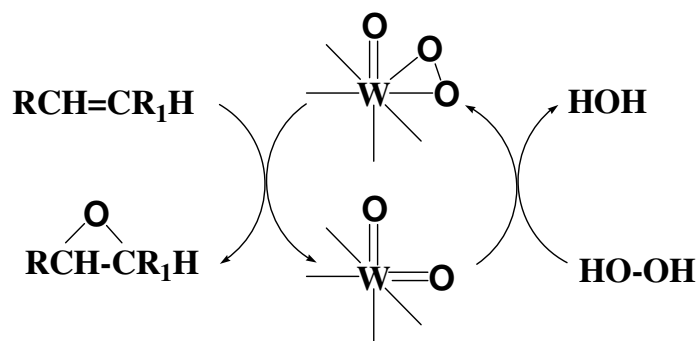
Scheme: 1 Proposed model for reaction mechanism for epoxidation of alkenes

(Only single tungsten octahedra is shown for clarity)
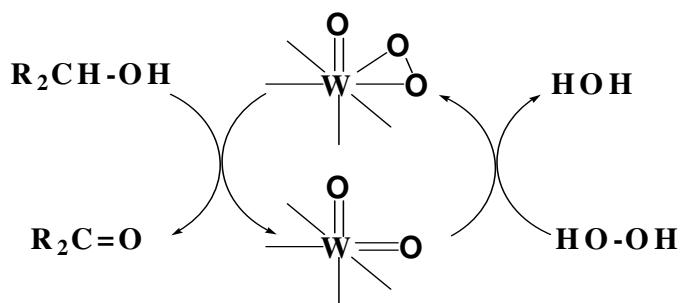
Scheme: 2 Proposed model for reaction mechanism for oxidation of alcohols

(Only single tungsten octahedra is shown for clarity)

2.4 Summary and Conclusion

The results clearly indicate that $Na_9[SbW_9O_{33}]$ in conjunction with a phase transfer catalyst $[MTCA]^+Cl^-$ is capable of selectively oxidizing a number of structurally different alkenes as well as a variety of secondary and allylic in high yields. In most of the cases the selectivity for epoxide (in the case of alkenes) or ketone (in the case of alcohols) was excellent. Importantly, there is no need of any solvent for the reaction (except when the substrate is a solid). It can be unambiguously seen from the controlled experiments that tungstate species are indeed the active center and transition metal ions do not play any major role. The IR studies indicate the formation of a tungsten-peroxo intermediate on the interaction of polyoxotungstate with *aq.* H_2O_2 in presence of $[MTCA]^+Cl^-$, and this intermediate was observed for both the transition metal containing polyoxotungstate as well as the transition metal free precursor. IR studies also reveal that the catalyst is stable in the presence of PTC when *aq.* H_2O_2 was used as the oxidant.

References

1. G. Cainelli, G. Cardillo, Chromium Oxidations in Organic Chemistry, Springer, Berlin, 1984

2. H. Ehara, M. Noguchi, S. Sayama, T. Onami, J. Chem. Soc., Perkin Trans. 1 (2000) 1429

3. Ullmann's Encyclopedia of Industrial Chemistry, 5th ed.: W. Gerhartz, Y. S. Yamamoto, L. Kaudy, J. F. Rounsaville, G. Schulz, Eds. Verlag Chemie: Weinheim, 1987; Vol. A9, p 531

4. S.-I. Murahashi, Y. Oda, T. Naota. J. Am. Chem. Soc. 114 (1992) 7913

5. S.-I. Murahashi, T. Naota, N. Hirai, J. Org. Chem. 58 (1993) 7318

6. 1. R. Neumann, A. M. Khenkin, Inorg Chem. 34 (1995) 5753

7. R. S. Drago, Coord Chem. Rev 117 (1992) 185

8. B. Meunier, Chem. Rev 92 (1992) 1411

9. Cytochrome P-450, Structure, Mechanism and Biochemistry, Ortizde Montellano, P. R., Ed; Plenum Press: New York and London, 1986, pp 1-28

10. M. J. Naughton, R. S. Drago, J. Catal. 155 (1995) 383

11. J. P. Arhancet, M. E. Davis, J. S. Merola, B. E. Hanson, Nature 339 (1989) 454

12. G. A. Ozin, C. Gil, Chem. Rev. 89 (1989) 1749

13. E. Byambajav, Y. Ohtsuka, Appl. Catal. A: General 252 (2003) 193

14. R. Grommen, P. Manikandan, Y. Gao, T. Shane, J. J. Shane, R. A. Schoonheydt, B. M. Weckhuysen, D. Goldfarb, J. Am. Chem. Soc. 122 (2000) 11488

15. D. Mansuy, J-F Bartoli, P. Battioni, D. K. Lyon, R. G. Finke J. Am. Chem. Soc. 113 (1991) 7222

16. N. K. K. Raj, A. V. Ramaswamy, P. Manikandan, J. Mol. Catal. A: Chemical 227 (2004) 37

17. R. Neumann, M. Gara, J. Am. Chem. Soc. 117 (1995) 5066

18. M. Bösing, A. Nöh, I. Loose, B. Krebs, J. Am. Chem. Soc. 120 (1998) 7252

19. R. Neumann, M. Dahan, J. Am. Chem. Soc. 120 (1998) 11969

20. G. Barak, J. Dakka, Y. Sasson, J. Org. Chem. 53 (1988) 3553

21. K. Sato, M. Aoki, M. Ogawa, T. Hashimoto, R. Noyori, J. Org. Chem. 61 (1996) 8310

22. R. Neumann, M. Gara, J. Am. Chem. Soc. 117 (1995) 5066

23. A. J. Appleton, S. Evans, J. R. L. Smith, J. Chem. Soc, Perkin Trans-2 (1996) 281

24. A. I. Vogel, A Text-book of Quantitative Inorganic Analysis, third ed., Longman, London, 1961

Chapter 3:

Alkenes epoxidation catalyzed by vanadium heteropoly acids heterogenized on amine functionalized SBA-15 materials

3.1 Introduction

Heterogenization of homogeneous catalytic materials has been an attractive strategy to overcome the difficulties involved in the separation and reusability of homogeneous catalysts [1, 2]. Many strategies have been adopted in the literature to heterogenize the homogeneous catalysts. Conventionally they are immobilized/anchored on polymeric organic materials such as resins [3, 4], supported on inert porous solids such as alumina and silica [5, 6] or encapsulated in the pores and cavities of microporous and mesoporous materials such as zeolites, MCM-41 and SBA-15 [7-9]. There are certain disadvantages with polymeric supports due to their vulnerability of their organic part to some chemicals and solvents, and due to leaching of catalysts from the immobilized material over the period of reactions [10]. On the other hand, porous inorganic material supports are structurally stable and more resistant to organic chemicals and solvents. However, mere encapsulation of the homogeneous catalytic molecules into the porous materials may also lead to partial leaching of catalysts. Moreover, controlling the amount of catalysts loading is limited when encapsulation technique is adopted [11].

To overcome the leaching problem, efforts have been made to immobilize the catalytic molecules on a functionalized silica surface, for example, microporous and mesoporous materials with organic chain containing terminal functional groups like amine, phosphine, sulfide etc [2]. Anchoring of the homogeneous catalysts onto these functionalized materials is proven to be effective in reducing the leaching problem. These inorganic materials are more versatile than polymeric supports since pore dimensions, specific surface area and mesoporous structure of them can be controlled to a large extend. A great deal of research work has been done on X and Y-type zeolites and M41 based mesoporous materials. Amongst mesoporous materials, SBA type support materials are more attractive due to their better hydrothermal stability, large pores and thick walls.

Transition metal ion substituted heteropoly compounds are, in general, promising catalysts for many catalytic applications including selective oxidation reactions [12]. High solubility of these molecules often makes their separation from the reaction mixture difficult. Heterogenizing these homogeneous molecules by immobilizing on mesoporous materials (e.g. MCM-41, SBA-15) were successful and found to be stable and active [13-16]. It was found that the encapsulation technique

enhanced easy separation of these heteropoly anions from the reaction mixture, however, weak bonding interaction of heteropoly anion with the silanol group of these silicate materials leads to partial leaching especially with polar solvent media [17, 18]. In the recent literature, anchoring of homogeneous catalyst molecules onto amine funtionalized silica materials like propyl amine functionalized mesoporous materials was found to be a promising strategy to reduce the leaching of active sites [18-20].

The present chapter describes the anchoring of vanadium substituted phosphomolybdic acids viz. $H_4PMo_{11}VO_{40}$, $H_5PMo_{10}V_2O_{40}$ and $H_6PMo_9V_3O_{40}$ on amine functionalized SBA-15 and their physicochemical characterization. Catalytic reactions towards the epoxidation of alkenes over aq. H_2O_2 and TBHP as the oxidants have been carried out, to demonstrate the heterogeneous nature and reusability of the immobilized catalyst. A comparative study of the activity of these three heteropoly acids in neat or anchored condition have been also been studied for the epoxidation reactions over both aq. H_2O_2 and TBHP as oxidants. In addition to this, we have also attempted to elucidate the plausible mechanism of the reactions for neat catalysts with our set of conditions, taking the aid of various techniques like UV-visible, ^{51}V NMR and EPR spectroscopy, as shall be seen in further sections.

3.2 Experimental

3.2.1 Materials

All chemicals used are of analytical reagent grade. Sodium phosphate dibasic dodecahydrate, sodium molybdate dihydrate and sodium metavanadate, conc. H_2SO_4 (Loba Chemicals Ltd) were used as received for the preparation of vanadium substituted phosphomolybdic acids. Aq. H_2O_2 (30%) and aq. TBHP (70%) were purchased from Merck India Ltd. Diethyl ether acetonitrile and 1,2 dichloroethane (S. D. Fine Chemicals Ltd) were of analytical grade and used without further purification. The exact strength of hydrogen peroxide was determined by redox titration with $KMnO_4$ solution. 30% TBHP/DCE was prepared by shaking appropriate volumes of 70% aq. TBHP and 1,2 dichloroethane in a separating funnel, and then collecting the lower dichloroethane (DCE) layer, followed by it's drying over anhydrous sodium sulfate. Tetraethyl orthosilicate (TEOS), (3-aminopropyl)-triethoxysilane (APTES), and the triblock copolymer, poly (ethylene glycol)-blockpoly (propylene glycol)-block-poly (ethylene glycol) [EO_{20}-PO_{70}-EO_{20}) were used as received (Aldrich).

Hydrochloric acid (2 M) was prepared from 37% fuming hydrochloric acid (Merck). The substrates norbornene, cyclooctene, cyclohexene and styrene were purchased from Sigma Aldrich Chemical Ltd. and were used without further purification.

3.2.2 Synthesis of SBA-15

SBA-15 was prepared by a known method as per the reported procedure [21]. In a typical procedure, 4 g of triblock copolymer, poly-(ethylene glycol)-block-poly-(propylene glycol)-block-poly (ethylene glycol) [EO_{20}-PO_{70}-EO_{20}, a template], was dispersed in 30 g distilled water and stirred for 3 h. To the resultant solution, 120 g of 2 M HCl was added under stirring and finally 8.5 g of tetraethyl orthosilicate (TEOS, a silicate precursor) was added dropwise. The resultant mixture was maintained at 40°C for 24 h under stirring and then at 110°C for 48 h under static condition in Teflon bottle. The crystallized product was filtered, washed with warm distilled water and dried at 110°C for 24 h. The dried sample was then calcined at 550°C at 1°C/min rate and holding it at 550°C for 6 h. The structure was confirmed by small angle X-ray scattering (SAXS) analysis. The surface area was determined by N_2 BET measurement at liquid nitrogen temperature. The calcined sample is referred as SBA-15 here after.

3.2.3 Preparation of amine-functionalized SBA-15

The surface modification of SBA-15 using 3-aminopropyl triethoxysilane (APTES) was carried out using a grafting method by adopting reported procedure [21]. In a typical preparation freshly activated SBA-15 (2 g) was refluxed with 50 ml of toluene (distilled over sodium and dried) to remove the occluded moisture azeotropically for 4 h. To that APTES (1 g) in 10 ml of toluene was added with stirring and refluxed for 4 h. After distilling off the solvent, the solid was filtered, washed in a soxhlet apparatus with dichloromethane, and then dried at room temperature. The product is designated as NH_2-SBA. The nitrogen elemental analysis estimated 2.3 mmol of NH_2 per gram of NH_2-SBA.

3.2.4 Preparation of vanadomolybdophosphoric acids

The three heteropoly acids of $H_4PMo_{11}VO_{40}$, $H_5PMo_{10}V_2O_{40}$ and $H_6PMo_9V_3O_{40}$ were synthesized by known procedures [22]. All the three heteropoly

acids were subjected to FT-IR and elemental analysis, to check the formation and purity of the same [13].

3.2.4.1 Monovanadomolybdophosphoric acid, $H_4PMo_{11}VO_{40}$ (V_1HPA)

Sodium phosphate dibasic dodecahydrate (1.77 gm, 5 mmol), was dissolved in 25 ml water and mixed with sodium metavanadate (1.52 gm, 12.5 mmol) that was dissolved in 25 ml boiling water. The mixture was cooled and acidified to red color with 1.25 ml concentrated sulfuric acid. To this colored solution was added sodium molybdate dihydrate (33.25 gm, 137.42 mmol) in 50 ml of water. Finally 21.25 ml of concentrated sulfuric acid was added. Color of the solution became light red. After cooling the solution was extracted with four fractions each of 25 ml diethyl ether to isolate the heteropoly acid in a separating funnel. In this extraction the heteropoly etherate was present as the middle layer. After separation, a stream of air was passed through the heteropoly etherate layer to free it of ether. The orange solid that separated was dissolved in water, concentrated to the first appearance of crystal in a vacuum desiccator over concentrated sulfuric acid and then allowed to crystallize further. The orange crystals that formed were dried, crushed and used for further studies.

3.2.4.2 Divanadomolybdophosphoric acid, $H_5PMo_{10}V_2O_{40}$ (V_2HPA)

Sodium metavanadate (4.06gm, 33.29 mmol) was dissolved by boiling in 16.6 ml water and then mixed with a solution of sodium phosphate dibasic dodecahydrate (1.18 gm, 3.29 mmol) in 16.6 ml water. To the cooled solution was added 0.83 ml of concentrated sulfuric acid. The resulting solution developed a red color. Addition of sodium molybdate dihydrate (20.16 gm, 83.32 mmol) in 50 ml water was then done. While the solution was stirred vigorously 14.16 ml of concentrated sulfuric acid was added slowly and then the hot solution was cooled to room temperature. The title compound was then extracted with four fractions each of 20 ml diethyl ether in a separating funnel. The heteropoly acid was present as the etherate in the bottom layer. This layer was isolated and dried in order to make it ether free. Orange colored solid was obtained after complete drying. Pure complex was obtained after recrystallization in water. The crystals that formed were dried and crushed for further use.

3.2.4.3 Trivanadomolybdophosphoric acid, $H_6PMo_9V_3O_{40}$ (V_3HPA)

Sodium phosphate dibasic dodecahydrate (1.77 gm, 4.95 gm) was dissolved in 12 ml water. Sodium metavanadate (9.15 gm, 75.04 mmol) was made soluble by boiling in 50 ml water. The sodium phosphate solution was mixed with the sodium metavanadate solution. The resulting solution was cooled, followed by the addition of 1.25 ml of concentrated sulfuric acid. This red colored solution was then added to a solution of sodium molybdate dihydrate (13.62 gm, 56.3 mmol) in 37.5 ml water. This solution was stirred vigorously and simultaneously 21.25 ml of concentrated sulfuric acid was added. The hot solution was cooled to ambient conditions. The heteropoly acid formed was extracted with four fractions, each of 25 ml diethyl ether in a separating funnel. The heteropoly acid is present as the etherate in the middle fraction. The middle layer was then isolated, dried to free of ether. The resulting red colored solid obtained was dissolved in water, concentrated to first crystal formation and allowed to crystallize further. The red crystals that formed were dried and powdered prior to further use.

3.2.5 Anchoring of vanadomolybdophosphoric acids onto NH_2-SBA

Freshly activated NH_2-SBA (0.9 g) was added 50 ml of acetonitrile solution containing 0.1 g of vanadomolybdophosphoric acids (V_xHPA, x: 1, 2 or 3) and refluxed for 3 h. The sample was then filtered, washed, and soxhleted using acetonitrile solvent for 12 h and dried at 100°C under vacuum. The final materials are designated as NH_2- SBA-V_xHPA (x: 1, 2 or 3). The nitrogen elemental analysis estimated 2.1 mmol of NH_2 per gram of NH_2-SBA-V_1HPA. Vanadium content estimated by ICP-OES and was 0.24 ppm for NH_2-SBA-V_1HPA.

3.2.6 Characterization

SAXS pattern of the samples was obtained in reflection mode using a Rigaku D_{max} 2500 diffractometer and Ni filtered copper radiation. The samples were scanned in the range 2θ = 0.5 - 6 and the generator was operated at 40 kV and 150 mA. Nitrogen adsorption measurements were measured on a NOVA 1200 (Quantachrome) at 77 K. First the samples were activated at 453 K for 3 h under vacuum and then the adsorption-desorption was conducted by passing N_2 into the sample, which was kept under liquid nitrogen. The specific surface area of the samples were calculated using

the multiple-point Brunauer-Emmett-Teller (BET) method in the relative pressure range P/P_0 = 0.05-0.3. The pore size distribution curves were computed by using the Barrett-Joyner-Halenda (BJH) method. The pore sizes were obtained from the peak positions of the distribution curves. Thermal analysis was performed on a Seiko model instrument (TG DTA 32) and the thermograms recorded at a heating rate of 10°C min^{-1} from 30 to 600°C under nitrogen atmosphere.

The elemental analysis (C and N) was carried out with an EA 1108 Elemental Analyser (Carlo Erba Instruments). V and Mo contents were estimated by ICP (Perkin Elmer Plasma 1000 Emission Spectrometer). The FT-IR spectra for the powdered samples were obtained over a range of 4000 - 400 cm^{-1} on a Shimadzu FT-IR 8201 PC and the spectra were recorded as a mull in fluorolube for the region 4000 - 1350 cm^{-1} and as a nujol mull for 1350 - 400 cm^{-1} range. UV-visible spectra were recorded on a Shimadzu UV-visible spectrophotometer (UV-2500 PC). High-resolution NMR studies were carried out on a Bruker DRX-500 MHz spectrometer. ^{31}P NMR chemical shifts were referenced to external phosphoric acid and ^{51}V chemical shifts were referenced to VOCl$_3$. SEM pictures of the samples were recorded on a JEOL-JSM-5200 scanning electron microscope with a resolution of 5.5 nm. Room-temperature EPR spectra were recorded on a Bruker EMX X-band spectrometer operating at 100 kHz field modulation at microwave frequency, 9.766 GHz. The microwave frequency was calibrated using a frequency counter of the microwave bridge ER 041 XGD. Bruker Simfonia and WINEPR software packages were used in the spectral simulations and to calculate hyperfine coupling constant.

3.2.7 Catalytic activity

All the reactions were carried out in a glass reactor at 60°C in acetonitrile solvent. Typically 0.01 mol of substrate and 0.01 mol of aqueous hydrogen peroxide (30%) were taken in 10 ml of solvent and the catalyst, 1 g NH$_2$- SBA-V$_x$HPA (1 g contains 5 μmol of V content) where, (x: 1, 2 or 3) was added. The reaction mixture was stirred constantly at the required temperature and was subjected to GC analysis (SPB^{TM}-5, 30m x 0.53mm, 3.0μm film thickness Supelco fused silica capillary column, N$_2$, FID, internal standard-chlorobenzene) periodically to monitor the conversion of the substrate and selectivity of the products. In the case of the immobilized sample, amount of catalyst containing 5 μmol of V content was taken for

the reaction. After the reactions, the immobilized catalyst was removed by careful filtration, washed several times with acetonitrile, dried in air and reused. Reactions were also carried out by adding 10 mg of neat V_xHPA as the catalyst for comparison.

3.3 Results and Discussions

3.3.1 Synthesis and Characterization

The Keggin structure of the vanadomolybdophosphoric acids was confirmed by FT-IR spectroscopy. The major FT-IR peaks were: 1060 cm^{-1} for P-O$_I$-Mo, 960 cm^{-1} for Mo=O$_t$ and 807 cm^{-1} and 783 cm^{-1} for Mo-O$_b$-Mo, where O$_I$, O$_t$ and O$_b$ are the inner, terminal and the bridging oxygen atoms respectively, in the Keggin anionic framework [13]. The water of crystallization was determined by thermo gravimetric analysis and was found to be 19, 14 and 14 for $H_4PMo_{11}VO_{40}$, $H_5PMo_{10}V_2O_{40}$ and $H_6PMo_9V_3O_{40}$ respectively. The UV-visible spectrum of the catalysts in acetonitrile showed absorption maxima at 218 and 308 nm, which are typical for the Keggin structure. These bands are due to the ligand to metal charge transfer transitions associated with octahedrally coordinated Mo^{6+} unit [13].

Amine functionalization of SBA-15 and the subsequent immobilization of molybdovanadophosphoric acids onto the mesoporous support are shown as a schematic representation in Figure 1. Vanadium substituted heteropoly acid samples were orange to red in color and the color becomes nearly colorless during the immobilization procedure. The combined filtrate after washing and soxhleting was subjected to UV-visible analysis and did not show any characteristic bands for molybdovanadophosphoric acids, possibly indicating retention of V_xHPA in the pores of NH$_2$-SBA. The ICP analysis of immobilized samples supports the above observation.
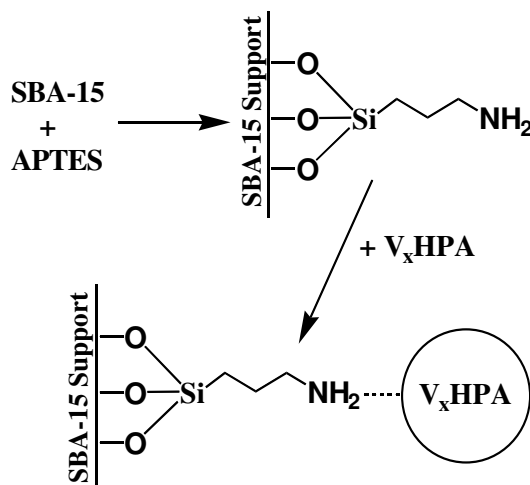
Figure 1: Schematic representation of functionalization of SBA-15 and the subsequent heterogenization of molybdovanadophosphoric acid (VHPA) on amine functionalized SBA-15

The small angle X-ray scattering (SAXS) patterns for SBA-15, NH_2-SBA and NH_2-SBA-V_xHPA (x: 1, 2 or 3) are depicted in Figure 2. Three reflections, one strong reflection at (100) and two with low intensity at (110) and (200) planes, are seen in the range $2\theta = 0.9$-$2.0°$ for all the samples, indicating retention of long-range order structure and well-formed hexagonal pore arrays. The d_{100} positions are similar for all the samples that probably indicate the structural ordering of SBA-15 is not affected upon modification with APTES, and on anchoring with V_xHPA. A small reduction in intensity of reflection (100) was noticed for the immobilized samples compared to pure SBA-15 and NH_2-SBA indicating anchoring of V_xHPA has indeed occurred inside the pores of SBA-15 [20, 23].
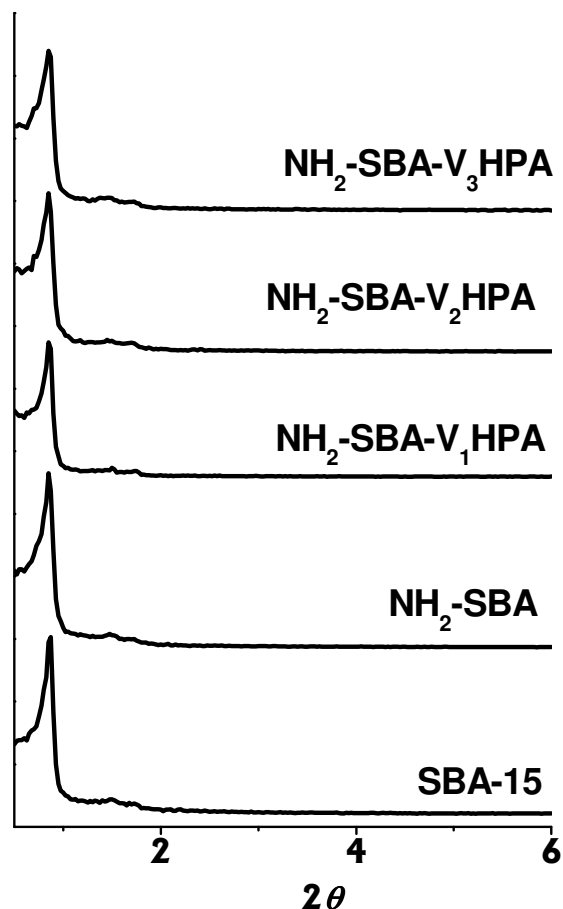
Figure 2: SAXS patterns of (a) SBA-15, (b) NH$_2$-SBA and (c) NH$_2$-SBA-V$_1$HPA, (d) NH$_2$-SBA-V$_2$HPA and (e) NH$_2$-SBA-V$_3$HPA

The nitrogen sorption isotherms for SBA, NH$_2$-SBA and NH$_2$-SBA-V$_1$HPA samples were carried out by BET method at 77 K. The parameters calculated from nitrogen adsorption data using the BJH method are listed in Table 1. The isotherm patterns of these samples display a type IV isotherm with H1 hysteresis and a sharp increase in volume adsorbed above $P/P_0 \sim 0.7$ which is characteristic of highly ordered mesoporous materials and are depicted in Figure 3. The textural properties of SBA-15 are substantially maintained over amine functionalization and on subsequent immobilization of V$_1$HPA. Surface area of SBA-15 has reduced from 859 m^2/g to 365 $\pm$ 15 m^2/g on amine functionalization and upon anchoring the V$_x$HPA [23, 24]. Similarly there was a reduction in pore volume on functionalization and on loading of V$_x$HPA compared with that of the pure SBA-15. These observations indirectly

confirm the anchoring of V_1HPA onto NH_2-SBA. The reduction in surface area and pore volume might be due to the filling of pores by bulkier trisiloxypropyl amine group and the heteropoly acid anions. The BJH pore size distribution curves (Figure 3, inset) derived from the desorption isotherm were similar for all the samples. The observation of similar pore size distribution for all the samples again indicates the integrity of ordered pore structure.

Table 1: Structural properties of SBA-15, NH_2-SBA and NH_2-SBA-VHPA samples characterized by N_2 adsorption

Samples	S_{BET} (m^2/g)	Total pore volume (cm^3/g)	Average pore diameter (nm)
SBA-15	859	1.10	8.9
NH_2-SBA	360	0.64	7.1
NH_2-SBA-V_1HPA	347	0.60	6.9
NH_2-SBA-V_2HPA	349	0.62	6.7
NH_2-SBA-V_3HPA	348	0.60	6.8
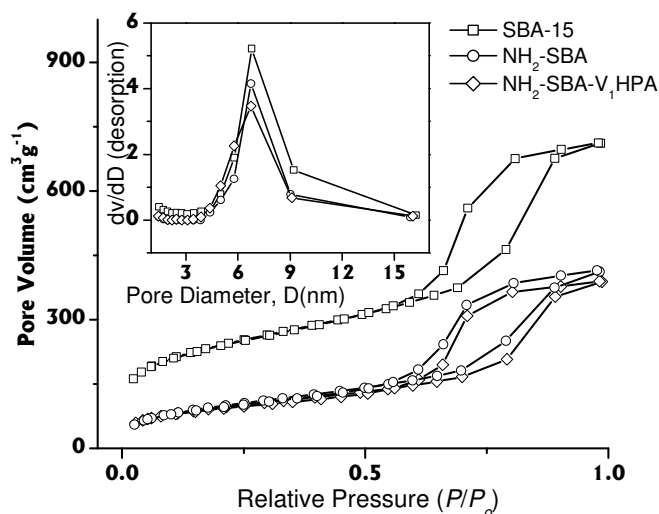
Figure 3: Nitrogen adsorption-desorption isotherms for (a) SBA-15, (b) NH_2-SBA and (c) NH_2-SBA-V_1HPA (Inset: Effective pore distribution of the above samples)

The SEM images of SBA (A), NH$_2$-SBA (B) and NH$_2$-SBA-V$_1$HPA samples (C) are shown in Figure 4 and the images are similar to the reported ones [25-27]. SEM images of other two vanadium loadings were also similar. The images of all the samples show hexagonal particles organized into rope-like structures, which are further agglomerated into elongated particles.

| A | B | C |
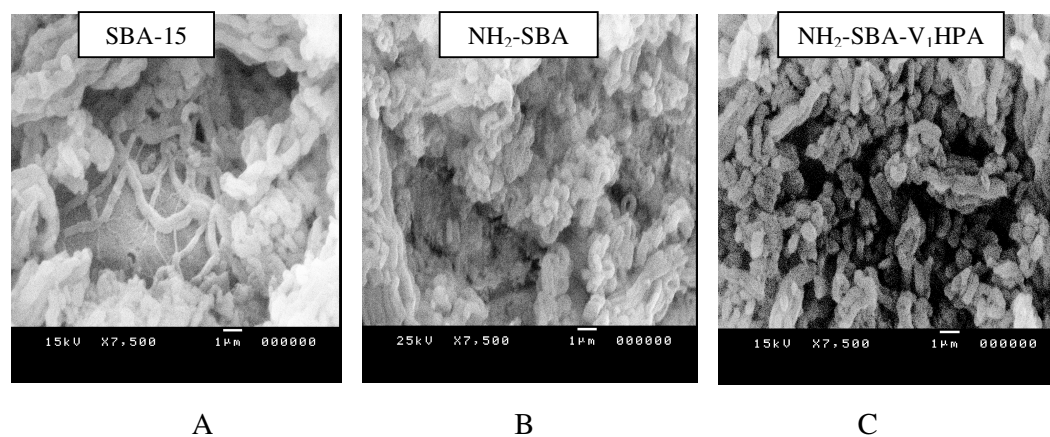
Figure 4: SEM images of (A) pure SBA-15, (B) NH$_2$-SBA and (C) NH$_2$-SBA-VHPA

3.3.2 Spectroscopic studies

Anchoring of V$_x$HPA on NH$_2$-SBA was investigated by different spectroscopic tools. The FT-IR spectra of NH$_2$-SBA, NH$_2$-SBA-V$_1$HPA and neat V$_1$HPA are compared as can be seen in Figure 5 [20]. Neat V$_1$HPA show peaks 1059, 958, 873, 722 cm^{-1}, characteristic of phosphomolybdic acid. Since most of the FT-IR bands of NH$_2$-SBA sample (1059, 958, 800 cm^{-1}) overlap with that of the neat V$_1$HPA, the bands associated with heteropoly unit were not clearly noticed in FT-IR spectrum of NH$_2$-SBA-V$_1$HPA. However, increase in intensity of bands at 800, 958 and 1059 cm^{-1} and appearance of a new shoulder at 894 cm^{-1} in NH$_2$-SBA-V$_1$HPA with respect to that of NH$_2$-SBA may be considered as an indication for the presence of V$_1$HPA in the pores of NH$_2$-SBA [13].
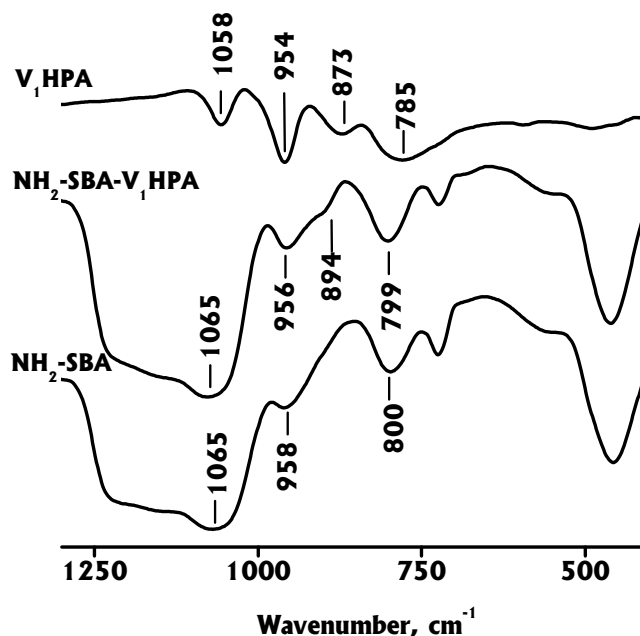
Figure 5: FT-IR spectra of (A) pure VHPA, (B) NH$_2$-SBA-VHPA and (C) NH$_2$-SBA

Similarly, V$_x$HPA samples show characteristic UV-visible bands and therefore their existence in SBA-15 can be identified by UV-visible spectroscopy. While SBA-15 and NH$_2$-SBA do not show any characteristic peaks in 220-400 nm region, NH$_2$-SBA-V$_x$HPA samples exhibit features of metal to ligand charge transfer transitions in this region as shown in Figure 6. These bands are compared with that of the neat V$_1$HPA (Figure 6, inset) which exhibits characteristic bands around 320 and 479 nm. Upon immobilization these bands are slightly shifted and broad features are seen at 348 and 451 nm. Some bands are shown in expanded scale for clarity. The presence of these bands indicates the occupation of V$_x$HPA in the pores of NH$_2$-SBA and small shifts in wavelength of these bands should be due to constraints around the heteropoly anion and/or due to its interaction with NH$_2$-SBA.

85
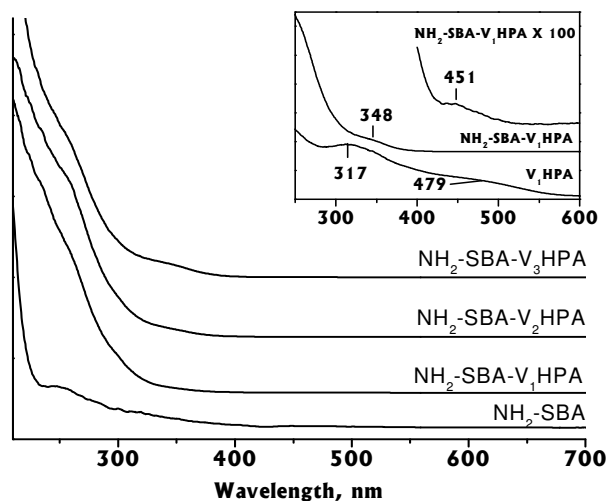
Figure 6: Diffuse reflectance UV-Visible spectra of NH_2-SBA-V_1HPA and neat V_1HPA

Additional evidence for the immobilization of V_xHPA on the amine functionalized SBA was showed by ^{31}P-NMR. ^{31}P MAS NMR spectrum was recorded for NH_2-SBA-V_1HPA as a representative sample and compared with neat V_1HPA sample in Figure 7. A ^{31}P signal was seen for the neat V_1HPA at -4.9 ppm and it was shifted to 1.85 ppm for NH_2-SBA-V_1HPA. Due to the extreme sensitivity of ^{31}P nucleus to its local environment, any slight changes in the chemical environment due to the interaction between the support and V_1HPA could have caused the difference. The difference in the chemical shift can also be due to the difference in degree of hydration of V_1HPA upon immobilization as it is known that ^{31}P NMR signal of the heteropoly acid anion is sensitive to degree of hydration [28-30]. Thus, the above spectral studies along with the small-angle X-ray and surface studies clearly provide evidence for the presence of V_xHPA inside NH_2-SBA.
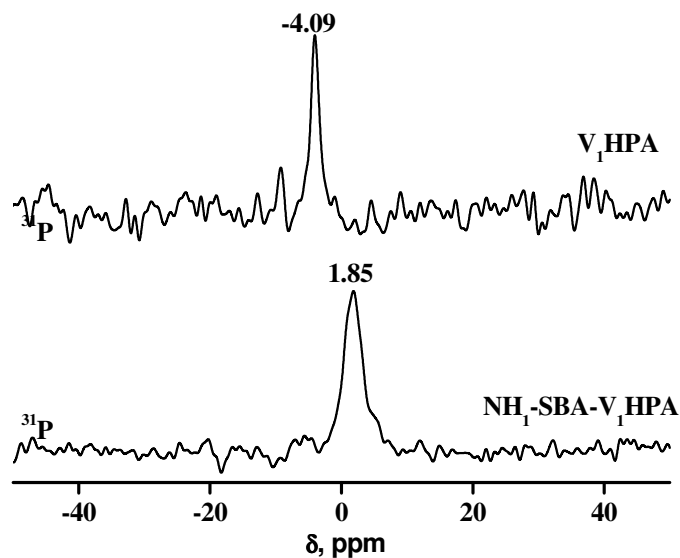
Figure 7: ^{31}P MAS NMR spectra of neat V_1HPA and NH$_2$-SBA-V$_1$HPA samples.

3.3.3 Catalytic activity and catalyst recycling

Vanadomolybdophosphoric acids are active catalysts (mostly as neat catalysts) for the selective oxidation of several organic substrates with peroxides as oxidants [31-32]. In the present work, catalytic activity of vanadomolybdophosphoric acids immobilized on the functionalized mesoporous material, NH$_2$-SBA-V$_x$HPA (x =1-3), were examined for oxygenation of cyclooctene and norbornene with oxidants in aqueous (aq. H$_2$O$_2$) and non-aqueous (TBHP/DCE) medium. Reactions with the neat V$_x$HPA (homogeneous) catalysts were also carried out with both the oxidants under the same experimental conditions and the results are compared with the respective immobilized catalysts (NH$_2$-SBA-V$_x$HPA).

In Figure 8, kinetic plots of cyclooctene conversion of the reactions with aq. H$_2$O$_2$ and TBHP/DCE in acetonitrile are given for V$_1$HPA, V$_2$HPA and V$_3$HPA catalysts. The reactions were carried out for 5 h as there after not much appreciable conversion was noticed. For V$_1$HPA the conversion of cyclooctene with aq. H$_2$O$_2$ was gradual and steady with time and reached around 42 % after 5 h of reaction time. However, with the other two catalysts the conversions were faster, especially with V$_3$HPA in the beginning and reached a steady state at lower conversions compared to

V_1HPA. These observations suggest faster decomposition of aq. H_2O_2 with higher vanadium contents (as noticed by the effervescence soon after the addition of H_2O_2). In other words, the dismutation reaction of H_2O_2 which leads to formation of O_2 and H_2O dominates the V-oxo species formation. It should be noted here that the V-oxo species is responsible for the formation of desired products.
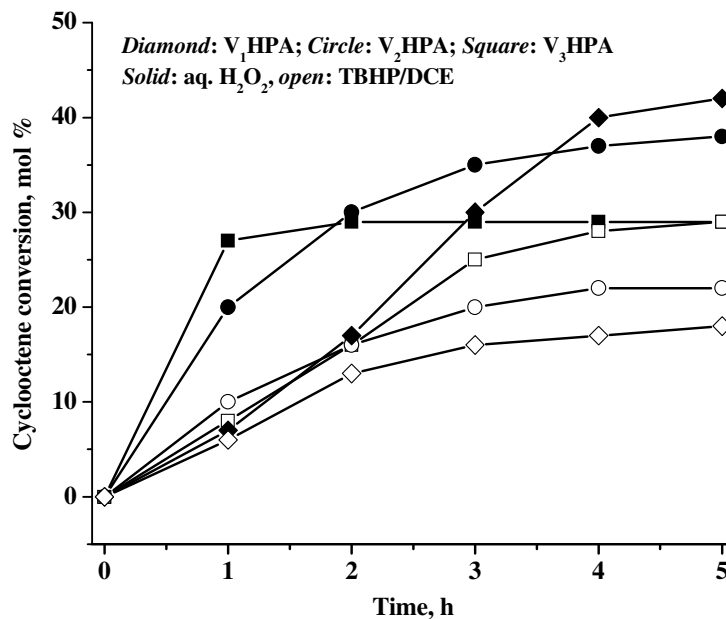
Figure 8: Reaction profiles of cyclooctene oxidation with aq. H_2O_2 and TBHP/DCE with the neat catalysts V_xHPA. Reaction condition: catalyst = 100 mg; cyclooctene = 0.01 mol; aqueous H_2O_2 /TBHP/DCE = 0.01 mol, 60 °C, acetonitrile

With the TBHP/DCE, the reverse trends were observed i.e. conversions are higher with higher amounts of vanadium contents though the overall conversions with TBHP/DCE were lower than that of the reactions with aq. H_2O_2. The lower conversion with TBHP should be due to slow decomposition of peroxides. However, here it should be noted that epoxide was only the product with TBHP/DCE but with aq. H_2O_2 apart from cyclooctene epoxide as a major product, other minor products such as cyclooctanol and cyclooctanone were also observed (Table 2). Formation of cyclooctanol is due to acid catalyzed reaction by protons coming from aq. H_2O_2

decomposition and subsequent secondary oxidation of cyclooctanol by the redox center leads to cyclooctanone (Scheme 1). Such acid catalyzed reaction may not be possible with TBHP decomposition.
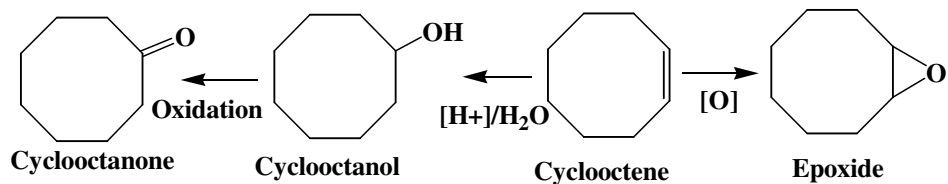
Scheme 1 Different possible products during cyclooctene oxidation reaction catalyzed by $H_4[PMo_{11}VO_{40}]$ in the presence of aq. H_2O_2

The above reactions were also tested with the heterogenized catalysts (NH_2-SBA-V_xHPA) with aq. H_2O_2 and TBHP/DCE in acetonitrile solvent. The reactions with TBHP/DCE were found to be slow due to slow decomposition of TBHP and so they were monitored for 12 h while reactions with aq. H_2O_2 were monitored for 5 h. The results (Table 2) show that epoxide was the only product for the both the oxidants. It may be noted here that the products were non-selective with the neat catalysts when aq. H_2O_2 was used. Absence of alcohol or ketone formation with the immobilized catalysts might be due to the non-availability of protons (which are responsible for alcohol formation) in the presence of NH_2-SBA. Thus epoxide was the only product.

Table 2-*A*: Oxidation of cyclooctene and norbornene with aq. H_2O_2 and TBHP/DCE using the neat (V_1HPA) and heterogenized (NH_2-SBA-V_1HPA) catalysts

Substrate	Oxidant	V_1HPA		NH_2-SBA-V_1HPA	
		% Conv.	Products (% Selectivity)	*%* Conv.	Products (% Selectivity)
Cyclooctene	H_2O_2	42	Epoxide(75)	21	Epoxide (>99)
			Cyclooctanol (13)		
			Cyclooctanone (12)		
	TBHP	18	Epoxide (>99)	34	Epoxide (>99)
				32*	Epoxide (>99)*
Norbornene	H_2O_2	70	Epoxide (58)	50	Epoxide (>99)
			Norborneol(17)		
			Norbornanone(25)		
	TBHP	32	Epoxide (>99)	40	Epoxide (>99)
				38*	Epoxide (>99)*

***Reaction conditions*:** V_1HPA catalyst: 5 μM, NH_2-SBA-V_1HPA (corresponding to 5 μM of heteropoly anion): 100 mg, substrate: 0.01 mol, aq. H_2O_2: 0.01 mol, TBHP/DCE: 0.01 mol, acetonitrile (10 ml), 60°C, time: 5 h (Reaction time with TBHP/DCE: 12 h), *: recovered catalyst (second run)

Table 2-*B*: Oxidation of cyclooctene and norbornene with aq. H_2O_2 and TBHP/DCE using the neat (V_2HPA) and heterogenized (NH_2-SBA-V_2HPA) catalysts

Substrate	Oxidant	V_1HPA		NH_2-SBA-V_1HPA	
		% Conv.	Products (% Selectivity)	*%* Conv.	Products (% Selectivity)
Cyclooctene	H_2O_2	38	Epoxide(70)	25	Epoxide (>99)
			Cyclooctanol (18)		
			Cyclooctanone (12)		
	TBHP	22	Epoxide (>99)	26	Epoxide (>99)
				25*	Epoxide (>99)*
Norbornene	H_2O_2	51	Epoxide (55)	32	Epoxide (>99)
			Norborneol(20)		
			Norbornanone(25)		
	TBHP	26	Epoxide (>99)	30	Epoxide (>99)
				28*	Epoxide (>99)*

***Reaction conditions*:** V_2HPA catalyst: 5 µM, NH_2-SBA-V_2HPA (corresponding to 5 µM of heteropoly anion): 100 mg, substrate: 0.01 mol, aq. H_2O_2: 0.01 mol, TBHP/DCE: 0.01 mol, acetonitrile (10 ml), 60°C, time: 5 h (Reaction time with TBHP/DCE: 12 h), *: recovered catalyst (second run)

Table 2-C: Oxidation of cyclooctene and norbornene with aq. H_2O_2 and TBHP/DCE using the neat (V_3HPA) and heterogenized (NH_2-SBA-V_3HPA) catalysts

Substrate	Oxidant	V_1HPA		NH_2-SBA-V_1HPA	
		% Conv.	Products (% Selectivity)	*%* Conv.	Products (% Selectivity)
Cyclooctene	H_2O_2	29	Epoxide(60)	22	Epoxide (>99)
			Cyclooctanol (22)		
			Cyclooctanone (18)		
	TBHP	29	Epoxide (>99)	24	Epoxide (>99)
				22*	Epoxide (>99)*
Norbornene	H_2O_2	45	Epoxide (55)	30	Epoxide (>99)
			Norborneol(22)		
			Norbornanone(23)		
	TBHP	21	Epoxide (>99)	29	Epoxide (>99)
				27*	Epoxide (>99)*

Reaction conditions: V_3HPA catalyst: 5 μM, NH_2-SBA-V_3HPA (corresponding to 5 μM of heteropoly anion): 100 mg, substrate: 0.01 mol, aq. H_2O_2: 0.01 mol, TBHP/DCE: 0.01 mol, acetonitrile (10 ml), 60°C, time: 5 h (Reaction time with TBHP/DCE: 12 h), *: recovered catalyst (second run)

To check the possibility of leaching of the active sites, the catalyst part was separated after 2 h of cyclooctene oxidation reaction with aq. H_2O_2 at the experimental condition and the filtrates containing reaction mixture were then allowed to continue further under the same experimental conditions. Conversions were monitored periodically and the results are plotted in Figure 9. As seen in the figure, with NH_2-SBA-V_1HPA the progress of the reaction was negligible after filtering the catalyst. The ICP analysis results indicate < 1.1 % of vanadium leaching (out of total amount of vanadium taken) into the solution when aq. H_2O_2 was used. Similar leaching experiments were carried out with NH_2-SBA-V_3HPA and it was found that the progress of reaction after filtering off the catalyst was almost same as that in the

presence of the NH_2-SBA-V_3HPA (Figure 9). The results simply indicate that the leaching of vanadium content was higher with the catalysts having higher vanadium loadings, however, selectivity of the product remains high i.e. cyclooctene epoxide was the only product. The reason for the high selectivity can be explained as discussed above.
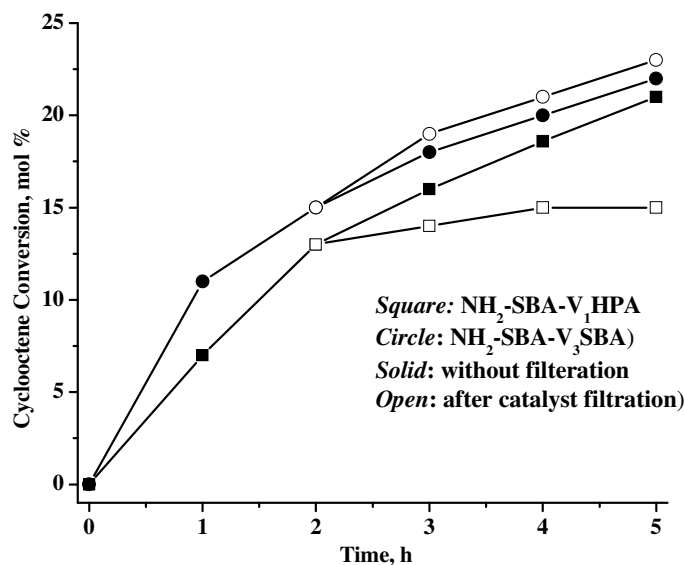
Figure 9: Reaction profiles of cyclooctene oxidation reactions with aq. H_2O_2 in the presence of NH2-SBA-V_1HPA and of NH_2-SBA-V_3HPA without filtration of the catalyst and after filtration of the catalyst at 2 h of reaction

Similar leaching experiments were also carried out with NH_2-SBA-V_xHPA (x: 1, 2 or 3) when TBHP/DCE oxidant was used under identical experimental condition. Slow decomposition of TBHP indicates the reactions are diffusion controlled due to the bulkiness of *t*-butyl group of TBHP. Leaching of vanadium was found to be negligible (< 0.2 % of total vanadium used) with all the three catalysts namely NH_2-SBA-V_xHPA (x: 1, 2 or 3) and the reaction results are given in Table 2. The reusability of the heterogenized catalyst was tested as follows: after 12 h of cyclooctene oxidation reaction, the NH_2-SBA-V_xHPA catalysts were filtered from the reaction mixture, washed with acetonitrile, dried in air and reused for the fresh reaction under identical experimental conditions. This cycle was repeated twice and the results are given in Table 2. It was found that with the recycled catalyst the conversion was bit low, however, selectivity remains very high.

The catalysts were also tested for oxidation of another substrate, norbornene, with the neat as well as the immobilized catalyst using both aq. H_2O_2 and TBHP/DCE oxidants and the results are give in Table 2. As seen in the table, with aq. H_2O_2 the neat catalysts always lead to multiple products formation with high conversion of substrates due the fast decomposition of H_2O_2. The formation of the minor products like norborneol and 2-norbornanone apart from the main product *i.e.* norbornene epoxide, can be explained due to the acidic nature associated with aq. H_2O_2 decomposition as discussed above. However, epoxide was the only product when TBHP/DCE was used. The norbornene oxidation reactions were also carried out with the anchored catalysts, NH_2-SBA-V_xHPA, with aq. H_2O_2 as well as TBHP/DCE oxidants and it was found that norbornene epoxide was the only product. The results are summarized in Table 2.

3.3.4 Reaction mechanism for neat V_xHPA

3.3.4.1 UV-visible spectroscopy

In our further studies, an attempt was made to propose the plausible mechanism of the reaction based on the UV-visible, ^{51}V NMR and EPR results, as seen below. Since amongst the three neat V_XHPA catalysts, V_1HPA was the most active catalyst for the epoxidation reactions, only V_1HPA was considered for the detailed mechanistic studies, over aq. H_2O_2 as the oxidant. For V_2HPA and V_3HPA catalysts, we expect a similar kind of mechanism.

A small amount of the reaction mixture was drawn periodically during the course of the reaction and was monitored by UV-visible spectroscopy in 200 - 900 nm region. Acetonitrile solution of the pure catalyst exhibits a characteristic band at around 308 nm (Figure 10, a) with a long tail at higher wavelength, which is associated with the ligand-metal transfer transitions. The above broad band is deconvoluted into two bands viz. a strong band at 308 nm and a weak one at 355 nm (Figure 10, dashed lines), and the line-width of both the bands are about 50 nm. Upon addition of aq. H_2O_2 (trace, b) or alkene + aq.H_2O_2 (trace, c) to the above catalyst, a distortion in the shape or line width could be noticed in the LMCT band, indicating the changes in the environment around heteropoly anion. However, the bands are not resolved enough to be noticed clearly to extract any further information. Similar was the case with the trace (d) and (e) in figure 10 corresponding to reaction mixtures at different reaction times.

V^{4+} ions with d^1 configuration are expected to show a *d-d* band around 750 nm; however, V^{5+} ions with no electron in d-orbital do not show any such a band [33-34]. A broad band around 750 nm was seen for acetonitrile solution of the pure catalyst (Figure 10, inset a) indicating that part of vanadium is in 4+ oxidation state as also evidenced by EPR spectroscopy as seen further. However, it is interesting to note that upon addition of aq. H_2O_2 the broad *d-d* band vanishes (Figure 10, inset b). This may indicate that the V^{4+} ions are oxidized to V^{5+} during the reaction. However, not much information could be obtained from UV-visible studies about the vanadium-peroxide interaction.
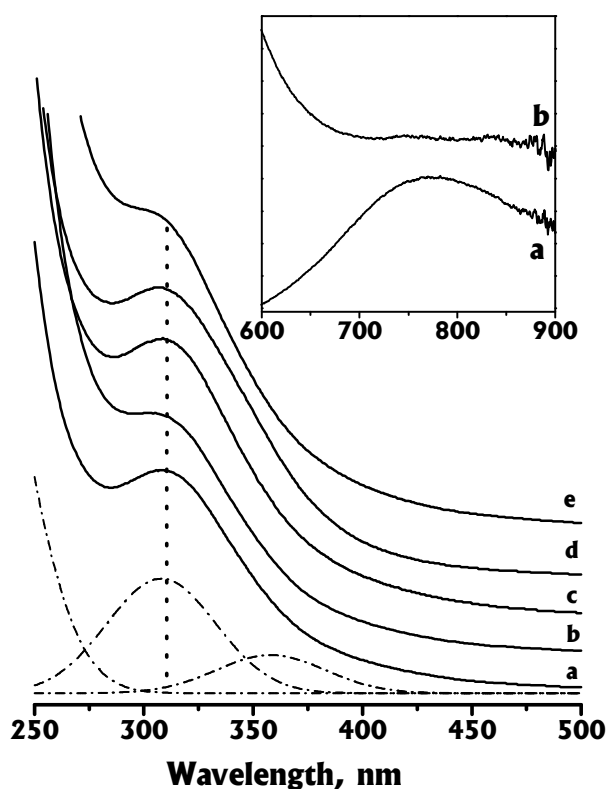
Figure 10: UV–visible spectra of LMCT region for (a)$H_4[PMo_{11}VO_{40}]$ in acetonitrile solution, (b) catalyst + aq. H_2O_2 in acetonitrile, (c) catalyst + norbornene in acetonitrile, reaction mixture at (d) 0.5 h and (e) 2 h (Deconvoluted bands of spectrum of (a) are given in dashed lines). (Inset: d–d band region for (a) $H_4[PMo_{11}VO_{40}]$ in acetonitrile solution, (b) $H_4[PMo_{11}VO_{40}]$ + aq. H_2O_2 in acetonitrile)

3.3.4.2 ^{51}V *NMR spectroscopy*

^{51}V NMR spectroscopy was used to gain information on the possible catalytic intermediates formed during alkene oxidation reactions. ^{51}V NMR spectra of pure $H_4[PMo_{11}VO_{40}]$ in acetonitrile solution, of $H_4[PMo_{11}VO_{40}]$ treated with aq. H_2O_2 (in acetonitrile) and of the reaction mixture are shown in Figure 11. The pure sample mainly shows a single peak at -540.1 ppm (Figure 11, bottom) indicating all the five isomers of $H_4[PMo_{11}VO_{40}]$ are not resolved in acetonitrile solvent [35]. There are other tiny peaks around −548 ppm most probably due to the presence of other isomers in small amount, or any vanadyl species. However, upon addition of aq. H_2O_2, a set of three broad signals appeared in the upfield positions at -640.8, -651.3, -671.6 ppm (Figure 11, center). This large upfield chemical shift can be attributed to $H_4[PMo_{11}VO_{40}]$-peroxo compounds as discussed in the case of hydrogen peroxide-treated $H_4[PMo_{10}V_2O_{40}]$ species in acetic acid [36], and no strong peaks were seen around -540 ppm except a small peak at -534.5 ppm. However, for the reaction mixture ($H_4[PMo_{11}VO_{40}]$ + aq. H_2O_2 + alkene in acetonitrile), the upfield broad bands disappeared but a narrow signal at -529 ppm (figure 11, top) was exhibited along with a peak with lower intensity at -548.1 ppm.

Disappearance of the broad upfield peaks on addition of alkenes (which is equivalent to the reaction mixture) and appearance of the narrow peak at around -548 ppm clearly indicates that the bound peroxide moiety is released from Keggin unit and the heteropoly anion unit has retained its structure after completion of the reaction. The small downfield shift of ^{51}V NMR signal for the reaction mixture compared with that of pure catalyst sample may be an indication of small structural changes like different degrees of hydration around the vanadium centers.
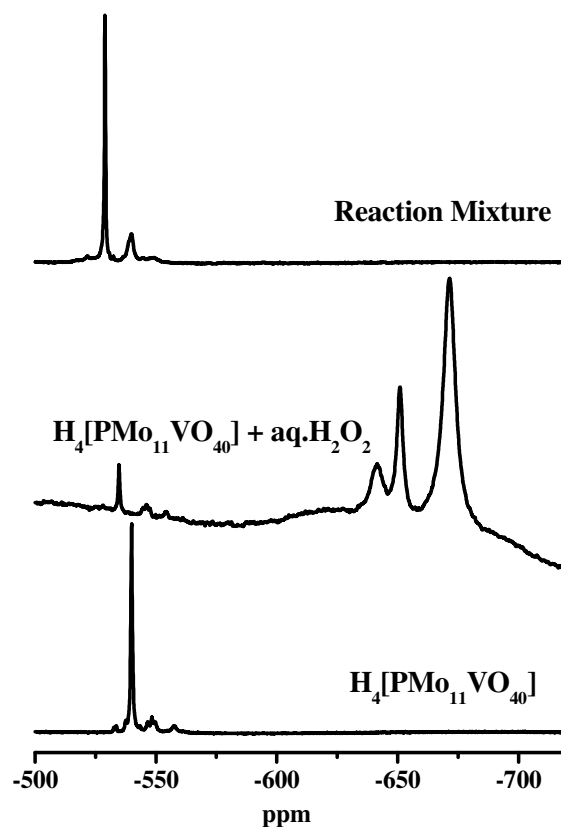
Figure 11: ^{51}V NMR spectra at room temperature for (a) H$_4$[PMo$_{11}$VO$_{40}$] in acetonitrile solution, (b) H$_4$[PMo$_{11}$VO$_{40}$] + aq. H$_2$O$_2$ in acetonitrile and (c) reaction mixture at 0.5 h

3.3.4.3 EPR spectroscopy

EPR spectroscopy can be used to monitor V^{4+} ion and any paramagnetic transient species formed during the course of the reaction. In an effort to understand the reaction intermediates and to throw light on the reaction mechanism, a small amount of sample was drawn from the reaction mixture at different time intervals and EPR spectra were recorded after the sample was quenched at room temperature. To gain a better understanding, the EPR spectra of acetonitrile solution of the catalyst before and after addition of aq. H$_2$O$_2$ and the substrate were also recorded. Representative spectra of such experiments are given in Figure 12. The acetonitrile solutions of the pure catalyst at room temperature exhibits isotropic ^{51}V hyperfine lines (figure 12, top) due to the presence of trace amounts of V^{4+} ion species in the catalyst or alternatively due to the vanadyl counter cations. Bayer *et al* have reported

that a small quantity of vanadium is probably present as VO^{2+} ions outside the Keggin structure compensating for two H^+ ions viz. $(VO)^{2+}H_2[PMo_{11}VO_{40}]$ during the synthesis of $H_4[PMo_{11}VO_{40}]$ [37].

The EPR spectrum contains eight hyperfine lines pattern due to the interaction of paramagnetic electron of V^{4+} with its nucleus (I = 7/2). The Hamiltonian parameters of this species based on the computer simulation are: g_{iso} = 1.97 and A_{iso} = 109 G. A small difference between the eight different lines is noticed due to the second order hyperfine effect. Addition of aq. H_2O_2 to the above acetonitrile solution with or without the substrate leads to the disappearance of the V^{4+} signal instantaneously (Figure 12, center). This observation probably indicates that V^{4+} center is oxidized to V^{5+}. The vanadium ions generate V^{5+}-peroxo species (Scheme 2, species II) on interaction with H_2O_2, which may partly be in equilibrium with V^{4+}-superoxo species (Scheme 2, species III) [38].

Possibility for the presence of any other species like superoxo radical bound to V^{5+} may be ruled out as its characteristic EPR signals with small hyperfine value are not observed in the present work [39]. It is noteworthy here that the EPR of the above solution was measured subsequently at various time intervals and it was found that the solution remains EPR silent even after 24 h (Figure 12, bottom).
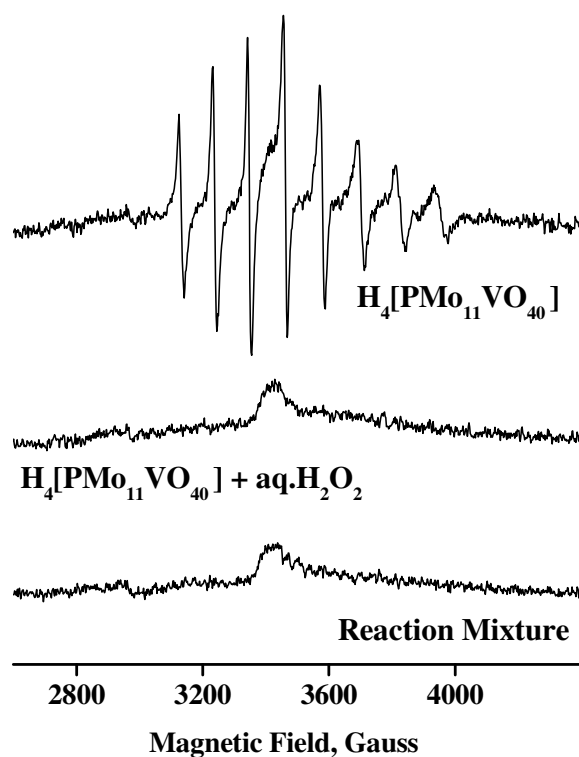
Figure 12: Room temperature EPR spectra of (a) $H_4[PMo_{11}VO_{40}]$ in acetonitrile, (b) $H_4[PMo_{11}VO_{40}]$ + aq. H2O2 in acetonitrile and (c) the reaction mixture at 0.5 h

3.3.4.4 Mechanism

Based on the catalytic studies, it is clear that the main products of norbornene or cyclooctene oxidation reaction with the V_xHPA catalyst are the corresponding epoxides and the minor products are the alcohols and ketones as can be seen in Table 2. Formation of epoxides along with hydroxylated products (alcohols) and ketones indicates that more than one mechanistic path ways are involved or subsequent reactions have proceeded after epoxide formations.

Absence of characteristic EPR signal of V^{5+}-peroxo species and appearance of upfield shift in ^{51}V NMR for the H_2O_2 interacted V_xHPA catalyst indicate that V^{5+}-peroxo (Scheme 2, species II) is the possible active intermediate species, which may partially be in equilibrium with V^{4+}-superoxo species (Scheme 2, species III). The V^{5+}-peroxo species might have formed via unstable V^{5+}-hydroxy-hydroperoxy species (Scheme 2, species I). A plausible reaction mechanism has been proposed in Scheme

2 [38]. The mechanism involves the formation of stable V^{5+}-peroxo species, as described in Scheme 2, which is partially in equilibrium with V^{4+}- superoxo radical transient species. This transient species then interacts rapidly with the alkenes to form the metallo-peroxy-alkene intermediate (Scheme 2, species IV). In the subsequent step, breakage of bonds between the oxygen atoms in this intermediate species leads to the formation of epoxides.

A mixture of corresponding alcohols and ketones are always seen as the side products in the oxidation reaction when aq. H_2O_2 is used as an oxidant (Table 2). The formation of hydroxylated products (alcohols) is due to the acid catalyzed hydration reaction with the alkenes (Scheme 1), where the acidity came from the protons formed upon H_2O_2 activation by the vanadium centers of the catalyst. The other minor products of ketones are formed by the oxidation of the alcohols (Scheme 1). Such acid catalyzed reaction may not be possible with TBHP decomposition. Thus, when TBHP was used as the oxidant, 100 % selectivity towards the epoxide was observed for both the alkenes, with all the three V_xHPA (x = 1, 2 or 3) catalysts (irrespective of whether used in a neat manner or in an anchored fashion) as can be seen in the Table 2.
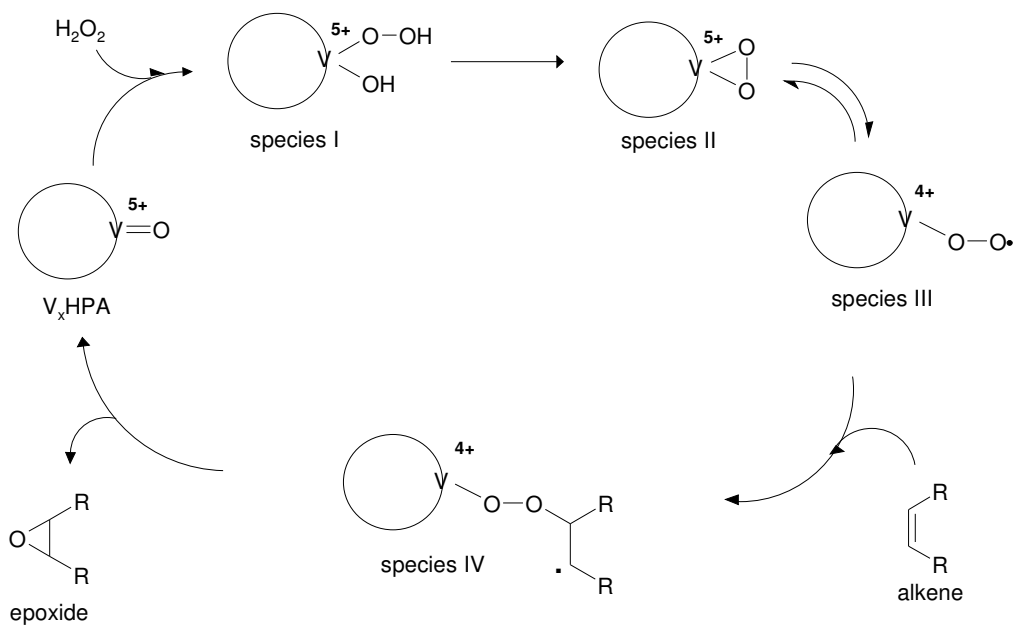
Scheme 2: A schematic representation of proposed reaction mechanism for the epoxidation of norbornene catalyzed by $H_4[PMo_{11}VO_{40}]$ in the presence of aq. H_2O_2. The heteropoly anion framework is represented as HPA. The bonds, which undergo changes, are alone shown for clarity

3.4 Summary and Conclusion

Vanadium substituted molybdovanadophosphoric acids (V_xHPA) were immobilized on amine functionalized SBA-15 and was characterized by different techniques. Small angle X-ray scattering analysis provides evidence for the structural integrity of the amine functionalized SBA even after immobilizing with molybdovanadophosphoric acid. The synthesized materials were also characterized by nitrogen sorption studies, UV-Visible, NMR, and IR studies provided evidence for the presence of V_xHPA inside the NH_2-SBA. The catalytic activity of the immobilized sample (NH_2-SBA-V_xHPA) were studied for few substrates with aqueous hydrogen peroxide at 60 °C and compared with the neat V_xHPA catalyst. It was found that selectivity of the products is higher with the immobilized catalyst. The catalyst part can be separated after the reaction and can be reused for few cycles without losing its further activity, especially with TBHP as the oxidant.

References

1. G. Ertl, H. Knozinger, J. Weitkamp (Eds.), *Handbook of Heterogeneous Catalysis*, Wiley–VCH, Weinheim, 1997.

2. H. Kosslick, I. Mönnich, E. Paetzold, H. Fuhrmann, R. Fricke, D. Müller and G. Oehme, Micropor. Mesopor. Mater. 44-45 (2001) 537.

3. D. C. Bailey and S. H. Langer, Chem. Rev. 81 (1981) 109.

4. D.E. De Vos and P. A. Jacobs, Catal. Today 57 (2000) 105.

5. M. J. Naughton and R. S. Drago, J. Catal. 155 (1995) 383.

6. J. P. Arhancet, M. E. Davis, J. S. Merola and B. E. Hanson, Nature 339 (1989) 454.

7. G. A. Ozin and C. Gil, Chem. Rev. 89 (1989) 1749.

8. R. Grommen, P. Manikandan, Y. Gao, T. Shane, J. J. Shane, R. A. Schoonheydt, B. M. Weckhuysen and D. Goldfarb, J. Am. Chem. Soc. 122 (2000) 11488.

9. E. Byambajav and Y. Ohtsuka, Appl. Catal. A: General 252 (2003) 193.

10. E. Brulé and Y. R. de Miguel, Tetrahedron Lett. 43 (2002) 8555.

11. L. C. Passoni, F. J. Luna, M. Wallau, R. Buffon and U. Schuchardt, J. Mol. Catal. A: Chemical 134 (1998) 229.

12. (a) A. M. Khenkin, R. Neumann, A. B. Sorokin and A. Tuel, Catal. Lett. 63 (1999) 189; (b) B. J. S. Johnson and A. Stein, Inorg. Chem. 40 (2001) 801.

13. K. Nowińska, R. Fórmaniak, W. Kaleta and A. Wąclaw, Appl. Catal. A. 256 (2003) 115.

14. X. -B. Lu, H. Wang and R. He, J. Mol. Catal. A: Chemical 186 (2002) 33.

15. A. Ghosh, C. R. Patra, P. Mukherjee, M. Sastry and R. Kumar, Micropor. Mesopor. Mater. 58 (2003) 201.

16. W. Kaleta and K. Nowińska, Chem. Commun. (2001) 535.

17. M. J. Verhoef, P. J. Kooyman, J. A. Peters, H. van Bekkum, Micropor. Mesopor. Mater. 27 (1999) 365.

18. K. Nowińska, W. Kaleta, Appl. Catal. A. Gen. 203 (2000) 91.

19. S. Zheng, L. Gao and J. Guo, J. Solid State Chem. 152 (2000) 447.

20. J. Horniakova, T. Raja, Y. Kubota, Y. Sugi, J. Mol. Catal. A. Chemical 217 (2004) 73.

21. P. Sutra, D. Brunel, Chem. Commun. (1996) 2485.

22. G. A. Tsigdinos and C. J. Hallada, Inorg. Chem. 7 (1968) 437.

23.   A. S. M. Chong, X. S. Zhao, J. Phys. Chem. B., 107 (2003) 12650.

24.   S. J. Gregg, K. S. W. Singh, Adsorption, surface area and porosity, 2nd Ed,; Academic Press, London, 1982.

25.   A. Lapkin, B. Bozkaya, T. Mays, L. Borello, K. Edler, B. Crittenden, Catal. Today, 81 (2003) 611.

26.   D. Zhao, J. Feng, Q. Huo, N. Melosh, G. H. Fredrickson, B. F. Chmelka, G. D. Stucky, Science 279 (1998) 548.

27.   M. -C. Chao, H. -P. Lin, H. -S. Sheu, C. -Y. Mou, Stud. Surf. Sci. Catal. 141 (2002) 387.

28.   A. G. Siahkali, A. Philippou, J. Dwyer, M. W. Anderson, Appl. Catal. A: General 192 (2000) 57.

29.   Y. Kanda, K.Y. Lee, S. Nakata, S. Asaoka, M. Misono. Chem. Lett. 1 (1988) 139.

30.   V. M. Mastikhin, S. M. Kulikov, A. V. Nosov, I. V. Kozhevnikov, I. L. Mudrakovsky, M. N. Timofeeva. J. Mol. Catal. 60 (1990) 65.

31.   R. Neumann, M. Cohan, Angew. Chem. Int. Ed. Engl. 36 (1997) 1738.

32.   K. Nomiya, K. Yagishita, Y. Nemoto, T. -A. Kamataki, J. Mol. Catal. A. Chemical 126 (1997) 43.

33.   A.M. Khenkin, A. Rosenberger, R. Neumann, J. Catal. 182 (1999) 82

34.   M. Kaliva, T. Giannadaki, A. Salifoglou, C.P. Raptopoulou, A. Terzis, V. Tangoulis, Inorg. Chem. 40 (2001) 3711

35.   S.E. O'Donnell, M.T. Pope, J. Chem. Soc., Dalton Trans. (1976) 2290

36.   R. Neumann, M. de la Vega, J. Mol. Catal, 84 (1993) 93

37.   R. Bayer, C. Marchal, F. X. Liu, A. Teze, G. Herve, J. Mol. Catal. A, 110 (1996) 65

38.   H. Mimoun, L. Saussine, E. Daire, M. Postel, J. Fischer, R. Weiss, J. Am. Chem. Soc. 105 (1983) 3101

39.   A.E. Gekhman, I.P. Stolarov, N.I. Moiseeva, V.L. Rubaijlo, M.N. Vargaftik, I.I. Moiseev, Inorg. Chim. Acta 275–276 (1998) 453

Chapter 4:

Alkene epoxidation catalyzed by vanadium heteropoly acids dispersed on hydrated titania

4.1 Introduction

Epoxides are one of the essential precursors for the synthesis of various important substances like plasticizers, perfumes, epoxy resins, etc, thus epoxidation reactions assume significant importance in the chemical industries. Many catalytic systems containing transition metal ions have been exploited for the epoxidation of alkenes in the past. In recent years, transition metal-substituted polyoxometalates based catalysts have gained considerable interest due to their multi versatilities for the oxidation of organic substrates [1-3]. Transition metal substituted polyoxometalates (TMSP) generally provide higher conversion and better selectivity for epoxides [4-7]. Amongst the TMSP, vanadium-substituted polyoxometalates are the most studied ones that have attracted the attention as catalysts for a variety of catalytic oxidation reactions like hydroxylation of benzene, oxidation of toluene and nitrobenzene with aqueous hydrogen peroxide, oxidation of isobutyric acid to methacrylic acid with molecular oxygen and so on [8-15].

Although, the activity of vanadomolybdophosphoric acids is well documented, most of the current examples demonstrate their catalytic applications as a homogenous catalyst [16-18]. Alternatively, they are heterogenized by anchoring them onto amine-functionalized SBA-15 and other mesoporous materials [19-20] or by impregnation on inert supports like silica, alumina or zirconia and further calcination at high temperatures [21-23]. The former strategy is generally applied for oxidation reactions while latter one is generally applied for acid catalyzed reactions. Both these methods have their own drawbacks like multi step synthesis of catalyst materials and time as well as energy consuming calcination steps respectively. So the simple strategy applied here was the wet impregnation of vanadomolybdophosphoric acids on a support and carry out the reactions in non-polar or hydrophobic solvents, so as to minimize the dissolution of these polar molecules and maintain the heterogeneity of the catalyst. Thus, in the current system vanadomolybdophosphoric acids were wet impregnated on two important support materials namely, $TiO_2.xH_2O$ or $ZrO_2.xH_2O$. After drying, these supported catalysts were tested for their activities in alkene epoxidation. Interestingly, amongst the two supports, titania supported vanadomolybdophosphoric acids showed a higher activity than the zirconia analogue. This higher activity of the former may be explained on the basis of the synergistic effect between heteropoly acid and the titania support, as we shall see further.

The mere wet-impregnation step of heteropoly acids on titania, however deprived us from using *aq.* H_2O_2 and *aq.* TBHP as oxidants, since the water component of these oxidants dissolves the heteropoly acids easily, thereby losing the heterogeneous behavior of these catalysts. Thus the oxidant used here was TBHP extracted in dichloroethane, or other hydrophobic solvents. This has refrained in having a comparative data of the catalytic activity with different oxidants for this system. Although the use of hydrophilic solvent like acetonitrile increased the catalytic activity as compared to the activity in dichloroethane, most of the heteropoly acid was lost due to its dissolution in the former. As a result the subsequent catalytic activity reduced drastically in further runs for such hydrophilic solvent systems. The dissolution of heteropoly acids in hydrophilic solvents may be the reason behind the initial higher activity displayed in the same. Although the additives like TBHP dissolve the heteropoly acid to some extent even in the dichloroethane solvent system, it is observed that there is not much loss in activity for next two subsequent runs, as shall be seen further. Importantly, in all the cases the major product was always the corresponding epoxide.

4.2 Experimental

4.2.1 Materials

Phosphomolybdic acid (PMA), phosphotungstic acid (PTA), titanium *t*-butoxide and zirconyl nitrate were purchased from Loba Chemie India Ltd. 1,2-dichloroethane, acetonitrile, methanol, ether and other solvents were procured from Merck India Ltd. All the alkenes were obtained from Aldrich, while 70% aqueous TBHP was obtained from Fluka. Sodium molybdate and sodium metavanadate were availed from S.D. fine chemicals India Ltd. All the chemicals were used as received without further purification. TBHP/DCE was prepared by shaking appropriate volumes of 70% aq. TBHP and 1,2 dichloroethane in a separating funnel and collecting the dichloroethane (DCE) layer, and drying it over anhydrous sodium sulfate.

4.2.2 Preparation of vanadomolybdophosphoric acids

Mono, di and tri vanadomolybdophosphoric acids (hereafter denoted by V_xHPA, where x = 1, 2 and 3 respectively) were synthesized by a reported procedure and their formation was checked by FT-IR and elemental analysis [24, 25].

4.2.2.1 Monovanadomolybdophosphoric acid, $H_4PMo_{11}VO_{40}$ (V_1HPA)

Sodium phosphate dibasic dodecahydrate (1.77 gm, 5 mmol), was dissolved in 25 ml water and mixed with sodium metavanadate (1.52 gm, 12.5 mmol) that was dissolved in 25 ml boiling water. The mixture was cooled and acidified to red color with 1.25 ml concentrated sulfuric acid. To this colored solution was added sodium molybdate dihydrate (33.25 gm, 137.42 mmol) in 50 ml of water. Finally 21.25 ml of concentrated sulfuric acid was added. Color of the solution became light red. After cooling the solution was extracted with four fractions each of 25 ml diethyl ether to isolate the heteropoly acid in a separating funnel. In this extraction the heteropoly etherate was present as the middle layer. After separation, a stream of air was passed through the heteropoly etherate layer to free it of ether. The orange solid that separated was dissolved in water, concentrated to the first appearance of crystal in a vacuum desiccator over concentrated sulfuric acid and then allowed to crystallize further. The orange crystals that formed were dried, crushed and used for further studies.

4.2.2.2 Divanadomolybdophosphoric acid, $H_5PMo_{10}V_2O_{40}$ (V_2HPA)

Sodium metavanadate (4.06gm, 33.29 mmol) was dissolved by boiling in 16.6 ml water and then mixed with a solution of sodium phosphate dibasic dodecahydrate (1.18 gm, 3.29 mmol) in 16.6 ml water. To the cooled solution was added 0.83 ml of concentrated sulfuric acid. The resulting solution developed a red color. Addition of sodium molybdate dihydrate (20.16 gm, 83.32 mmol) in 50 ml water was then done. While the solution was stirred vigorously 14.16 ml of concentrated sulfuric acid was added slowly and then the hot solution was cooled to room temperature. The title compound was then extracted with four fractions each of 20 ml diethyl ether in a separating funnel. The heteropoly acid was present as the etherate in the bottom layer. This layer was isolated and dried in order to make it ether free. Orange colored solid was obtained after complete drying. Pure complex was obtained after recrystallization in water. The crystals that formed were dried and crushed for further use.

4.2.2.3 Trivanadomolybdophosphoric acid, $H_6PMo_9V_3O_{40}$ (V_3HPA)

Sodium phosphate dibasic dodecahydrate (1.77 gm, 4.95 gm) was dissolved in 12 ml water. Sodium metavanadate (9.15 gm, 75.04 mmol) was made soluble by boiling in 50 ml water. The sodium phosphate solution was mixed with the sodium

metavanadate solution. The resulting solution was cooled, followed by the addition of 1.25 ml of concentrated sulfuric acid. This red colored solution was then added to a solution of sodium molybdate dihydrate (13.62 gm, 56.3 mmol) in 37.5 ml water. This solution was stirred vigorously and simultaneously 21.25 ml of concentrated sulfuric acid was added. The hot solution was cooled to ambient conditions. The heteropoly acid formed was extracted with four fractions, each of 25 ml diethyl ether in a separating funnel. The heteropoly acid is present as the etherate in the middle fraction. The middle layer was then isolated, dried to free of ether. The resulting red colored solid obtained was dissolved in water, concentrated to first crystal formation and allowed to crystallize further. The red crystals that formed were dried and powdered prior to further use.

4.2.3 Sample Preparation

Hydrated titania ($TiO_2.xH_2O$) was prepared by hydrolysis of 1M titanium *t*-butoxide solution (in ethanol) with distilled water and hydrated zirconia ($ZrO_2.xH_2O$) was prepared by treating 1M zirconyl nitrate solution (aqueous) with 1:1 ammonia solution. Both the supports $TiO_2.xH_2O$ and $ZrO_2.xH_2O$ were dried at 110°C prior to use. 15 wt% HPA/MO_2 samples were prepared by wet impregnation method. Here HPA stands for heteropoly acids and MO_2 stand for hydrated titania or hydrated zirconia. In a typical procedure 0.15 g of the heteropoly acid was dissolved in 4 ml of methanol, and to the same solution 0.85 g of hydrated titania or hydrated zirconia was added and stirred at room temperature overnight (approximately 12 h). Excess of solvent was removed on a rota-vapor and the solid samples were dried at 110°C.

4.2.4 Characterization

The room temperature powder X-ray diffraction patterns of the samples were collected on a Philips X' Pert Pro 3040/60 diffractometer using Cu Kα radiation (l =1.5418 °A), nickel filter and X'celerator as detector. Solid state UV-visible spectra were recorded on Perkin-Elmer lambda-350 UV visible spectrophotometer. FT-IR spectra were recorded on Shimadzu FTIR 8201 PC instrument. ICP analysis was done on Perkin Elmer Plasma 1000 Emission Spectrometer.

4.2.5 Catalytic activity

The liquid phase epoxidation reactions were carried out in a two-necked 50 ml round bottom flask immersed in a thermostated oil bath maintained at desired temperature between 40-80°C. Prior to use the HPA/MO_2 catalysts were activated at 110°C. A typical reaction mixture consisted of 0.1 g of activated catalyst, 10 mmol of substrate, 20 mmol of 30% TBHP and 10 ml of dichloroethane. The reaction mixture was stirred with a Teflon-coated magnetic bar for a stipulated time interval of 5 h every time. Progress of the reaction was monitored by drawing small aliquots of the reaction mixture at regular intervals and subjecting them to GC analysis (Hewlett-Packard 5890 gas chromatograph with a flame ionization detector and 50 m × 0.32 mm 5% phenyl methylsilicone capillary column). The products were unambiguously identified by GC-MS (Shimadzu gas chromatograph, G-17A fitted with QP-500 MS Mass spectrometer) as per requirement.

## 4.3 Results and Discussion

4.3.1 Catalyst Characterization

Experimental data showed that the 15 wt% V_2HPA/TiO_2 was exceptionally active as catalyst for various epoxidation reactions, hence only this catalyst was studied in detail. The 15 wt% V_2HPA/TiO_2 was characterized using powder XRD, FTIR and UV-visible spectroscopy and the results of which are discussed in this chapter. The 15 wt% V_2HPA/TiO_2 catalyst along with the neat V_2PMA and $TiO_2.xH_2O$ dried at 110°C were subjected to powder XRD, and the XRD patterns can be seen in Figure 1. No additional peak of divanadomolybdophosphoric acid (V_2PMA) was seen in the XRD pattern of 15 wt% V_2PMA/TiO_2 indicating that the supported compounds are amorphous or their size is too small and cannot be detected by XRD.

To show the presence of V_2PMA on the surface of titania, the catalyst (15 wt% V_2PMA/TiO_2), the support ($TiO_2.xH_2O$) and the neat V_2PMA acid were also subjected to solid state UV-visible spectroscopy and the spectra can be seen Figure 2. The absence of any peaks in the visible region (400-800 nm) for $TiO_2.xH_2O$, but the sharp bands seen at 470 nm for 15 wt% V_2PMA/TiO_2 corresponding to V_2PMA indicate that the presence of the V_2HPA on the surface of $TiO_2.xH_2O$. The minimal shift in the bands from neat V_2PMA to the impregnated one may be due to change in

environment, degree of hydration or additional interactions with the hydroxyl groups of the support. The bands corresponding to V_2PMA and TiO_2 overlap with each other in the ultraviolet region (200-400 nm).
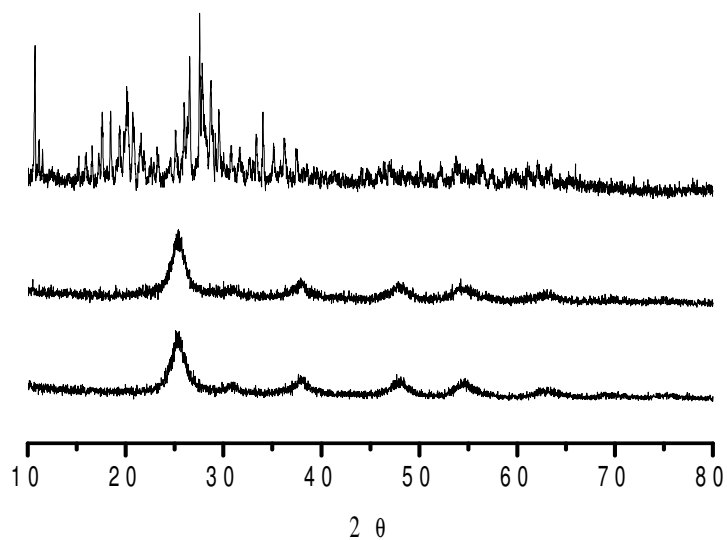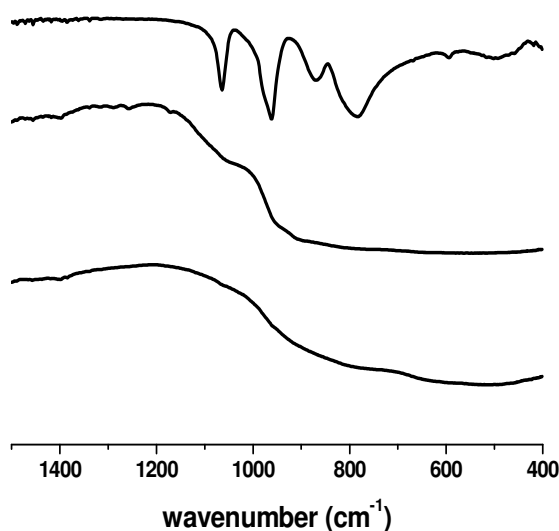

Figure 1: Powder XRD patterns of (a) neat V_2PMA (top), (b) 15% V_2PMA/TiO_2 (center) and (c) $TiO_2.xH_2O$ dried at 110°C (bottom)
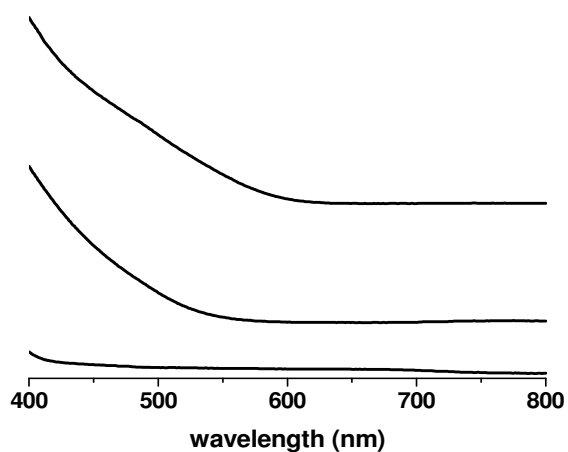
Figure 2: Solid state UV-visible spectra of (a) neat V_2PMA (top), (b) 15% V_2PMA/TiO_2 (center) and (c) $TiO_2.xH_2O$ dried at 110°C (bottom)

Additional evidence to show the presence of divanadomolybdophosphoric acid on the support hydrated titania is given by FTIR. As seen in figure 3, the first line shows the FTIR spectrum of divanadomolybdophosphoric acid. The characteristic peaks of 1063 cm^{-1} for P-O_I-Mo, 961 cm^{-1} for Mo=O_t and 870 cm^{-1} and 785 cm^{-1} for Mo-O_b-Mo, where O_I, O_t and O_b are the inner, terminal and the bridging oxygen atoms respectively in a Keggin unit, can be seen clearly in the same [25]. Similarly the third line shows the FTIR spectrum of hydrated titania. In this spectrum no intense peak is observed in the region from 1200 to 400 cm^{-1}. Although the second line, which corresponds to 15 wt% V_2HPA/TiO_2, also does not show any bands in the above seen region, very small peaks at 1063 and 961 cm^{-1} are clearly seen in this line. These peaks correspond to divanadomolybdophosphoric acid as shown in line 1 (Fig 3). This gives sufficient evidence to show that divanadomolybdophosphoric acid is present on the surface of titania, and that it has maintained its Keggin structure even after impregnation on hydrated titania and also during its activation, at 110°C.

Figure 3: FT-IR spectra of (a) neat V_2PMA (top), (b) 15% V_2PMA/TiO_2 (center) and (c) $TiO_2.xH_2O$ dried at 110°C (bottom)

4.3.2 Effect of solvent on the reaction

The solvents used for the reaction were either dichloroethane or acetonitrile and in both the cases the oxidant used was 30% TBHP/DCE. Thus cyclooctene gave 94% conversion in dichloroethane solvent after 5 h of reaction time and 98% conversion in acetonitrile solvent after 3 h of reaction time, at 80°C reaction temperature for both the solvent systems. Hence, acetonitrile is a better solvent for the above reaction. However, when the reaction was stopped after 1.5 h and continued again after filtering off the catalyst, for both the solvent systems, it was observed that there was not much increase in the conversion for dichloroethane (*ca* 6%), but for acetonitrile, the conversion continues to increase steeply and steadily with time and the total increase in conversion was *ca* 37% as can be seen in Figure 4.
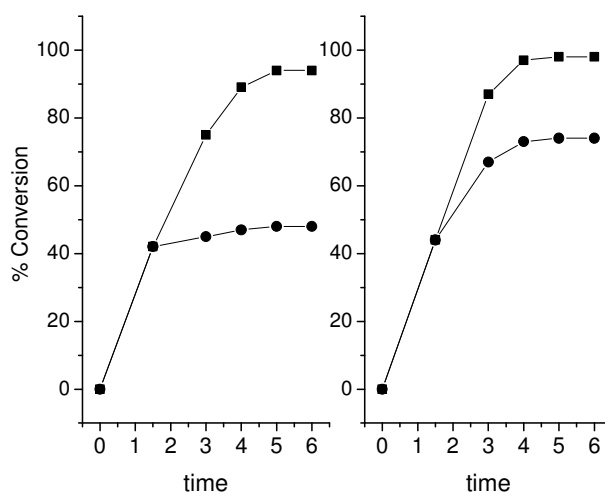
Figure 4: Leaching test for cyclooctene epoxidation over 15% V_2PMA/TiO_2 in 1, 2 dichloroethane (left) and acetonitrile (right) solvents. *Reaction conditions*: catalyst: 0.1 g, alkene: 10 mmol, TBHP/DCE: 20 mmol, Solvent: 10 ml, temperature: 80°C. (■: without filtration, ●: after filtration)

Thus, it was seen that substantial amount of divanadomolybdophosphoric acid had leached into the reaction mixture in acetonitrile as compared to dichloroethane, owing to the high solubility of heteropoly acids in the former. To substantiate this point, the above filtrates were subjected to ICP analysis and it was found that 7.1% of the total vanadium and 6.8% of the total molybdenum present in the reaction mixture had leached in the case of dichloroethane; however for acetonitrile 41.4% vanadium

and 42.2% molybdenum were observed to have leached. This obviously led us to check the recycling behavior of the catalyst in dichloroethane solvent. It was found that the conversion of cyclooctene had slightly decreased from 94% to 91% in the second run, and further to 86% in the third run. Thus, although the conversion had decreased, the magnitude was very small (8%). Similarly, recycling behavior of the catalyst (15 wt% V_2HPA/TiO_2) was investigated for some other alkenes *viz.* norbornene and limonene in dichloroethane solvent. Even for these two alkenes, there was not much drop in conversion up to first three runs (7% and 5% respectively). The minimal leaching of divanadomolybdophosphoric acid, in the case of dichloroethane solvent system is attributed to the slight dissolution of the heteropoly acids in the additives *viz.* TBHP and *t*-butanol formed during the course of reaction from TBHP. Importantly, no leaching of divanadomolybdophosphoric acid (from 15 wt% V_2HPA/TiO_2) was observed in neat dichloroethane, even at refluxing conditions. Further, consistency in the catalytic activity of 15 wt% V_2HPA/TiO_2 for three consecutive runs reiterates the fact that heteropolyacids do not decompose when TBHP is used as the oxidant. It is known that heteropolyacids decompose very rapidly when aqueous hydrogen peroxide is used as the oxidant.

4.3.3 Epoxidation of cyclooctene with different 15 wt% HPA/MO₂

Epoxidation of cyclooctene was performed with different 15 wt% HPA/MO_2 catalysts. Amongst them 15 wt% V_2HPA/TiO_2 was a better catalyst for the reaction as can be seen in Table 1. In order to investigate its higher activity over other 15 wt% HPA/MO_2 catalysts, an attempt was made to explore the role of vanadium, titanium and other transition metal ions in the system. So few controlled experiments were conducted with different 15 wt% HPA/MO_2 catalysts using TBHP/DCE as the oxidant and dichloroethane as the solvent, and the results are presented in Table 1. It can be seen from the results (Table 1) that even 15 wt% PMA/TiO_2 (where PMA stands for phosphomolybdic acid) was also active for this reaction but showed a poor activity. Thus for the same reaction with TBHP/DCE as the oxidant, only 32% Cyclooctene conversion was seen 15 wt% PMA/TiO_2 as against 94% conversion observed for 15 wt% V_2HPA/TiO_2 at the same set of reaction conditions, since vanadium substituted phosphomolybdic acids are better catalysts than neat phosphomolybdic acid [26]. Further, phosphomolybdic acid is a better catalyst than

phosphotungstic acid in oxidation reactions [26], thus 15 wt% PTA/TiO_2 (where PTA stands for phosphotungstic acid) failed to show any activity for the same reaction, with TBHP/DCE as oxidant. Although, phosphotungstic acid is known to have an excellent catalytic activity for oxidation reactions with aqueous H_2O_2 [27], it failed to show any activity with TBHP. TBHP/DCE was chosen as an oxidant over aqueous TBHP because the latter is typically immiscible with dichloroethane. Among the three vanadomolybdophosphoric acid catalysts, only 15 wt% V_2HPA/TiO_2 showed higher activity (94% conversion) in the oxidation of cyclooctene. The other two catalysts i.e. 15 wt% V_1HPA/TiO_2 and 15 wt% V_3HPA/TiO_2 gave only 44% and 89% conversion, respectively under the same reaction conditions. It is already known from the literature that as the number of vanadium subtituents in phosphomolybdic acid increases from one to two, the catalytic activity of the heteropoly acid also increases [18, 28]. However, on increasing the number of vanadium subtituents in phosphomolybdic acid from two to three, not much change in activity is observed. Similar to the role of vanadium, it was also checked whether titanium from the support is also playing any role or not. So two samples containing 15 wt% V_2HPA/TiO_2 and 15 wt% V_2HPA/ZrO_2 were prepared in similar manner and their activities were checked in oxidation of cyclooctene under similar conditions. The 15 wt% V_2HPA/TiO_2 catalyst showed *ca*. 94% conversion to give cyclooctene epoxide while 15 wt% V_2HPA/ZrO_2 catalyst gave only 20% conversion as seen in Table 1. It may also be seen in the table that the neat supports (neat 110°C dried $TiO_2.xH_2O$ and $ZrO_2. xH_2O$) do not catalyze the reaction at all. Thus, it is assumed that the higher activity of 15 wt% V_2HPA/TiO_2 catalyst is due to the synergistic effect between the heteropoly acid and titania support. Such synergistic effect between titania and heteropoly acids has earlier been observed in photo catalytic reactions [29].

Table 1: Selective oxidation of cyclooctene over various 15% HPA/MO$_2$ with 30% TBHP/DCE

Entry	Catalyst	% Conversion	% Selectivity (epoxide)
1.	PMA/TiO$_2$	32	>99
2.	V$_1$PMA/TiO$_2$	44	>99
3.	V$_2$PMA/TiO$_2$	94	>99
4.	V$_3$PMA/TiO$_2$	89	>99
5.	V$_2$PMA/ZrO$_2$	20	>99
6.	PTA/TiO$_2$	<1	-
7.	TiO$_2$.xH$_2$O	<1	-
8.	ZrO$_2$.xH$_2$O	<1	-

Reaction Conditions: 0.1 g of catalyst, 10 mmol of cyclooctene and 20 mmol of 30% TBHP and 10 ml of 1,2-dichloroethane, temperature: 80°C, time: 5 h.

### *4.3.4 Effect of temperature and substrate: oxidant ratio on cyclooctene epoxidation*

The oxidation of cyclooctene with the oxidant of TBHP/DCE over 15 wt% V$_2$HPA/TiO$_2$ catalyst was carried out with cyclooctene: TBHP/DCE mol ratio of 1:2 in the temperature range 40–80°C. The cyclooctene conversion increased with increase in temperature. Thus after 5 h of reaction, only 31%, 41% and 52% conversion of cyclooctene were observed at 40°C, 50°C and 60°C of temperatures, respectively, as against 94% conversion achieved at 80°C in the same time interval. Interestingly cyclooctene epoxide was the only product obtained at all these temperatures.

Kinetic measurements for cyclooctene oxidation were carried out as a function of temperature and the results are plotted in Figure 5 and the data showed the reaction to be first order with respect to cyclooctene concentration. The rate constants at different reaction temperature between 40°C and 60°C were obtained by subjecting the data to linear regression as shown in Figure 5. Arrhenius equation was used with above rate constant data to estimate the activation parameters for the cyclooctene epoxidation reaction (inset, Figure 5). The activation energy was 7.21 ± 0.32 kcal/mol and the enthalpy of activation was 6.61 ± 0.39 kcal/mol. The obtained activation energy although seems to be low, is typical for oxygen transfer reactions [30].
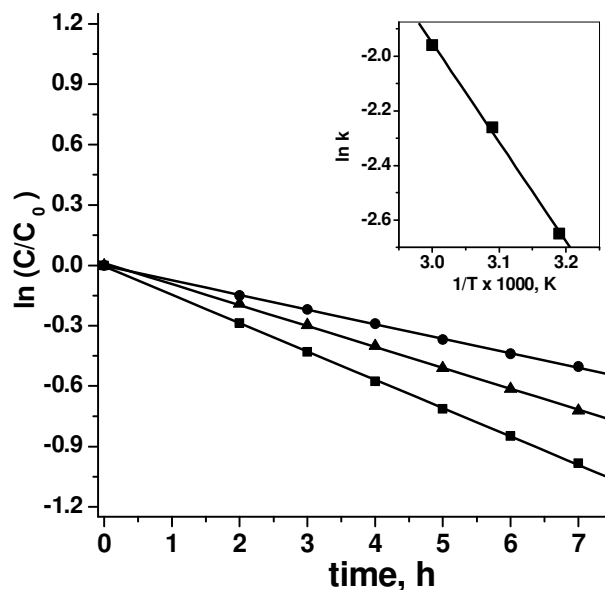
Figure 5: Kinetic profiles of cyclooctene epoxidation reaction as a function of temperature and their linear fittings (■: 60°C, ▲: 50°C, ●: 40°C). Reaction condition: catalyst: 0.1 g, alkene: 10 mmol, 30% TBHP/DCE: 20 mmol. (Inset: a plot of the measured rate constants as a function of temperatures in an Arrhenius plot)

In an attempt to optimize the amount oxidant TBHP/DCE needed for maximum cyclooctene conversion, experiments were carried out under similar reaction conditions and the results are shown in Figure 6. With cyclooctene: TBHP/DCE mol ratio of 1:1, the maximum conversion was 46% after 5 h. With cyclooctene: TBHP/DCE mol ratio of 1:2, it was 94% in the same time interval, and with 1:3 mol ratio, the cyclooctene conversion was nearly the same as that of 1:2 mol ratio. Thus it was indicated that the cyclooctene: TBHP/DCE mol ratio of 1:2 was optimum to obtain a satisfactory yield of the corresponding epoxide with this catalyst. Thus the substrate: TBHP/DCE mol ratio of 1:2 was employed in further epoxidation reactions.
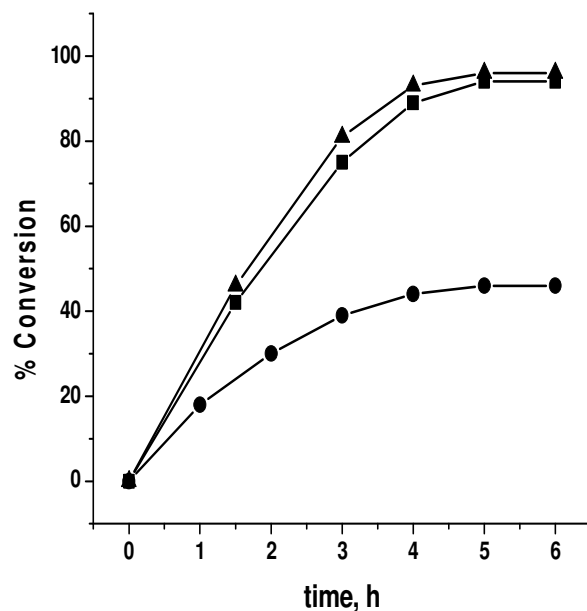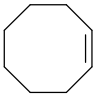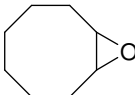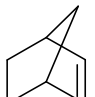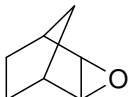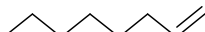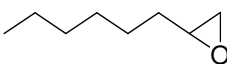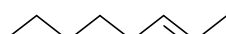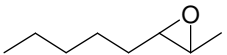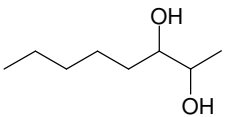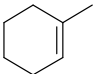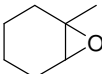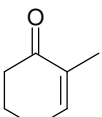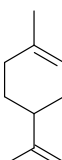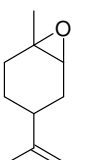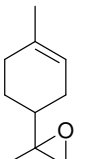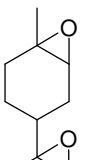
Figure 6: Epoxidation of cyclooctene with different substrate: oxidant ratios. Reaction conditions: Reaction condition: catalyst: 0.1 g, alkene: 10 mmol, 30% TBHP/DCE: 20 mmol

4.3.5 Epoxidation of other alkenes

Apart from cyclooctene, the epoxidation behavior of yet another industrially important alkene viz. norbornene was investigated, over 15 wt% V_2PMA/TiO_2 catalyst, with TBHP/DCE as oxidant and dichloroethane as the solvent at 80°C. In this case also, almost 100% selectivity for the corresponding epoxide was obtained at 87% conversion after 5 h, as can be seen in Table 2. Similarly, epoxidation of some more alkenes like 1-octene, trans-2-octene, and 1-methyl-1-cyclohexene was studied over 15 wt% V_2PMA/TiO_2 catalyst. The results are presented in Table 2. It was observed that an increase in the number of substitutions on the carbon-carbon double bond enhanced the reactivity of the alkenes. Thus, for 1-octene which is a mono-substituted alkene with respect to the olefinic bond, the conversion was 11% after 5 h, however, for a di-substituted alkene like trans-2-octene it was 21% and for a tri-substituted alkene like 1-methyl-1-cyclohexene was 40%, after the same time interval.

Table 2: Selective oxidation of various alkenes over 15% V_2HPA/TiO_2 with 30% TBHP/DCE

Entry	Substrate	% Conversion	Product	% Selectivity
1.		94		>99
2.		87		>99
3.		11		>99
4.		21		87
				13
5.		40		75
				25
6.		73		54
				29
				17

Reaction Conditions: 0.1 g of catalyst, 10 mmol of alkene and 20 mmol of 30% TBHP and 10 ml of 1,2-dichloroethane, temperature: 80°C, time: 5 h.

For all these alkenes, epoxide was always the major product (> 75 %). The by-product of glycol in the case of *trans*-2-octene possibly formed further from the epoxide, under the virtue of acidity present in heteropoly acid part of the catalyst system. The by-product of ketone in the case of 1-methyl-1-cylohexene might have formed owing to the allylic oxidation. Similar by-products were also observed by others [30]. The activity was further extrapolated to limonene, a diene with one di-substituted and one tri-substituted double bond. Here, the two individual mono-epoxides along with some di-epoxide were obtained and as seen above the selectivity for epoxidized tri-substituted double bond was more than the di-substituted counterpart.

4.4 Summary and Conclusion

The results clearly indicate that divanadomolybdophosphoric acid wet-impregnated on hydrated titania ($TiO_2.xH_2O$) makes an excellent catalyst system for alkene epoxidation, with TBHP extracted in dichloroethane as the oxidant. The catalysts can be recycled without much loss in activity at least three times by choosing appropriate solvent for the reaction. For all the alkenes seen here the major product is always the corresponding epoxide. The controlled experiments unambiguously indicate that the vanadium substitutions in the heteropoly acid as well as the titanium species from the support have a role to play. Thus a simple catalytic system, which is free of high temperature calcination steps and tedious multi-step procedures, normally encountered in heterogenization of heteropoly acids, is demonstrated hereby.

References

1. C.L. Hill, C.M. Prosser-McCartha, Coord. Chem. Rev. 143 (1995) 407

2. Y. Nishiyama, Y. Nakagawa, N. Mizuno, Angew. Chem. Int. Ed. 40 (2001) 3639

3. C.L. Hill, I.A. Weinstock, Nature 388 (1997) 332

4. M. Bosing, A. Nöh, I. Loose, B. Krebs, J. Am. Chem. Soc. 120 (1998) 7252

5. X. Zhang, T.M. Anderson, Q. Chen, C.L. Hill, Inorg. Chem. 40 (2001) 418

6. R. Neumann, M. Gara, J. Am. Chem. Soc. 116 (1994) 5509

7. A.M. Khenkin, R. Neumann, A.B. Sorokin, A. Tuel, Catal. Lett.,63 (1999) 189

8. K. Nomiya, S. Matsuoka, T. Hasegawa, Y. Nemoto, J. Mol. Catal. A: Chem. 156 (2000) 143

9. K. Nomiya, H. Yanagibayashi, C. Nozaki, K. Kondoh, E. Hiramatsu, Y. Shimizu, J. Mol. Catal. A: Chem. 114 (1996) 181

10. K. Nomiya, K. Yagishita, Y. Nemoto, T. Kamataki, J. Mol. Catal. A: Chem. 126 (1997) 43

11. M. Misono, N. Mizuno, K. Inumaru, G. Koyano, Lu Xin-Hong, Stud. Surf. Sci. Catal. 110 (1997) 35

12. K. Nomiya, Y. Nemoto, T. Hasegawa, S. Matsuoka, J. Mol. Catal. A: Chem. 152 (2000) 55

13. K. Nomiya, K. Hashino, Y. Nemoto, M. Watanabe, J. Mol. Catal. A: Chem. 176 (2001) 79

14. T. Ilkenhans, B. Herzog, T. Braun, R. Schlogl, J. Catal. 153 (1995) 275

15. M. Akimoto, K. Shima, H. Ikeda, E. Echigoya, J. Catal. 86 (1984) 173

16. Ben-Daniel, R. Neumann, Angew. Chem. Intl. Ed. 42 (2003) 92

17. M. de la Vega, R. Neumann, J. Mol. Catal. 84 (1993) 93

18. S. Shinachi, M. Matsushita, K. Yamaguchi, N. Mizuno, J. Catal 233 (2005) 81

19. N. K. K. Raj, S. S. Deshpande, R. H. Ingle, T. Raja, P. Manikandan, Catal. Lett. 98 (2004) 217

20. N. K. K. Raj, S. S. Deshpande, R. H. Ingle, T. Raja, P. Manikandan, Stud. Sur. Sci. and Catal.156 (2005) 769

21. A. S. Dias, M. Pillinger, A. A. Valente, Micro. Meso. Mat. 94 (2006) 214

22. E. Caliman, J. A. Dias, S.C.L. Dias, A.G.S. Prado, Catal. Today 107-108 (2005) 816

23. B. M. Devassy, S.B. Halligudi, J. Catal. 236 (2005) 313

24. G. A. Tsigdinos and C. J. Hallada, Inorg. Chem. 7 (1968) 437

25. K. Nowińska, R. Fórmaniak, W. Kaleta and A. Wąclaw, Appl. Catal. A. 256 (2003) 115

26. F Cavani, Catal. Today 41 (1998) 73

27. Y. Ishii, K. Yamawaki, T. Ura, H. Yamada, T. Yoshida, M. Ogawa, J. Org. Chem. 53 (1988) 3587

28. A. Predoeva, S. Damyanova, E. M. Gaigneaux, L Petrov, App. Catal. A 319 (2007) 14

29. Yu Yang, Y. Guo, C. Hu, C. Jiang, E. Wang, J. Mater Chem. 13 (2003) 1686

30. R. Neumann, M. Gara, J. Am. Chem. Soc. 117 (1995) 5066

Chapter 5:

Selective oxidation of ethane to acetic acid over MoVAlO$_x$ based catalytic system with molecular oxygen

5.1 Introduction

Research activity on the selective oxidation of lower alkanes, especially C_2-C_4 alkanes, to the corresponding alkenes or oxygenates (acetic acid, acrylic acid, etc) has gained a high momentum in recent years [1, 2]. Selective oxidation of lower alkanes is an attractive path towards the chemical utilization of cheap natural gas resources. For instance, one-step direct oxidation of ethane and propane to acetic acid and acrylic acid, respectively, is an alternative method to the currently employed alkene based routes [2-5]. Generally, lower alkanes are less reactive due to the non-availability of a lone pair electrons and little polarity of the C-H bonds, and hence, their oxidation is usually encountered with difficulties. Furthermore, a high selectivity to the required products is obtained generally at low conversion. Higher conversion invariably leads to less selective to the required products, due to the formation of thermodynamically stable, undesirable combustion products. In spite of the above limitation, a great deal of efforts have been attempted to achieve selective functionalization of lower alkanes. However, in the case of selective oxidation of ethane only a few catalysts are known that are efficient in terms of acetic acid and ethylene yield at a relatively mild experimental condition [1, 2, 6].

Oxidation of ethane involves several micro intermediate steps that demand a multifunctional catalyst. Thus, the selection of a suitable catalyst containing many active phases (multifunctionality) for the ethane oxidation and maximizing the selectivity to ethylene and/or acetic acid under appropriate operating condition is a complex and challenging task. Several research groups have studied a broad spectrum of catalysts using various techniques to understand the active sites responsible for the selective oxidation of ethane. However, the knowledge available on the reaction mechanism is still rather limited and hence there is a need for systematic studies on the wide range of catalyst systems in order to understand the structure-activity correlations [2, 7, 8].

There have been many reports emphasizing the importance of elements like Te and Nb ions along with Mo-V containing basic composition for the formation/ stabilization of the active phases responsible for the selective oxidation of ethane [1, 5, 10, 11]. Reports are also available indicating the importance of the initial elemental composition, the pH, the preparation methodologies and the treatment temperatures for a better yield of the required alkenes and oxygenates, however, these dependencies vary with catalyst to catalyst [4, 6].

The initial report on MoVAlO$_x$ by Ueda *et al* at an atmospheric pressure and at 340 ºC showed less than 4 mol % ethane conversion with a low selectivity to acetic acid [12]. In the present paper, we report on the catalytic activity of MoVAlO$_x$ type catalysts for the selective oxidation of ethane to produce ethylene and acetic acid at moderate ethane conversion, as a function of the pH of the preparative gel of the catalysts synthesized. MoVAlO*x* type catalysts prepared at different pH conditions were also tested at different experimental conditions *viz.* pressure, temperature and ethane/O$_2$/H$_2$O feed ratios in order to obtain acetic acid and ethylene in high yield. Interestingly, the catalyst prepared from a gel at pH 2 was found to have superior activity than other catalysts. We have also identified different phases present in the catalysts prepared at different pH conditions. Structure-activity correlations were made based on the detailed characterization of the catalysts by powder XRD, Raman, UV-visible, and EPR spectral techniques.

5.2 Experimental

5.2.1 Catalyst preparation and Characterization

Catalyst composition of general formula MoVAlO$_x$ with a preparative composition of the elements Mo, V and Al in the atomic ratio 1.0:0.333:0.167 respectively was synthesized using a hydrothermal method [12]. Anderson type heteropoly molybdate, $(NH_4)_3AlMo_6H_6O_{24}.7H_2O$, prepared from the mixed aqueous solution of ammonium heptamolybdate and aluminum sulfate [12, 13] and was used as a source for Mo and Al. Typically, the catalyst compositions of MoVAlO$_x$ were prepared as follows: aqueous solutions of $(NH_4)_3AlMo_6H_6O_{24}.7H_2O$ and $VOSO_4$ were mixed at room temperature, the slurry was adjusted to the required pH value (1, 2, 3 or 4) using NH_4OH or HNO_3 and the final mixture was transferred to a PTFE lined autoclave (200 ml capacity). The autoclave was heated to 175 ºC for 48 h under constant rotation (40 rpm). After 48 h, the autoclave was cooled and the dark solid mass obtained at the bottom of the autoclave was separated from the solution, washed with water several times and dried at 100 ºC overnight in an oven. The final catalyst compositions were named as MoVAlO$_x$-1, MoVAlO$_x$-2, MoVAlO$_x$-3 and MoVAlO$_x$-4, where the numerical values indicate the pH at which the catalysts were prepared.

The bulk compositions of Mo, V and Al were analyzed by ICP using a Plasma 400 Perkin Elmer spectrometer and their surface composition was done using EDX method. The surface area of the catalysts was determined by N$_2$ adsorption at 77 K,
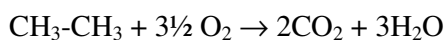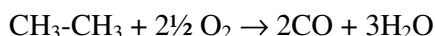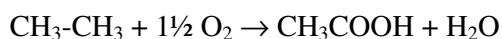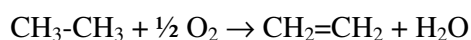
using the multipoint BET analysis method with an Autosorb-1 Quantachrome flow apparatus. The catalysts were dehydrated in vacuum at 250 °C for 10 h prior to the measurements. The room temperature powder X-ray diffraction (XRD) patterns of calcined catalysts were collected on a Philips X'Pert Pro 3040/60 diffractometer using Cu Kα radiation (l = 1.5418°A), nickel filter and X'celerator as detector which employs the real time multiple strip (RTMS) detection technique. XRD patterns were collected in the 2θ range 5 -75° steps of 0.017°. Scan type was the continuous scanning mode and the scan time per step was 50 s. Scanning electron microscopy (SEM) and EDX microanalyses were performed on a JEOL JSM 6300 LINK ISIS instrument.

The FT-IR and Raman spectra of the catalysts were recorded on a Shimadzu FTIR 8201 PC instrument and Ranishaw 2000 Raman Microscope excited with 633 nm Laser respectively. Diffuse reflectance UV-visible spectra were collected on a Perkin Elmer Lambda 900 series, equipped with a 'Praying Mantis' attachment from Harrick. The spectra were recorded for $VOSO_4$, MoO_3, V_2O_5 and the as-synthesized and calcined $(NH_4)_3AlMo_6H_6O_{24}.7H_2O$ (hereafter referred as Mo_6Al-AS and Mo_6Al-Cal respectively) as references for the analysis. The electron paramagnetic resonance (EPR) spectra were recorded at room temperature on a Bruker EMX X-band spectrometer operating at 100 kHz field modulation. The microwave frequency was calibrated using a frequency counter of the microwave bridge ER 041 XG-D. Bruker Simfonia and WINEPR software packages were used in the spectral simulations and to calculate hyperfine coupling constant.

5.2.2 Catalytic activity testing

The ethane oxidation experiments were performed in a typical laboratory fixed bed reactor using a corrosion resistant stainless steel tubular reactor of internal diameter of 9 mm and 450 mm height which was kept in a tubular furnace. The catalyst (0.3-0.5 mm particle size) was introduced in the reactor and diluted with 2-4 g of silicon carbide with similar in size in order to keep a constant volume in the catalyst bed. A thermocouple was installed in the center of the catalyst bed in contact with the catalyst particles to measure the reaction temperature. The heating zones at the inlet and the outlet of the reactor were filled with inert porcelain particles. The catalyst was activated by heating the reactor to 350 °C at a heating rate of 2 °C/min

under air flow for 4 h and then to 400 °C under He flow for 4 h. The reactor was then brought to the required temperature, and pressurized to the required level with a feed using a back pressure controller placed on the reactor outlet stream. A typical composition of the feed was ethane/air/steam: 27.6/47.6/24.8 mol %. The water (steam) feed was preheated at 250 °C and then thoroughly mixed with the other gas feed prior to their contact with the catalyst. The flow rate was varied (from 40 to 100 ml/min) in order to achieve different ethane conversion levels. Experiments were carried out at temperatures in the range 250-350 °C to achieve the highest combined selectivity for ethylene and acetic acid at a moderate ethane conversion. The liquid products (mainly acetic acid and water) were separated from the gas products by an ice cold condenser, collected in high pressure liquid-gas separator and analyzed using offline gas liquid chromatography (GC: HP 5890 series 11 using a 1.5 m by 3 mm column packed with material sold under the trademark PORAPAQ^{TM}-QS). Acetic acid was also estimated by standard volumetric titration method. The gas products were analyzed online by gas chromatography (GC: Chemito 1000) operating with three columns. Oxygen, nitrogen and carbon monoxide were analyzed using a 2.5 m by 3 mm column of 13X molecular sieve. Carbon dioxide, ethane and ethylene were analyzed using a 0.5 m x 3 mm column packed with material sold under the trade name PORAPAQ^{TM}-N. The carbon balance was in the range 93-97 %. In all cases, the conversion and selectivity calculations were based on the following stoichiometries:

$$CH_3\text{-}CH_3 + \tfrac{1}{2}\,O_2 \rightarrow CH_2=CH_2 + H_2O$$

$$CH_3\text{-}CH_3 + 1\tfrac{1}{2}\,O_2 \rightarrow CH_3COOH + H_2O$$

$$CH_3\text{-}CH_3 + 2\tfrac{1}{2}\,O_2 \rightarrow 2CO + 3H_2O$$

$$CH_3\text{-}CH_3 + 3\tfrac{1}{2}\,O_2 \rightarrow 2CO_2 + 3H_2O$$

The selectivity data were calculated on the basis of product sum. Details of the reaction conditions are described in the footnotes of the Tables and Figures. The conversion of ethane in an experiment using an empty volume reactor (blank run) was lower than 1 %, confirming that the homogeneous reaction is negligible at the experimental conditions employed for the present catalytic activities.

5.3 Results

5.3.1 Synthesis and Characterization

5.3.1.1 Synthesis, elemental composition and surface properties

The elemental composition of catalysts of general formula $MoVAlO_x$ prepared hydrothermally at four different pH values and the yield of the final catalysts (calcined catalysts) are given in Table 1. The catalyst yield was found to decrease at higher pH condition as seen in the Table 1. The bulk elemental composition of the catalysts was obtained from ICP analysis. The data clearly indicate that the final composition of the catalyst is different from the initial preparative composition depending on the pH values. Also, Mo/V and Mo/Al molar ratios decrease with increase in pH indicating that the Mo content is lower at the higher pH value.

The surface elemental composition for all the catalysts was determined by EDX method (Table 1) and it was found that these elemental compositions are different from the bulk composition. The amount of vanadium at the surface of the catalysts was higher as compared to that of the bulk except with the $MoVAlO_x$-4 catalyst, indicating its mobility to the surface of the catalysts. BET surface area measurements have also been carried out for these catalysts and the data are presented in Table 1. The surface area of the catalyst $MoVAlO_x$-1 was 7 m^2/g, while for the other catalysts it was in the range 16- 17 m^2/g.

Table 1: Elemental compositions and surface properties of hydrothermally synthesized MoVAlOx catalysts prepared at different pH values.

Catalyst	[a] Yield, %	Elemental Composition		
		ICP Analysis	EDX Analysis	Surface area, m^2/g
$MoVAlO_x$-1	99	$Mo_1V_{0.15}Al_{0.20}O_x$	$Mo_1V_{0.26}Al_{0.11}O_x$	6
$MoVAlO_x$-2	96	$Mo_1V_{0.34}Al_{0.09}O_x$	$Mo_1V_{0.36}Al_{0.30}O_x$	16
$MoVAlO_x$-3	33	$Mo_1V_{0.7}Al_{0.28}O_x$	$Mo_1V_{0.78}Al_{0.69}O_x$	17
$MoVAlO_x$-4	13	$Mo_1V_{1.75}Al_{0.49}O_x$	$Mo_1V_{1.27}Al_{1.05}O_x$	17

[a] Yield of calcined catalysts, calculated on the basis of concentration of Mo with respect to initial elemental composition taken for the synthesis

5.3.1.2 Powder X-Ray diffraction

The powder XRD patterns of the four calcined catalysts prepared at different pH values can be seen in Figure 1. The calcination was carried out at 400 °C under N_2 after treating the catalysts in air up to 350 °C for 2 h. The catalysts $MoVAlO_x$-1 and $MoVAlO_x$-2 showed a similar XRD patterns exhibiting predominantly MoO_3 [JCPDS, 76-1003] and MoV_2O_8 [JCPDS, 74-1510] phases. Although, the quantification of different phases was not carried out, the relative intensity of MoO_3 is much higher in $MoVAlO_x$-1. Relative amount of MoV_2O_8 phase was higher in $MoVAlO_x$-2 compared to $MoVAlO_x$-1. In other words, the relative intensity ratio of $[MoV_2O_8]$/ $[MoO_3]$ is higher in $MoVAlO_x$-2 than in $MoVAlO_x$-1. In addition, traces of Mo_4O_{11} [JCPDS, 13-0142], a reduced phase, is also seen in both catalysts (which is more prominent in $MoVAlO_x$-2). The XRD pattern of $MoVAlO_x$-3 exhibits MoV_2O_8 as a major phase along with a minor phase of $Mo_4V_6O_{25}$ [JCPDS, 34-0530]. Interestingly, MoO_3 phase is totally absent in MoVAlOx-3. In addition, low intensity peaks were seen at 2θ values 17.63(23)°, 29.51(15)°, 38.12(3) and 46.19(12)° could not be fitted with any of the known single phases. For $MoVAlO_x$-4, the pattern was dominated by V_2O_5 [JSPDS, 85-0604] phase as a major phase along with a medium intensity Mo_4O_{11} and $MoVAlO_4$ [JSPDS, 89-0871] phases. A trace amount of $Mo_4V_6O_{25}$ phase was also seen in $MoVAlO_x$-4.
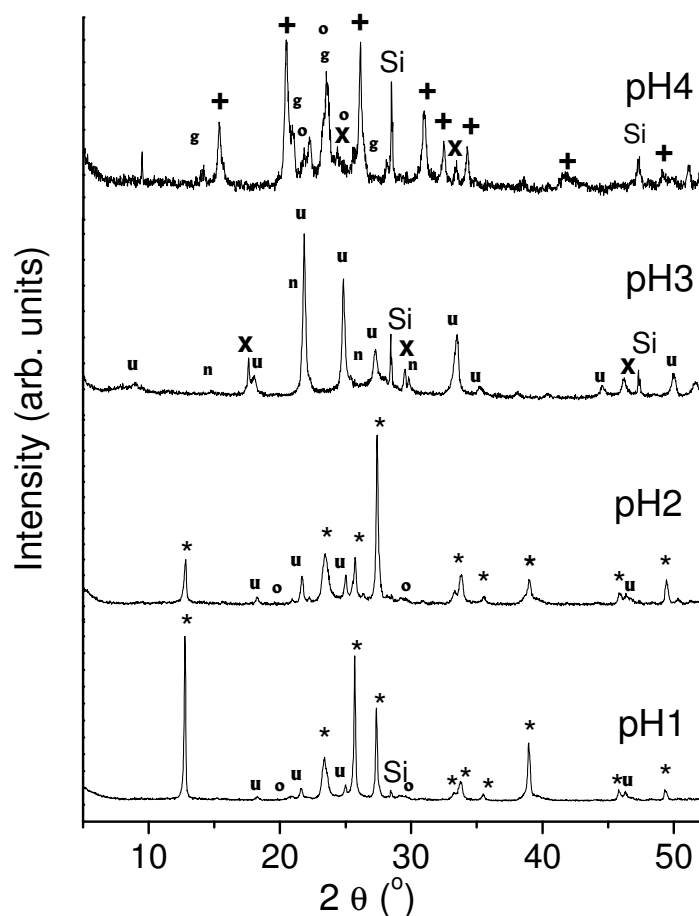
Figure 1: Powder XRD pattern of the catalyst. ∗: MoO_3, ♦: MoV_2O_8, □:Mo_4O_{11}, +: V_2O_5, ●: $Mo_4V_6O_{25}$, ■: $MoVAlO_7$, x: unidentified phase, Si: silicon standard.

5.3.1.3 Morphology of MoAlVO$_x$ catalysts

The morphology of calcined catalysts was investigated by SEM analysis. All the four catalysts were found to have completely different morphologies and the images are given in Figure 2. Long rod or needle shaped crystals with a length about 4-40 μm were observed in the case of MoVAlO$_x$-1. These needle or rod shaped crystals have collapsed into smaller sizes in MoVAlO$_x$-2 catalyst as shown in the Figure 2. For the catalysts prepared at higher pH values *viz*., MoVAlO$_x$-3 and MoVAlO$_x$-4, the images are more of microcrystalline and spongy in nature respectively.
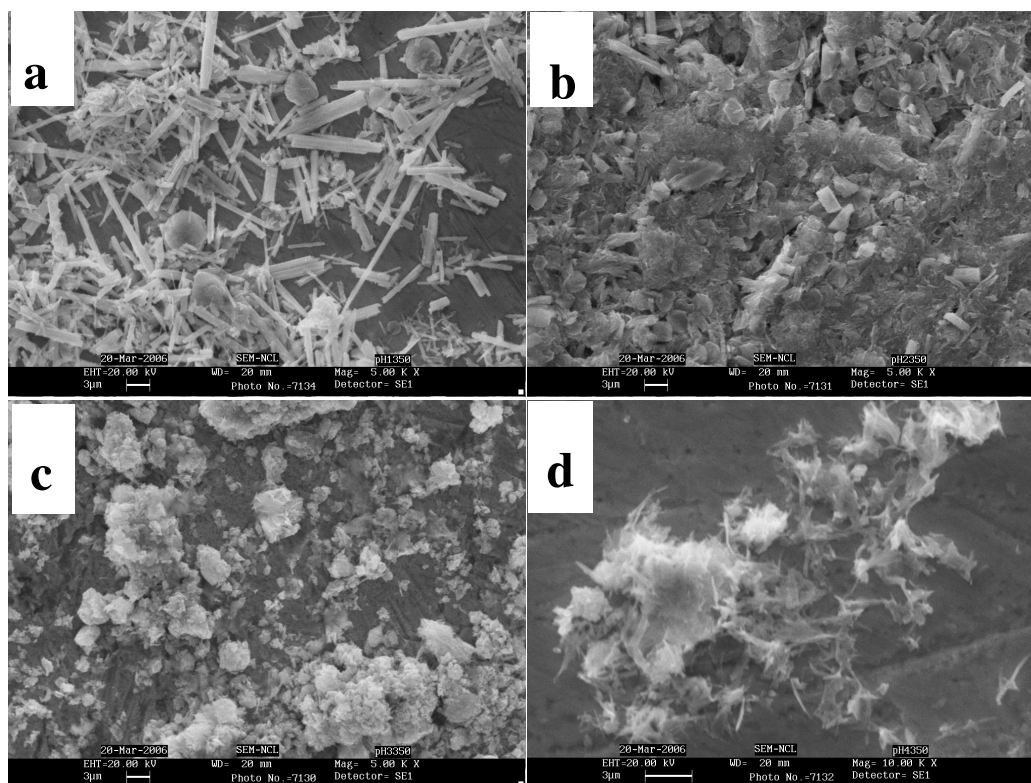
Figure 2: SEM images of (a) MoVAlO$_x$-1, (b) MoVAlO$_x$-2, (c) MoVAlO$_x$-3 and (d) MoVAlO$_x$-4

5.3.1.4 Raman Spectroscopy

Raman spectroscopy was used to identify different moieties/phases having different coordination symmetry present in the catalytic catalysts. The Raman spectra of all the calcined catalysts recorded at room temperature are shown in Figure 3. The spectra of MoVAlO$_x$-1 and MoVAlO$_x$-2 catalysts showed bands at 992, 820, 664 cm^{-1} which are characteristic of α-MoO$_3$ species and its presence was also supported by the XRD data.

A broad shoulder band around 700 cm^{-1} and a peak at 992 cm^{-1} (the latter band might be overlapped with that of α-MoO$_3$) indicate the presence of phases containing V$_2$O$_5$ unit *viz*. MoV$_2$O$_8$ phase [14]. Interestingly, for MoVAlO$_x$-3 and MoVAlO$_x$-4 catalysts, the intensity of 820 cm^{-1} band diminished to a broad shoulder. However, the band centered around 700 cm^{-1} increased many fold and became a broader band for MoVAlO$_x$-4 catalyst. The above features indicate the absence or negligible amount of α-MoO$_3$ species and increased amount of pure V$_2$O$_5$/ (V$_2$O$_5$- containing phases e.g.

MoV_2O_8) in these catalysts. This is quite understandable as the relative amount of vanadium content was higher in this catalyst compared to the catalysts prepared at a low pH. In the case of MoVAlO$_x$-4, the V content was more than that of Mo as seen in Table 1. The bands at 900 and 850 cm^{-1} are generally attributed to the stretching mode of Mo-O-Mo bonds of polymerized surface molybdenum oxide containing species in different configurations (dimers, oligomers) [15, 16]. The broad bands centered around 920, 900 and 850 cm^{-1} are attributed to crystalline Mo_4O_{11} and $Mo_4V_6O_{25}$ species in addition to MoO_3 type compounds. The spectra of all catalysts showed a broad band in the region 700-675 cm^{-1} (which were stronger in MoVAlO$_x$-3 and MoVAlO$_x$-4) and a band around 400 cm^{-1}. These bands are assigned to V-O-V (or V-O-Mo) stretching vibrations of polymeric surface species e.g. $MoVAlO_4$, $Mo_4V_6O_{25}$ etc [17]. The bands can also be partly attributed to the presence of a bulk V_2O_5 especially for MoVAlO$_x$-4 catalyst as characteristic bands of V_2O_5 appear at 282, 405, 695 and 993 cm^{-1} [14]. The absence of 760 or 937 cm^{-1} band in all the catalysts indicates that monomeric tetrahedral vanadate species (~760 cm^{-1}) and surface metavanadate species (937 cm^{-1}) are either absent or present in negligible quantities [18]. An isolated monovanadate group having terminal V=O stretching mode which generally exhibits a distinct narrow band at 1030-1020 cm^{-1}, is absent in the catalysts [14, 19]. Also, bands associated with $AlVO_4$ (characteristic bands are: 1003, 970, 943 cm^{-1}) are absent in the calcined catalysts [20].
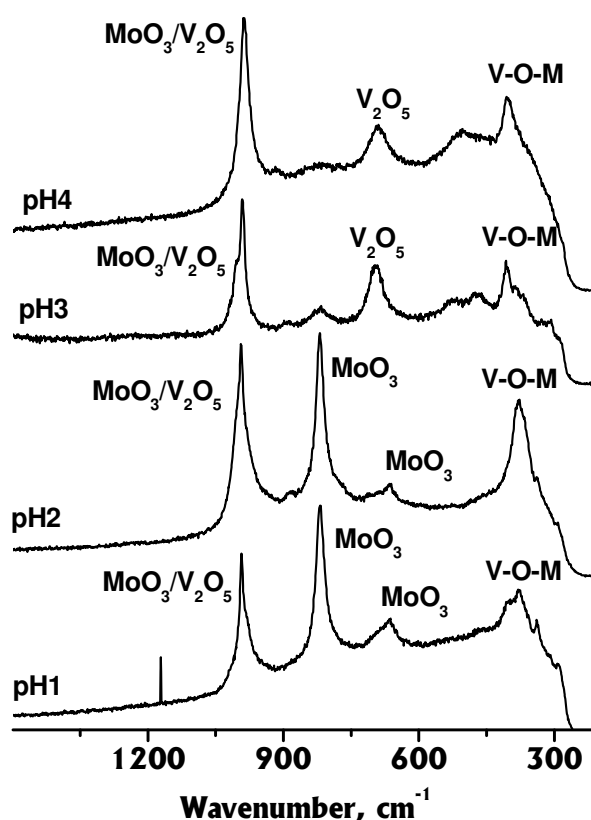
Figure 3: Raman spectra of (a) MoVAlO$_x$-1, (b) MoVAlO$_x$-2, (c) MoVAlO$_x$-3 and (d) MoVAlO$_x$-4 (calcined samples)

5.3.1.5 UV-visible spectroscopy

The diffuse reflectance UV-visible spectra of the calcined catalysts prepared at different pH values were recorded at room temperature and are shown in Figure 4. The spectra were deconvoluted to identify different bands present especially in the region 200-500 nm. Accordingly, the spectra could be deconvoluted into five major bands centered on 234, 265, 307, 376, 452 nm and however, their intensities vary with catalysts prepared at different pH. The UV-visible spectra of few reference catalysts namely VOSO$_4$, V$_2$O$_5$, MoO$_3$ and as synthesized and calcined (NH$_4$)$_3$AlMo$_6$H$_6$O$_{24}$.7H$_2$O catalysts, represented as Mo$_6$Al-*AS* and Mo$_6$Al-*Cal* respectively were also recorded for a comparison and the spectra are given in Figure 5.

The UV-visible spectra of all the calcined catalysts were dominated by five major peaks centered around 234, 265, 307 (br), 376, 452 (vs) nm and also a broad

band above 500 nm. The intensity of the bands centered on 234, 265 and 307 nm was stronger and the peaks at 376 and 452 nm appear as a shoulder for the catalysts. While the relative intensity of 234 and 265 nm bands are more or less same for both $MoVAlO_x$-2 and $MoVAlO_x$-1, bands in the region 305-480 nm became stronger for $MoVAlO_x$-2. The features of $MoVAlO_x$-3 and $MoVAlO_x$-4 were almost similar and the bands in the region 305-480 nm became more intense and a broad shoulder at 452 nm became clearly visible.

The bands in the range of 230-310 nm present in all the catalysts were assigned to Mo^{6+} in octahedral coordination with different structural arrangement [5, 18, 19, 21]. The above assignment was further substantiated by the UV-visible spectra of the reference catalysts namely MoO_3, Mo_6Al-*AS* and Mo_6Al-*Cal* catalysts (Figure 5) and their spectra are dominated by characteristic bands in the region 200-350 nm. The broad bands appeared above 550 nm are assigned to a *d-d* band associated with Mo and V ions with lower oxidation states e.g. Mo^{5+}/Mo^{4+} or V^{4+}/V^{3+} as they are expected to exhibit bands in the region 400-750 nm [22]. The above assignments were further supported by comparing the spectra of reference samples, Mo_6Al-*Cal* and $VOSO_4$, which have a substantial amount of Mo^{5+} and V^{4+} respectively, showing characteristic of *d-d* band above 500 nm. The dominant band centered on 376 nm in all the calcined catalysts were assigned to penta coordinated V^{5+} [5, 18, 19]. The assignment was also confirmed by comparing with the UV-visible spectrum of reference V_2O_5 catalyst where the vanadium is in five coordination state. The intensity of the above band increases at higher pH values due to the increase in V content at higher pH.
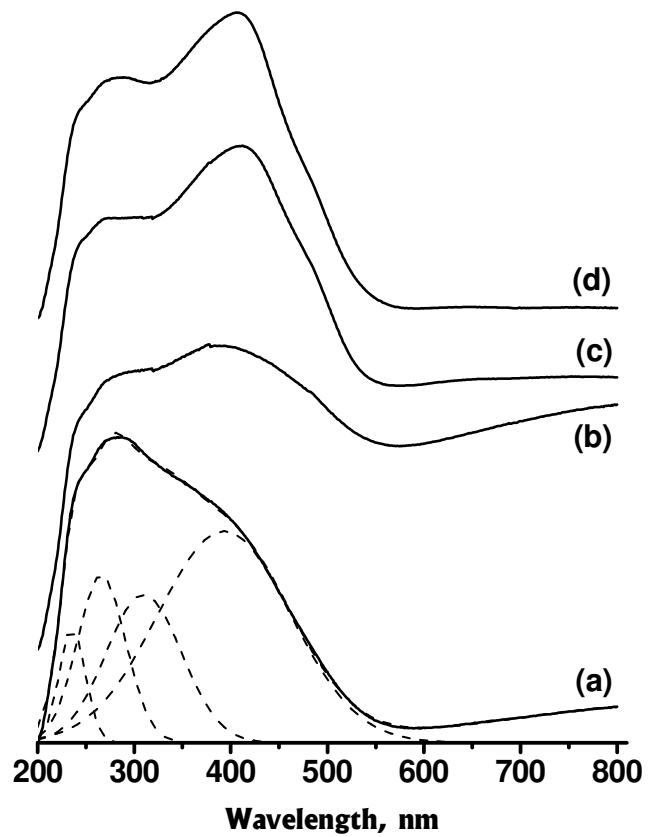
Figure 4: DRS UV-visible spectra of (a) $MoVAlO_x$-1, (b) $MoVAlO_x$-2, (c) $MoVAlO_x$-3 and (d) $MoVAlO_x$-4 (calcined samples)
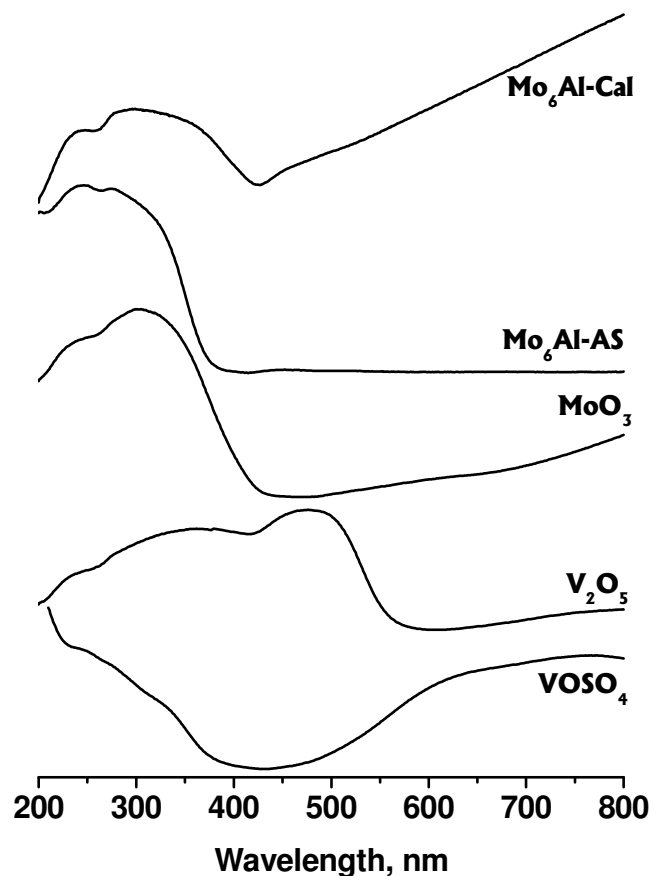
Figure 5: DRS UV-visible spectra of different standard samples

5.3.1.6 EPR Spectroscopy

Figure 6 shows the EPR spectra of all the four calcined catalysts were recorded at room temperature. While the EPR spectra of $MoVAlO_x$-1 and $MoVAlO_x$-2 catalysts showed overlapped signals corresponding to Mo^{5+} and V^{4+}, $MoVAlO_x$-3 and $MoVAlO_x$-4 catalysts gave signals corresponding to mainly of Mo^{5+} with no trace of V^{4+} signal. The EPR spectra of V^{4+} centers are characteristic of an axial symmetry typical for orthogonal geometry [23]. The EPR spectra of V^{4+} of $MoVAlO_x$-1 and $MoVAlO_x$-2 were best fitted with Hamiltonian parameters, $g_{\parallel} = 1.926$, $g_{\perp} = 1.985$, $A_{\parallel} = 183$, $A_{\perp} = 53$ at operating microwave frequency, 9.457 GHz.

Normalization of the simulated spectrum with the parallel components of V^{4+} EPR signal clearly showed that EPR spectra of $MoVAlO_x$-1 and $MoVAlO_x$-2 consist of overlapped signals from V^{4+} and Mo^{5+} species. EPR spectrum of Mo^{5+} showed

unresolved broad isotropic pattern (peak to peak line width of 90 G). The assignment of the EPR signal to Mo^{5+} was also substantiated by that of the reference catalyst, Mo_6Al-*Cal*, which showed a characteristic Mo^{5+} signal with 70 G line width (Figure 6). The broad line width may be due to the presence of more than one Mo^{5+} sites and/or due to magnetic interactions between the paramagnetic Mo^{5+} centers those are in close proximity. In order to quantify the amount of paramagnetic centers *viz.*, V^{4+} and Mo^{5+}, with respect to the total V and Mo contents respectively, the area under the peak of all the EPR spectra (double integration) was calculated using vanadyl sulfate as a standard.

Accordingly, V^{4+}/V_{total} was estimated to be around 0.8 % in $MoVAlO_x$-1 as well as $MoVAlO_x$-2 whereas Mo^{5+}/Mo_{total} was around 2.5 % for all the catalysts indicating that the majority of Mo and V species are in their higher oxidation states namely Mo^{6+} and V^{5+} respectively which are diamagnetic. For $MoVAlO_x$-1 and $MoVAlO_x$-2 catalysts, the area corresponding to V^{4+} was determined separately based on the simulation before estimating the Mo^{5+} content.
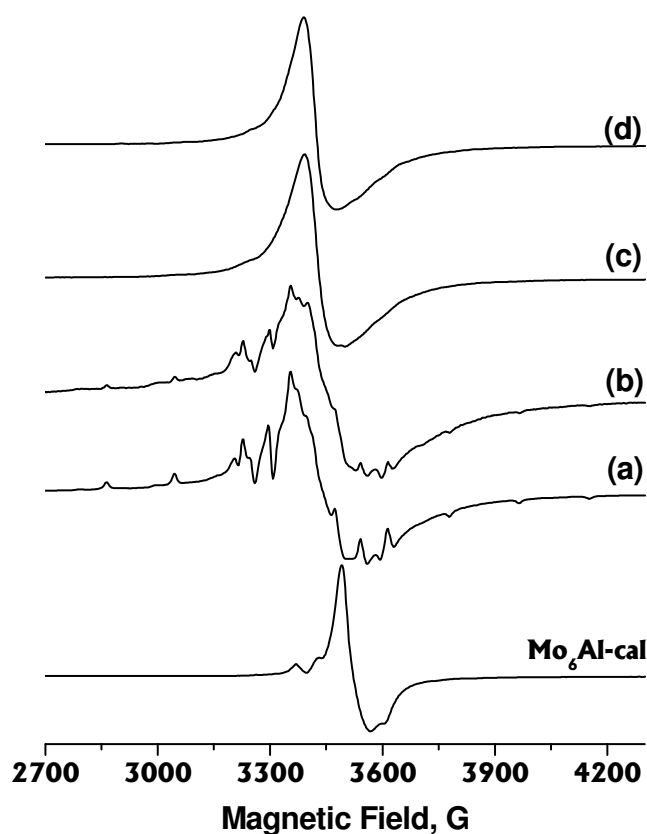
Figure 6: EPR of (a) $MoVAlO_x$-1, (b) $MoVAlO_x$-2, (c) $MoVAlO_x$-3, (d) $MoVAlO_x$-4 and Mo_6Al-*CAL* (calcined samples)

5.3.2 Selective Oxidation of ethane

All the four catalysts were tested for selective oxidation of ethane in a fixed bed reactor as described in the experimental section. The reaction was carried out typically at the experimental condition of 300 °C and 15 bar with a flow rate of 48.33 ml/min using ethane/air/steam: 27.6/47.6/24.8 mol % over 2 g of catalyst loading. The reaction was allowed to run for several hours (~ 10 h) to attain saturation and then the products were analyzed for every 3 h and the results are summarized in Table 2. Each data point is an average of three measurements. In all these cases, acetic acid and ethylene were the main products apart from CO and CO_2. Other products like ethanol, methanol and acetaldehyde were also seen but in less than 150 ppm level and are not discussed further. As seen in Table 2, $MoVAlO_x$-1 gave 30 mol % selectivity to acetic acid and 32 mol % selectivity to ethylene at the ethane conversion of 9.7 mol %.

Interestingly, $MoVAlO_x$-2 showed an excellent activity with 23 mol % ethane conversion with a combined ethylene and acetic acid selectivity of 80.6 mol % where acetic acid selectivity alone was 40.2 mol %.

$MoVAlO_x$-3 showed a moderate ethane conversion (10.5 mol %) with a better acetic acid selectivity of 46 mol % where the combined ethylene and acetic acid selectivity of 82 mol %. In both $MoVAlO_x$-2 and $MoVAlO_x$-3 catalysts, the selectivity to CO and CO_2 was very low. The catalyst $MoVAlO_x$-4 showed the least activity of 8.2 mol % ethane conversion with lowest acetic acid selectivity of 3 mol % where selectivity to ethylene was 18 mol % and selectivity to CO_x was 79 mol %. $MoVAlO_x$-2 gave highest acetic acid yield of 9.25 mol % while $MoVAlO_x$-4 gave the least yield (0.25 mol %). The other catalysts viz., $MoVAlO_x$-1 and $MoVAlO_x$-3 gave an acetic acid yield of 2.91 and 3.78 mol % respectively as shown in Table 2.

Since $MoVAlO_x$-2 showed a better activity towards ethane oxidation than the other catalysts, $MoVAlO_x$-2 catalyst was alone tested at different experimental conditions to understand their effects on the ethane conversion and the products selectivity. Experiments were carried out at different reaction pressures in the range 5-20 bar with a feed of ethane/air/steam: 27.6/47.6/24.8 mol % at reaction temperature 300°C and the results are plotted in Figure 7. The reaction pressure has a definite influence on ethylene and acetic acid selectivity. As seen in the Figure, there is a gradual increase in the ethane conversion with increase in the reaction pressure and reached nearly a plateau above 15 bar pressure. The ethane conversion was around 8 % at 5 bar and increased to 23 % at 15 bar. The acetic acid selectivity was around 20 % and the ethylene selectivity was around 73 % at 5 bar and both reached around 40 % at 15 bar pressure and thereafter, the selectivity of ethylene and acetic acid were more or less the same until 20 bar pressure. Thus, the optimum reaction pressure was around 15 bar at 300°C. The variation in the selectivity to CO and CO_2 was small as compared to that of ethylene and acetic acid where the selectivity to CO was slightly higher than that of CO_2. Selectivity to CO was around 5 % at 5 bar which reached around 11 % at 20 bar and CO/CO_2 mole ratio remained around 1.6 ± 0.4 throughout the pressure range employed.

At an optimum reaction pressure of 15 bar with a feed composition of ethane/air/steam: 27.6/47.6/24.8 mol %, oxidation experiments were carried out at different reaction temperatures in the range of 260-340 ºC. The variation in the

selectivity of ethylene, acetic acid, CO and CO_2 along with the ethane conversion as a function of temperature is shown in Figure 8. The ethane conversion at 270 °C was 5 % and increased to 27 mol % at 340 °C. Although the combined selectivity to ethylene and acetic acid was around 80 % throughout the temperature range employed, the acetic acid selectivity decreased from 44 % to 36 % on increasing the temperature from 260 to 340°C. On the other hand, the trend for ethylene selectivity was reverse with increase in temperature. The other products were namely CO and CO_2 increase with temperature due to the combustion reactions of ethylene and acetic acid. The CO selectivity was slightly higher than that of CO_2 as shown in the Figure [24].

The time on stream study was carried out with $MoVAlO_x$-2 catalyst to test the stability and activity of the catalyst with time. The reaction was carried out for 50 h and was monitored at regular time intervals at 300 °C and 15 bar with the feed ethane/air/steam: 27.6/47.6/24.8 mol %. The profile of ethane conversion and the product selectivity with time is given in Figure 9 where each data point was the average of three experiments.

The influence of addition of water (steam) co-feed on the ethane conversion and the product selectivity was studied at the reaction temperature, 300 °C by varying the partial pressure of water at a constant partial pressure of ethane and oxygen. The ethane conversion and selectivity of the products namely acetic acid, ethylene and CO_2 are shown in Figure 10 as a function of partial pressure of water. The experiment was performed by varying the partial pressure of water between 1.55 to 6.23 bar at a constant total pressure of 15 bar at the reactor inlet where the partial pressure of ethane was 3.22 bar and that of oxygen were 5.63 bar (balance by nitrogen). As shown in the Figure, the conversion of ethane decreases gradually from 23.8 mol % to 16.1 mol % when the partial pressure of water was increased from at 1.55 to 6.23 bar. Addition of steam showed a positive influence on the acetic acid selectivity as the acetic acid selectivity increased from 36.1 mol % at 1.33 bar to 43.9 % at 6.23 bar partial pressure of water whereas ethylene selectivity showed an opposite trend, 41.8 % at 1.33 bar and 37 % at 6.23 bar. The CO_2 selectivity was almost constant for the entire range of water partial pressure where CO was seen only in traces.

Table 2: Selective oxidation of ethane over MoVAlOx catalysts prepared at different pH values.

Catalyst	Ethane Conversion (mol %)	Product selectivity (%)				CH_3COOH Yield (mol %)
		CH_3COOH	CH_2CH_2	CO	CO_2	
$MoVAlO_x$-1	9.7	30	32	19	19	2.91
$MoVAlO_x$-2	23	40	40	12	8	9.25
$MoVAlO_x$-3	10.5	36	46	10	8	3.78
$MoVAlO_x$-4	8.2	3	18	9	70	0.25

Reaction conditions: Pretreatment temperature: 400 ºC for 4 h in He stream (20 ml/min). Reaction conditions: temperature = 300 °C, pressure= 15 bar, ethane = 13.33 ml/min, air = 23 ml/min, steam = 12 ml/min

Figure 7: Conversion and selectivity profiles on selective oxidation of ethane over MoVAlO$_x$-2 catalyst with reaction pressure. Pretreatment temperature: 400 ℃ for 4 h in He stream (20 ml/min). Reaction conditions: temperature = 300 °C, ethane = 13.33 ml/min, air = 23 ml/min, steam = 12 ml/min
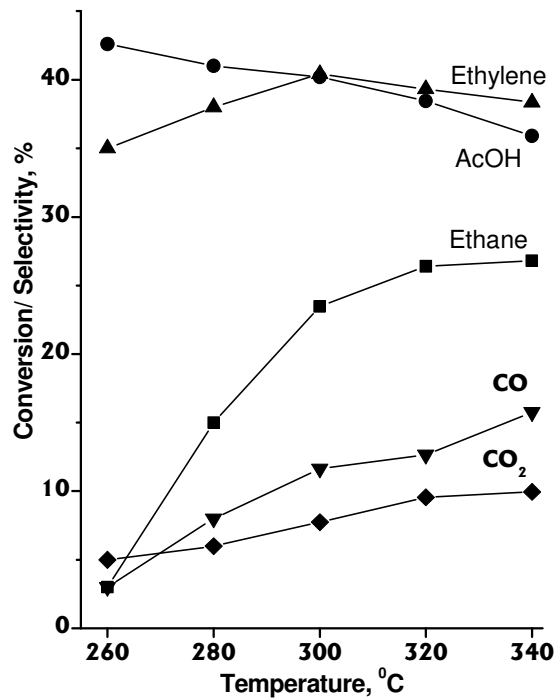
Figure 8: Conversion and selectivity profiles on selective oxidation of ethane over MoVAlO$_x$-2 catalyst with reaction temperature. Pretreatment temperature: 400°C for 4 h in He stream (20 ml/min). Reaction conditions: pressure= 15 bar, ethane = 13.33 ml/min, air = 23 ml/min, steam = 12 ml/min
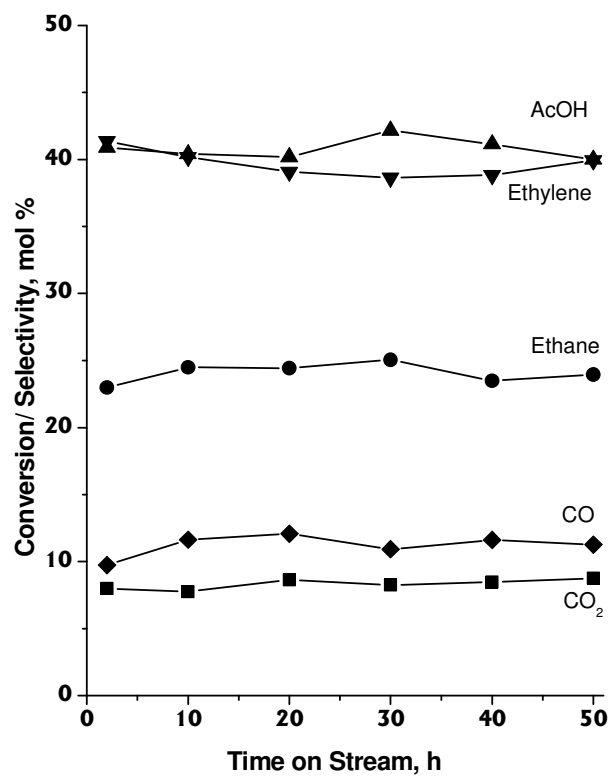
Figure 9: Time on stream study of selective oxidation of ethane over MoVAlO$_x$-2 catalyst with reaction temperature. Pretreatment temperature: 400ºC for 4 h in He stream (20 ml/min). Reaction conditions: temperature = 300 °C, pressure= 15 bar, ethane = 13.33 ml/min, air = 23 ml/min, steam = 12 ml/min

Figure 10: Effect of partial pressure of water on the ethane conversion and product selectivity during selective oxidation of ethane over MoVAlO$_x$-2 catalyst. Experimental conditions: temperature, 300°C; total pressure, 15 bar; catalyst, 2 g; PO_2 = 5.625 bar and PC_2H_6 = 3.22 bar, the partial pressure of water was varied between 1.55 to 6.23 bar, total pressure = 15 bar

5.4 Discussion

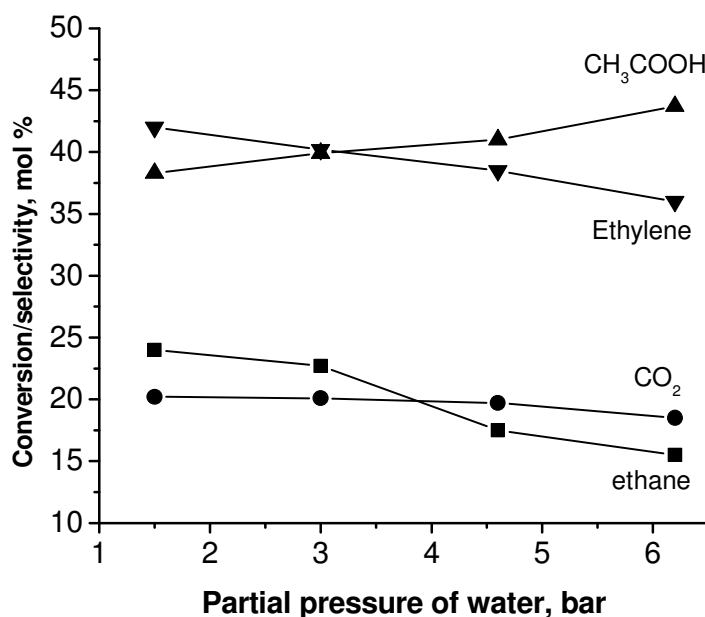Although the initial preparative elemental compositions were same, the pH at which the catalysts were made has a strong influence on the bulk and surface elemental compositions and the catalyst yield. Decreasing trend of Mo/V and Mo/Al ratios with increase in pH (Table 1) indicates that Mo content in the catalysts decreases with increase in the pH value. Also, the yield of the calcined catalysts decreased with increase in pH.

The decrease in the Mo content and the catalyst yield should be associated with the higher solubility of Mo or dissociation of Anderson heteropoly compound, $(NH_4)_3AlMo_6H_6O_{24}.7H_2O$, at higher pH which creates a less favorable situation for the formation of mixed metal oxides with the expected elemental composition. Thus, the pH of the slurry has a profound effect on the nature of the precursors and their amount available for the formation of mixed metal oxide catalysts at the hydrothermal

condition and also on the formation of crystalline phases during the heat treatment as seen in the powder XRD patterns. While the surface area in the range 7-20 m^2/g is typical for the mixed metal oxide catalysts, observed lower surface area of MoVAlO$_x$-1 should be due to its highly crystalline nature [7].

The powder XRD patterns of the present MoVAlO$_x$ catalysts are different from that of the reported MoVAlO$_x$ having a similar elemental composition [25]. The reported XRD pattern of MoVAlO$_x$ showed mainly two sharp peaks at 2θ = 22 and 45° (001) reflections along with other diffractions at lower angles. The presence of strong peak line at 2θ = 22° (d = 4 A°) was reported to be responsible for the good catalytic activity of the catalyst. However, with the present catalyst systems the peak at 2θ = 22° is not strong. The difference in the XRD patterns of the present catalysts from the reported one may be attributed to the pH condition of the preparative composition and subsequent temperature treatments. All the four as-synthesized catalysts prepared at different pH values were calcined under the identical conditions *i.e.* heating up to 350 °C under static air and then to 400°C under the N$_2$ atmosphere. α-MoO$_3$ phase which is present in MoVAlO$_x$-1 and MoVAlO$_x$-2 is totally absent in the other two catalysts prepared at higher pH values. Thus, the present results show that the amount of MoO$_3$ can be controlled by pH of the initial preparative slurry. The presence of high amount of V$_2$O$_5$ in MoVAlO$_x$-4, MoO$_3$ in MoVAlO$_x$-1 and different elemental compositions at different pH conditions indicate that presence of the right amount of different elements during the temperature treatment is highly important for the formation of active species. It is generally observed that presence of additional metal ion like Nb to Mo$_y$V$_z$O$_x$ basic composition influences formation of partially reduced phase (Mo$_4$O$_{11}$ type) and decreases the formation of MoO$_3$ [26]. It appears that in the present catalyst systems, Al ion plays a role of Nb in stabilizing different active phases. Although Al containing phases are not observed except in MoVAlO$_x$-4, Al might have been incorporated in vanadomolybdate or highly dispersed on the other phases, owing to its low content such that it is not seen in XRD pattern, or it existed in an amorphous state.

A partial reduction of the catalysts with a temperature treatment is generally observed in the presence of oxalate and nitrate anions in the catalyst precursors [4, 27]. In some cases, the presence of NO$_x$ favors partial oxidation of metal ions with an enhanced activity [28]. Although neither oxalate nor nitrate salts were used in the

present catalyst systems, observed partial reduction of Mo^{6+} to Mo^{5+} might be due to ammonium ions present. The observation of EPR signal upon the heat treatment of a diamagnetic Mo_6Al-*AS* precursor substantiates the point that ammonium ions present in the precursor is responsible for the partial reduction of Mo^{6+}. Estimation of amount of V^{4+} and Mo^{5+} in the calcined catalysts showing $V^{4+}/V_{total} \sim 0.8$ % and Mo^{5+}/Mo_{total} ~ 2.5 % indicated that majority of Mo and V are in their higher oxidation states, *viz.,* Mo^{6+} and V^{5+} respectively which are diamagnetic. It may also be noted here that any paramagnetic centers connected through a super exchange pathway leading to strong antiferromagnetic interactions might not have contributed for the EPR intensity. Presence of such antiferromagnetic interactions in the present case can not be ruled out while all the catalysts prepared at different pH values were found to be active for the ethane oxidation as seen in the Table 1, the catalysts prepared at pH 1, 2 or 3 showed better selectivity to ethylene and acetic acid, with a moderate ethane conversion.

Based on the phases identified from the powder XRD, it appears that the MoV_2O_8 phase, which is present in the catalysts prepared at pH 1-3, are possibly responsible for the selective oxidation of ethane to acetic acid/ethylene. The XRD patterns of both $MoVAlO_x$-1 and $MoVAlO_x$-2 are nearly similar except for the fact that (020) reflection of MoO_3 is very strong (100 %) in $MoVAlO_x$-1 as compared to $MoVAlO_x$-2. The above observation is likely due to the preferential orientation of the MoO_3 crystals in $MoVAlO_x$-1.

The superior activity of $MoVAlO_x$-2 compared to $MoVAlO_x$-1 needs further investigations. The higher ratio of MoV_2O_8/MoO_3 in $MoVAlO_x$-2 compared to $MoVAlO_x$-1 may be due to the lower Mo/V ratio in $MoVAlO_x$-2. As seen in the elemental analysis data (Table 1) the Mo: V ratio was 1:0.15 in $MoVAlO_x$-1 compared to 1:0.34 in $MoVAlO_x$-2. The presence of MoV_2O_8 and $Mo_4V_6O_{25}$ in $MoVAlO_x$-3 and its moderate activity substantiate the conclusion that MoV_2O_8 might be an important phase responsible for the catalytic activity. The higher ethane conversion with the $MoVAlO_x$-2 catalyst compared to the $MoVAlO_x$-3 catalyst indicates that MoO_3 support is important for the better activity.

Apart from MoV_2O_8/MoO_3 ratio, the amount of the reduced phase Mo_4O_{11} was higher in $MoVAlO_x$-2 compared to $MoVAlO_x$-1 indicating the possibility that the MoV_2O_8 phase along with the reduced species may be important for the excellent activity. It may also be noted here that the surface area of $MoVAlO_x$-2 is higher than

$MoVAlO_x$-1 which may have some influence on the overall activity of the catalyst. With the above background, it is easy to understand the least catalytic activity of $MoVAlO_x$-4 catalyst where MoV_2O_8 and Mo_4O_{11} phases are minor phases and MoO_3 phase was totally absent. Presence of V_2O_5 and other high vanadium containing phases like $MoVAlO_4$ might be responsible for the over oxidation of the formed product namely ethylene and acetic acid.

It may be noted here that the partial reduction of catalyst precursors has been reported to have a positive influence on the activity and selectivity in selective oxidation of the lower alkanes, though the exact role of these species are yet to be understood [4, 26, 27]. The presence of reduced species with V^{4+} centers in $MoVAlO_x$-1 and $MoVAlO_x$-2 catalysts and Mo^{5+} in $MoVAlO_x$-3 and $MoVAlO_x$-4 catalysts is obvious from EPR results. However, the nature and location of V^{4+} is not clear from the present study. One possibility is that part of vanadium ion in MoV_2O_8 is in V^{4+} oxidation state as MoV_2O_8 is the only vanadium containing crystalline phase in $MoVAlO_x$-1 and $MoVAlO_x$-2. However, the absence of V^{4+} EPR signal in $MoVAlO_x$-3 where MoV_2O_8 phase is the major phase does indicate the presence of V^{4+} containing non-crystalline species can not be ruled out. Presence of Mo^{5+} and other reduced phases containing Mo^{5+} are clear from EPR, UV-visible and XRD data.

Thus, we believe that ethane is converted to ethylene by oxidative dehydrogenetion mechanism which in turn is adsorbed back on the catalyst to form acetic acid. Decrease in the acetic acid selectivity and increase in the ethylene selectivity on increasing the temperature is believed to be associated with adsorption and desorption phenomena. At high temperatures, the energy, kT (where k is Boltzmann constant) was enough to desorb the ethylene and thus making it not available for the acetic acid formation. The time on stream studies indicated that the catalyst is stable and active for several hours without any deactivation. Commonly occurring catalyst deactivation by coking is not expected in the present systems due to the oxidative experimental conditions. The studies of the effect of partial pressure of water co-feed on ethane oxidation indicated that the water co-feed has a positive influence on the acetic acid selectivity and negative influence on the ethylene selectivity and the ethane conversion rate. The positive influence of steam on the acetic acid selectivity is believed to be associated with the hydroxyl group formation on the surface of catalyst which in turn facilitates the conversion of ethylene to acetic acid [29-31]. A reduction in the rate of ethane oxidation by water co-feed has been

observed by others for various metal oxide systems [2, 8, 29]. The decrease of ethane conversion might be associated with adsorption of strong polar substrate like water and/or acetic acid, thus blocking the active sites that lead to the reduction of the ethane oxidation rate. Different effect of water co-feed on the formation of acetic acid and CO_2 indicates the possibility for different types of sites where water seems to be preferentially interacting on the site that is responsible for ethylene to acetic acid formation.

The efficiency of the present catalyst system for the selective ethane oxidation is assumed to be due to the presence of MoV_2O_8 and other reduced species supported on the MoO_3 phase. Activation of the C-H bond of ethane on the catalytic surface possibly via unstable ethoxy intermediate leads to ethylene formation. Part of the ethylene formed adsorbs either weakly or strongly on the selective site of the catalyst surface in the presence of water and oxygen that leads to the formation of intermediates like ethanol and acetaldehyde and further to acetic acid. Although alcohol/aldehyde products were not seen as major products, their concentrations up to 150 ppm were detected in the GC analysis. With the present experimental conditions, oxidation rate of these alcohol/aldehyde intermediates leading to acetic acid might be very high. Any of these intermediates, ethane and/or acetic acid will be oxidized to CO_x, if they are strongly adsorbed on any non-selective phase (e.g. Al_2O_3 or V_2O_5). Desorption of ethylene will be easier if it is bound on weak acid site like MoO_3.

5.5 Summary and Conclusion

Catalysts of general formula $MoVAlO_x$ prepared with initial elemental composition of 1.00: 0.34: 0.167 (Mo: V: Al) at different pH conditions showed pH dependant elemental compositions. While all of them found to be active for selective oxidation of ethane, catalysts prepared at pH 2 showed excellent activity with 23 % ethane conversion with 80 % combined selectivity to ethylene and acetic acid in equimolar ratio at optimum experimental conditions. From powder XRD and other spectroscopic studies, the high activity is attributed to the presence of MoV_2O_8 and other reduced species like Mo_4O_{11} phases supported on MoO_3. Although presence of any amorphous phase is not clear at present, presence of V and Mo ions in partially reduced form, as confirmed by Raman, UV-visible and EPR spectra, play a crucial role in the selective oxidation of ethane.

References

1. D. Vitry, Y. Morikawa, J. L. Dubois, W. Ueda, Appl. Catal. A. 252 (2003) 411

2. D. Linke, D. Wolf, M. Baerns, O. Timpe, R. Schlögl, S. Zey, U. Dingerdissen, J. Catal. 205 (2002) 16

3. M. M. Lin, Appl. Catal. A. 207 (2001) 1

4. J. M. Oliver, J. M. L. Nieto, P. Botella, A. Mifsud, Appl. Catal.A. 257 (2004) 67

5. Q. Smejkal, D. Linke and M. Baerns, Chem. Eng. Proc. 44 (2005) 421

6. J. M. L. Nieto, P. Botella, M. I. Vázquez, A. Dejoz, Chem. Commun. (2002) 1906

7. M. Roussel, M. Bouchard, K. Karim, S. Al-Sayari, E. Bordes-Richard, Appl.Catal. A 308 (2006) 62

8. E. Heracleous and A.A. Lemonidou, J. Catal. 237 (2006) 175

9. S. Zeyss, U. Dingerdissen, J. Fritch, US Patent 6,790,983, 2004

10. K. Oshihara, T. Hisano, W. Ueda, Topics.Catal. 15 (2001) 153

11. K. Asakura, K. Nakatani, T. Kubota, Y. Iwasawa, J. Catal. 194 (2000) 309

12. W. Ueda, N. F. Chen, K. Oshihara, Chem. Commun. (1999) 517

13. K. Nomiya, T. Takahashi, T. Shirai, M. Miwa, Polyhedron 6 (1987) 213

14. A. Khodakov, B. Olthof, A.T. Bell, E. Iglesia, J. Catal. 181 (1999) 205

15. M. Dieterle, G. Mestl, J. Jäger, Y. Uchida, H. Hibst, R. Schlögl, J. Mol.Catal.A. 174 (2001) 169

16. G. Mestl, Ch. Linsmeier, R. Gottschall, M. Dieterle, U. Wild, R. Schlögl, J. Mol.Catal.A. 162 (2000) 463

17. W. Daniell, A. Ponchel, S. Kuba, F. Anderle, T. Weingand, D.H. Gregory and H. Knozinger, Topics in Catal 20 (2002) 65

18. J. M. Jehng, I.E. Wachs, F. T. Clark, M.C. Springman, J. Mol. Catal. 81 (1993) 63

19. E. Heracleous, M. Machli, A. A. Lemonidou, I. A. Vasalos, J. Mol. Catal. A. 232(2005) 29

20. J. M. Kanervo, M. E. Harlin, A. O. I. Krause, M. A. Bañares, Catal. Today, 78 (2003) 171

21. J. M. Oliver, J. M. L. Nieto, P. Botella, Catal. Today 96 (2004) 241

22. A. Davidson, M. Che, J. Phys. Chem. 96 (1992) 9909

23. E. García-González, J. M. López Nieto, P. Botella and J. M.González-Calbet*,* Chem. Mater. 14 (2002) 4416

24. E. Heracleous, A. A. Lemonidoua*,* J. A. Lercher, Applied Catalysis A: General 264

25. K. Oshihara, Y. Nakamura, M. Sakuma, W. Ueda, Catal.Today 71 (2001), 153

26. M. Roussel, M. Bouchard, E. Bordes-Richard, K. Karim, S. Al-Sayari, Catal. Today 99 (2005) 77

27. H. Tsuji, Y. Koyasu, J. Am. Chem. Soc. 124 (2002) 5608

28. A. M. Gaffney, M. D. Heffner, R. Song, EP 1249274 (2002)

29. M. D. Argyle, K. Chen, A. T. Bell, E. Iglesia, J. Phys. Chem. B 106 (2002) 5029

30. A. B. Evnin, J. A. Rabo, P. H. Kasai, J. Catal. 30 (1973) 109

31. J. L. Seoane, P. Boutry, R. Montarnal, J. Catal. 63 (1980) 191

Chapter 6:

Summary and Conclusion

6.1 Introduction

Selective oxidation of olefins and alcohols to produce epoxides, aldehydes, and ketones is of great importance in the fine chemical and pharmaceutical industries. Traditionally, these catalytic procedures produce a great deal of environmentally undesirable wastes because inorganic oxidants and organic solvents are used. Replacing the conventional process by an environmentally benign procedure along with the use of environment friendly oxidants like molecular oxygen or hydrogen peroxide is highly desirable. However, it is known that both these eco friendly oxidants generally do not show any direct activity towards the organic substrates. There are various transition metal ions based catalyst systems that are known to activate molecular oxygen and hydrogen peroxide. Most of them are of metal-organic ligand in origin like the metal-salen complexes or metal-porphyrin complexes. The problem with these systems is that the organic part of the catalyst is vulnerable to oxidation thereby losing its activity. Thus, a catalyst system that activates both molecular oxygen and hydrogen peroxide for the selective oxidation reactions, without itself undergoing oxidative decomposition during the course of reaction is certainly desired. This thesis deals with the use of Polyoxometalates as catalysts for all such oxidation reactions. A detailed summary and conclusion derived from each chapter is explained below.

6.2 Selective oxidation of alkenes and alcohols over [SbW$_9$O$_{33}$] based catalyst system with *aq.* H$_2$O$_2$

This chapter deals with selective oxidation of alkenes and alcohols over Na$_9$[SbW$_9$O$_{33}$] in conjunction with a phase transfer catalyst [MTCA]$^+$Cl$^-$ catalytic system, with *aq.* H$_2$O$_2$ as the oxidant. The system was found to be capable of selectively oxidizing a number of structurally different alkenes as well as a variety of secondary and allylic in high yields. In most of the cases the selectivity for epoxide (in the case of alkenes) or ketone (in the case of alcohols) was excellent. Importantly, there was no need of any solvent for the reaction (except when the substrate was a solid). It could be unambiguously shown from the controlled experiments that tungstate species are indeed the active centers and that the incorporated transition metal ions do not play any major role. Spectroscopic studies indicated the formation of a tungsten-peroxo intermediate on the interaction of polyoxotungstate with aq. H$_2$O$_2$ in presence of [MTCA]$^+$Cl$^-$, and this intermediate was observed for both the

transition metal containing polyoxotungstate as well as the transition metal free precursor. Spectroscopic studies also revealed that the catalyst was stable in the presence of PTC when aq. H_2O_2 was used as the oxidant.

6.3 Alkenes epoxidation catalyzed by vanadium heteropoly acids heterogenized on amine functionalized SBA-15 materials

This chapter deals with vanadium substituted molybdophosphoric acids (V_xHPA) immobilized on amine functionalized SBA-15 as catalysts for epoxidation of alkenes, once again with the same oxidants of *aq.* H_2O_2 as well as TBHP. The synthesized materials were characterized by using various techniques prior to testing of their catalytic activities. Small angle X-ray scattering analysis provided evidence for the structural integrity of the amine functionalized SBA even after immobilizing with molybdovanadophosphoric acid. The synthesized materials were also characterized by nitrogen sorption studies, UV-Visible, NMR, and IR studies provided evidence for the presence of V_xHPA inside the NH_2-SBA. The catalytic activity of the immobilized sample (NH_2-SBA-V_xHPA) were studied for few substrates with aqueous hydrogen peroxide at 60 °C and compared with the neat V_xHPA catalyst. It was found that selectivity of the products is higher with the immobilized catalyst. The catalyst part can be separated after the epoxidation reactions and can be reused for few cycles without losing its further activity, especially with TBHP as the oxidant.

6.4 Alkene epoxidation catalyzed by vanadium heteropoly acids dispersed on hydrated titania

This chapter deals with alkene epoxidation catalyzed by vanadium substituted molybdophosphoric acids (V_xHPA) dispersed on hydrated titania, with organic solvent extracted TBHP as the oxidant, in a lipophilic solvent system. It was clearly demonstrated that divanadomolybdophosphoric acid wet-impregnated on hydrated titania ($TiO_2.xH_2O$) was an excellent catalyst system for alkene epoxidation, with TBHP extracted in dichloroethane as the oxidant. The catalysts could be recycled without much loss in activity at least three times by choosing appropriate solvent for the reaction. For all the alkenes studied here the major product was always the corresponding epoxide. The controlled experiments unambiguously indicated that the

vanadium substitutions in the heteropoly acid as well as the titanium species from the support had a role to play. Hence a simple catalytic system, which was free of high temperature calcination steps and tedious multi-step procedures, normally encountered in heterogenization of heteropoly acids, was thus demonstrated.

6.5 Selective oxidation of ethane to acetic acid over MoVAlO$_x$ based catalytic system with molecular oxygen

This chapter deals with selective oxidation of ethane to acetic acid over MoVAlO$_x$ catalysts in a fixed bed down flow reactor set up. Catalysts of general formula MoVAlO$_x$ were prepared with initial elemental composition of 1.00: 0.34: 0.167 (Mo: V: Al) at different pH conditions, showed pH dependent elemental compositions. While all of them found to be active for selective oxidation of ethane, catalysts prepared at pH 2 showed excellent activity with 23 % ethane conversion with 80 % combined selectivity to ethylene and acetic acid in equimolar ratio at optimum experimental conditions. From powder XRD and other spectroscopic studies, the high activity was attributed to the presence of MoV$_2$O$_8$ and other reduced species like Mo$_4$O$_{11}$ phases supported on MoO$_3$. Although presence of any amorphous phase was not clear at present, presence of V and Mo ions in partially reduced form, as confirmed by Raman, UV-visible and EPR spectra, played a crucial role in the selective oxidation of ethane.

6.6 Overall Conclusion

In this thesis, [SbW$_9$O$_{33}$] based polyoxotungstate in conjunction with a phase transfer catalyst (methyl trioctyl ammonium chloride) was used as catalyst for the selective oxidation of alkenes and alcohols with *aq.* H$_2$O$_2$ as the oxidant. This system does not require any solvent, except in the case of solid alkenes/alcohols. It was also demonstrated using FT-IR spectroscopy that the polyoxotungstate moiety is stable even in the presence of *aq.* H$_2$O$_2$, after extraction in organic medium under the virtue of PTC. The drawback of the system however, was difficulty in the separation of the epoxidized or ketonized product from the catalyst. High temperature distillation was required for the separation of the products, which is certainly not desired.

To overcome this problem of difficulty in separation of product from catalyst, two approaches were used; one was heterogenization of the polyoxometalate based catalyst on amine functionalized SBA-15 and the other approach was dispersion of

the same on hydrated titania, as we shall see one by one. The first approach was thus heterogenization of vanadium substituted molybdophosphoric acids on amine functionalized SBA-15. The presence of the heteropoly acids inside the pores of SBA-15 was neatly showed using various techniques. Recycling experiments were also carried out, to demonstrate the reusability of catalysts for successive runs. However, the only drawback of the system was multi-step and high temperature syntheses of the catalyst materials, thus consuming lot of time as well as energy, prior to the actual oxidation processes.

In order to overcome these problems the other approach was designed i.e. dispersion of vanadium substituted molybdophosphoric acids on hydrated titania, which was very easy to synthesize and did not require high temperature or multiple-steps for the catalyst syntheses. Here also recycling experiments were carried out to demonstrate the reusability of catalysts for successive runs. However, the disadvantage with this system was we had to restrict ourselves to lipophilic solvents like dichloroethane as well as hydrophobic oxidants like organic solvent extracted TBHP, which is normally less active and costlier than *aq.* H_2O_2.

In all the works seen till now we were in a position to carry out oxidation of alkenes or alcohols which are comparatively reactive as substrates and also, we have used either *aq.* H_2O_2 or TBHP as the oxidants, which are fairly better, as far as their activation by the catalysts is concerned. Thus for the final chapter of the thesis we have carried out the selective oxidation of ethane, which shows a very low reactivity, as compared to the other substrates *viz.* alkenes or alcohols, was chosen. Further, the selective oxidation of ethane to acetic acid was carried out using molecular oxygen, which is somewhat difficult to activate, when compared to other oxidants like *aq.* H_2O_2 or TBHP that were used in this thesis work. Normally, at high temperature and high pressure reaction conditions, the products are more reactive than the reactants itself and the easily end up in getting further oxidized to CO and CO_2, which are not the actual targets. Despite all these odds, selective oxidation of ethane to acetic acid has been successfully demonstrated in the current work.

LIST OF PUBLICATIONS

1.   Heterogenized molybdovanadophosphoric acid on amine-functionalized SBA-15 for selective oxidation of alkenes

        Raj, N. K. K., Deshpande, S.S., **Ingle, R. H.**, Raja, T., Manikandan, P., **2004**, *Catalysis Letters* 98 (4), pp. 217-223

2.   Immobilized molybdovanadophosphoric acids on SBA-15 for selective oxidation of alkenes

        Raj, N. K. K., Deshpande, S. S., **Ingle, R. H.**, Raja, T., Manikandan, P., **2005**, *Studies in Surface Science and Catalysis* 156, pp. 769-778

3. $[SbW_9O_{33}]$-based polyoxometalate combined with a phase transfer catalyst: A highly effective catalyst system for selective oxidation of alcohols with H_2O_2, and spectroscopic investigation

        Ingle, R. H., Kala Raj, N. K., Manikandan, P., **2007**, *Journal of Molecular Catalysis A: Chemical* 262 (1-2), pp. 52-58

4.   Alkene epoxidation catalyzed by vanadomolybdophosphoric acids supported on hydrated titania

        Rohit H. Ingle, A. Vinu and S.B. Halligudi, *Catalysis Communications*, **(In Press, Corrected Proof)**

5.   Selective Oxidation of Ethane Over Mo–V–Al–O Oxide Catalysts: Insight to the Factors Affecting the Selectivity of Ethylene and Acetic Acid and Structure-activity Correlation Studies

        T. M. Sankaranarayanan, **R. H. Ingle**, T. B. Gaikwad, S. K. Lokhande, T. Raja, R. N. Devi, V. Ramaswamy and P. Manikandan, *Catalysis letters,* **(Articles in Press)**

6.   Lacunary Keggin type polyoxotungstates in conjunction with a phase transfer catalyst: an effective catalyst system for epoxidation of alkenes with aqueous H_2O_2

        Rohit H. Ingle and N. K. Kala Raj, *Journal of Molecular Catalysis A: Chemical*, **(Communicated)**

SELECTED PRESENTATIONS IN SYMPOSIA/CONFERENCES

1. "Mn-based sandwich type Polyoxometalates: Effective Catalysts for Selective Epoxidation of Alkenes with Aqueous Hydrogen Peroxide", <u>Rohit H. Ingle,</u> N. K. Kala Raj and P. Manikandan, 7th National symposium on Catalysis, CSMCRI, Bhavnagar, Gujarat, India, January 18-20, 2005

2. "Molybdenum and vanadium based oxides as efficient catalysts for selective oxidation of ethane to ethylene and acetic acid", <u>R. H. Ingle</u>, T. M. Sankaranarayanan, T. B. Gaikwad, S. K. Lokhande, T. Raja, R. N. Devi, V. Ramaswamy and P. Manikandan, National Science Day Celebrations, National Chemical Laboratory, Pune, India, February 27, 2006